DESIGN, DEVELOPMENT AND PERFORMANCE PARAMETERS EVALUATION OF SMALL SCALE SOLAR UPDRAFT TOWER (SUT) PLANT

Submitted in partial fulfillment of the requirements
For the award of the degree of

DOCTOR OF PHILOSOPHY

In

MECHANICAL ENGINEERING

By

Mr. BALIJEPALLI RAMAKRISHNA
(Roll No. 716134)

Supervisor:

Dr. CHANDRAMOHAN V. P.
Associate Professor

Dr. K. KIRAN KUMAR
Associate Professor

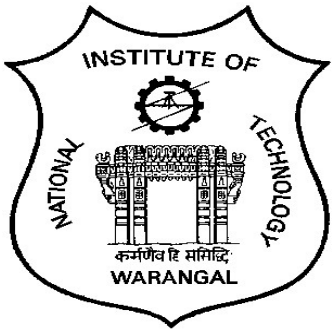

DEPARTMENT OF MECHANICAL ENGINEERING
NATIONAL INSTITUTE OF TECHNOLOGY
WARANGAL-506 004, TELANGANA,
INDIA

JANUARY 2020

DEDICATED

TO

MY PARENTS

NATIONAL INSTITUTE OF TECHNOLOGY- WARANGAL

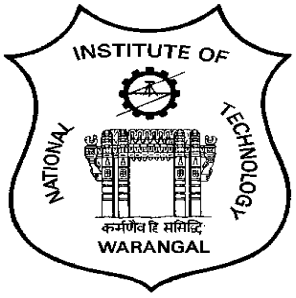

CERTIFICATE

This is to certify that the thesis entitled "**Design, Development and Performance Parameters Evaluation of Small Scale Solar Updraft Tower (SUT) Plant"** being submitted by **Mr. Balijepalli Ramakrishna** for the award of the degree of Doctor of Philosophy (Ph.D) in Mechanical Engineering to the National Institute of Technology, Warangal, India, is a record of the bonafide research work carried out by him under my supervision. The thesis has fulfilled the requirements according to the regulations of this Institute and in our opinion has reached the standards for submission. The results embodied in the thesis have not been submitted to any other University or Institute for the award of any degree or diploma.

Date:

Dr. Chandramohan V. P.
Associate Professor
Thesis Supervisor
Department of Mechanical Engineering,
National Institute of Technology,
Warangal

Dr. K. Kiran Kumar
Associate Professor
Thesis Supervisor
Department of Mechanical Engineering,
National Institute of Technology,
Warangal.

DECLARATION

This is to certify that the work presented in the thesis entitled "**Design, Development and Performance Parameters Evaluation of Small Scale Solar Updraft Tower (SUT) Plant"** is a bonafide work done by me under the supervision of Dr. Chandramohan V. P. and Dr. K. Kiran Kumar and was not submitted elsewhere for award of any degree.

I declare that this written submission represents my ideas in my own words and where others' ideas or words have been included, I have adequately cited and referenced the original sources. I also declare that I have adhered to all principles of academic honesty and integrity and have not misrepresented or fabricated or falsified any idea/data/fact/source in my submission. I understand that any violation of the above will be a cause for disciplinary action by the Institute and can also evoke penal action from the sources which have thus not been properly cited or from whom proper permission has not been taken when needed.

Mr. Balijepalli Ramakrishna
Roll No. 716134

ACKNOWLEDGEMENT

First and foremost I want to thank my supervisors **Dr. Chandramohan V. P. and Dr. K. Kiran Kumar.** It has been an honor to be that I am their Ph.D. student. They cultivated the seed of the research in me and inspired to apply this knowledge not only in laboratories but also in the personal life. Their invaluable contributions of time and ideas during Ph.D. stay provide me wealthy in experiences, which is productive and stimulating in all aspects. Their positive attitude at any diverse situations taught me how to tackles the hurdles at any stage with joy and enthusiasm. They provided me an excellent platform to nourish and grow my professional as well as personal life.

This work was not possible without the inspiration of my M. Tech. Supervisors **Prof. S.K. Dash (I.I.T Kharagpur, India),** and **Dr. S.K. Ajmani (Head, R&D, Tata Steel, India).** They inspired me during my post-graduation studies and accelerated my passion for pursuing higher studies with greater impact. They are my constant source of inspiration throughout my life.

I wish to sincerely thank university authorities, **Prof. N.V. Ramana Rao**, Director, National Institute of Technology, Warangal and other top officials who gave me an opportunity to carry out research work.

I also sincerely thank **Prof. N. Selvaraj (Dean, International Relations and Alumni Affairs)** and **Prof. R. Narasimha Rao**, Head, Mechanical Engineering Department, National Institute of Technology, Warangal for his continuous support towards carrying out research work.

I wish to express my sincere and whole hearted thanks and gratitude to my doctoral scrutiny committee (DSC) members **Prof. S. Srinivasarao,** Professor, Mechanical Engineering Department, **Dr. Jaya Krishna,** Associate Professor, Mechanical Engineering Department, **Dr. K. Thangaraju,** Associate Professor, Physics Department, National Institute of Technology, Warangal for their kind help, encouragement and valuable suggestions for successful completion of research work.

I would like to extend my thanks to all the faculty members in the Department of Mechanical Engineering for their valuable suggestions and encouragement. I am also thankful to all the supporting and technical staff of the Department of Mechanical Engineering who has directly or indirectly helped during the course of my work.

I am thankful to all my fellow research scholars especially, **Mr. Abhay Lingayat, Mr. Pritam Das, Mr. Manoj Kumar Dundi, Mr. Vishnu Vardhan Reddy and Mr. Ganesh Gawale** and M.Tech scholars, **Mr. Yashwant Kumar Reddy, Mr. Satyapal Yadav, Mr. Sajjan kesari** and **Mr. Ankit.**

I take this opportunity to sincerely acknowledge **the Center of Excellence (CoE) under TEQIP-II, National Institute of Technology Warangal for** providing the financial assistance for my project.

Last but not the least; I would like to thank my parents, sister, wife and children's, who are surely the happiest to see me complete this endeavor. To them, I owe all my accomplishments.

BALIJEPALLI RAMAKRISHNA

Abstract

Energy consumption has been increasing day by day because of population growth throughout the world. Present energy resources such as petroleum products may not sustain for long to meet human needs. The rapid utilization of limited fossil fuel reserves and other conventional energy sources are the main reasons for fuel scarcity in the globe. Use of fossil fuel and natural gas creates pollution, environmental problems etc. Also, their rising prices, diminishing availability in the future, force the society to find an alternate solution for fossil fuel. This has created awareness about alternative sources and therefore, much research is needed on non-conventional energy sources. Solar energy is one source which is freely and abundantly available and a huge amount of energy can be harnessed. One of the solar energy based plants is called solar updraft tower (SUT) power plant which has attracted attention of researchers because of its simple construction and novel technique.

Various kinds of solar power generating technologies such as thermo electric power generation, thermionic power generation, solar central power tower technology, parabolic trough solar thermal technology and dish solar thermal technology have been developed since so many years. However, this power generating technologies have some specific demerits such as high investment cost, low installed capacity and poor ability to resist wind force. To solve the problems of above said, SUT is one of the choices among the various solar technologies for producing power because of its simple design, easy fabrication, low operational and maintenance cost.

Estimation of solar input parameters such as radiation falls on collector, energy losses, radiation absorbed by absorber plate and consequently its heat losses is a very important thing in the design of a SUT system. Optimisation of geometrical dimensions of a SUT power plant is very much necessary for increasing the power production which avoids the unnecessary material usage. Enhancement of air velocity using guide vanes at chimney base is extremely required for increasing electric power generation. Material selection of SUT components (collector, chimney and turbine) is also one of the key issues to design the system effectively. Thermal energy storage (TES) system stores heat energy in day time and liberates the heat during no sunlight time region. Effective design of energy storage system can work the SUT system round-the-clock and produce more power. Design of wind turbine blade is also a crucial aspect to extract more energy from air. Therefore, a step is taken in this research work to address the above

issues in a very clear manner. To achieve all these objectives, the present research work is mainly focused on the design, development and performance parameters evaluation of a small scale SUT plant.

The three main divisions of this research work are: theoretical analysis, numerical analysis and experimental analysis of SUT plant. In the theoretical work, the performance of SUT was investigated and tabulated all the inputs and estimated parameters with the materials of a SUT power plant. All the three main components' (turbine, solar collector and a chimney) process parameters are estimated and discussed. The optimised geometrical dimensions of a small scale SUT were estimated and these were: collector diameter (D_{cp}) of 3.5 m, chimney height (H_{ch}) of 6 m and chimney diameter (D_{ch}) of 0.6 m. Appropriate materials are discussed and selected for solar collector, chimney, turbine and heat storage materials. Solar beam, diffuse and global radiation are estimated to analyze the performance of collector cover. Energy losses in solar collector cover and transmissivity estimations are performed to calculate theoretical energy collected in solar collector. Pressure drop inside the chimney is estimated and from that the actual power output of the turbine is calculated. The quantity of heat storage materials needed is evaluated in terms of both mass and volume. Theoretically the maximum velocity of air is achieved at the chimney base and is 2 m/s. The maximum overall efficiency and collector efficiency of the plant are estimated as 0.0028 % and 53.9 %. The maximum theoretical power output of the plant is 0.633 W.

In the numerical work, different cases (case-I, both collector and absorber plates are inclined; case-II, inclined collector and horizontal absorber plates; case-III, both horizontal collector and absorber plates), have been developed to examine the flow and thermodynamic characteristics of SUT power plant. A step is taken to find the location of turbine to absorb maximum kinetic energy for all the three cases. The practical domains of three cases were created and simulations were run using ANSYS FLUENT 16.0 CFD package. A turbulent, Realizable (k-ε) model and discrete ordinates (DO) radiation model were utilised to work out the mathematical governing equations of various cases. It came to a conclusion that the maximum and the average air velocities inside SUT were higher (3.06 and 1.63 m/s, respectively) in case-I compared to case-II (2.4 and 1.34 m/s) and case-III (2.9 and 1.57m/s). The maximum air temperature inside the setup is higher in case-II (322 K) compared to case-I (312 K) and case-III (318 K). Turbulent kinetic energy, power produced and overall efficiency of the setup were the best in case-II than other two models. Hence, it is suggested that case-II is better to choose.

Based up on theoretical and numerical analyses, a small scale SUT power plant was built at National institute of technology, Warangal, India. Appropriate location, dimensions of each component, selection of materials for different components and a detailed procedure followed during the fabrication of SUT plant are explained in this research work. The setup was constructed based on locally available materials. Velocity, pressure and temperature were measured at various locations inside the setup. Performance parameters of SUT plant were estimated. The maximum air velocity at a location below and above turbine was 4.7 and 5.5 m/s and the average was 2.18 and 2.98 m/s, respectively. The maximum pressure drop of 4 N/m^2 was noticed across the wind turbine. The theoretical and actual power outputs were 1.37 and 0.82 W, respectively. Chimney and overall plant efficiencies were estimated and these were 0.0187 % and 0.0128 %, respectively. Electrical power output from the system was estimated and based on that a list was made to power household devices. Uncertainty analysis was performed for all the observed and estimated parameters. The setup designed is enough to produce electrical power and therefore, the trial was successful. Finally, a comparison was made between theoretical, numerical and experimental results and found a good agreement.

Table of Contents

List of Figures

List of Tables

Nomenclature

a	Axial interference factor
a’	Tangential interference factor
A, B, and C	Constants (or) Coefficients
A	Surface area, (m^2)
A.P	Absorber plate
CB	Chimney base
C_m	Mass specific heat, (kJ/kg K)
C_v	Volumetric specific heat, (MJ/m^3 K)
c	Chord length of turbine blade, (m)
C_p	Specific heat of the air, (kJ/kg K)
C_L	Coefficient of lift
C_D	Coefficient of drag
dTa	Tangential force, (N)
dTh	Thrust force, (N)
dr	Blade segment thickness, (m)
D	Diameter, (m)
D_Y	The day of the year
E	Radiant energy, (W)
dF_L	Lift force, (N)
dF_D	Drag force, (N)
g	Acceleration due to gravity, (m/s^2)
H	Height, (m)
h_s	Hour angle, (°)
h_w	Wind loss coefficient, (W/m^2K)
h_L	Linearized radiation coefficient, (W/m^2-K)
h_c	Convective heat transfer coefficient, (W/m^2-K)
I	Solar radiation (or) heat flux, (W/m^2)
I_{bn}	Incident beam of flux, (W/m^2)
C_g	Glass extinction coefficient (m^{-1})
k	Turbulent kinetic energy, (m^2/s^2)

K	Thermal conductivity of air, (W/m-K)
L	Latitude, (°) (or) distance between absorber plate and collector, (m)
m_r	Mass of the material, (kg)
m	Mass flow rate, (kg/s)
n_1	Refractive index of medium 1
n_2	Refractive index of medium 2
N	Number of turbine blades
p	Pressure, (N/m^2)
P	Power output, (W)
Q_L	Rate of energy loss, (W)
Q_U	Useful energy available, (W)
Qa	Heat transfer rate of air, (W)
Q	Volumetric flow rate of air, (m^3/s)
r	Radius of blade segment from the hub, (m) (or) tilt factor
$\vec{r}$	Position vector
R	Radius, (m)
Ra	Rayleigh number
R_1	Resistance between the collector and absorber plate, (K/W)
R_2	Collector resistance, (K/W)
$\vec{s}$	Direction vector
SUT	Solar updraft tower
T	Temperature, (°C)
TKE	Turbulent kinetic energy, (m^2/s^2)
TES	Thermal energy storage material
U_t	Overall heat loss coefficient, ($W/m^2.K$)
u	Blade velocity, (m/s)
v	velocity, (m/s)
V	Volume, (m^3)
V_1	Upstream velocity, (m/s)
V_2	Air velocity at rotor upwind side, (m/s)
V_3	Air velocity at rotor upwind side, (m/s)

V_4	Downstream velocity, (m/s)
W	Relative wind speed, (m/s)
Z	Solar zenith angle, (°)

Greek Symbols

α	Angle of attack, (°) (or) absorptivity (or) Thermal diffusivity (m^2/s)
β	Turbine blade pitch angle, (°) (or) Coefficient of thermal expansion
γ	Surface azimuthal angle, (°)
Ø	Wind flow angle, (°)
γ_∞	Lapse rates of atmospheric temperature, (K/m)
η	Efficiency, (%)
ξ	Collector slope angle, (°)
δ	Solar declination, (°)
δ_c	Glass cover thickness, (m)
ε	Emmittance, (or) turbulent dissipation rate, (m^2/s^3)
υ	Kinematic viscosity of air, (m^2/s)
ρ	Reflectivity
ρ_a	Density of the air, (kg/m^3)
Δ	Difference
σ	Stephan-Boltzmann constant, ($W/m^2 K^4$)
θ	Solar incident angle, (°)
θ_1	Angle of incidence, (°)
θ_s	Central angle of sector, (°)
τ	Transmissivity of the collector cover
μ	Dynamic viscosity, (Pa-s)
$\tau\alpha$	Transmissivity absorptivity product
ω	Rotational speed of the turbine, (rpm)
ω_s	Hour angle, (°)
ω_{st}	The hour angle at sunset and sunrise, (°)
$d\Omega'$	Solid angle, (sr)
λ	Wave length, (m)

δ_k	Turbulent Prandtl number for k
δ_ε	Turbulent Prandtl number for ε

Subscripts

a	ambient air
act	actual
A	absorber plate
b	beam
c	collector
ch	chimney
d	diffuse
g	glass transition
G	global
h	hot air
m	glass melting
max	maximum
o	overall
R.C	required collector
s	scattering
SKY	sky
th	theoretical

Chapter 1

Introduction and Literature Review

Chapter 1

1. Introduction, Motivation, Solar power generating technologies

In past few decades, a greater amount of carbon dioxide, carbon monoxide and other dangerous gases were released in to atmosphere by direct or indirect human activities. These results in increase of earth temperature and also make a remarkable and harmful effects on environment. Investigations have been carried out by researchers saving the environment using alternative energy sources, especially by consuming natural green energy [1]. Moreover, utilization of sustainable energy sources expands consistently. Among the various sources of energy, solar energy is a most appropriate and cleanest source that can provide a noteworthy amount of energy for various applications while it is the most abundant. Furthermore, the price of sustainable power source accessories has been decreased constantly during past few years, for example a 60% reduction in a solar panel cost since 2011 [2].

The working fluids (or) any other receiving devices which can convert the solar energy in to electric power eventually by means of few ways are generally referred to as solar power generation technologies. Presently, there are two categories of solar power generation technologies.

1) Solar energy $\xrightarrow{\text{Convert}}$ Thermal energy $\xrightarrow{\text{Convert}}$ Electrical energy

In the first kind, the solar radiation converts in to heat, followed by a specific power generation method which converts the thermal energy in to electrical energy. Some of the examples are thermo electric power generation (semiconductor or metallic materials), thermionic power generation (vacuum devices), alkali metal thermal power generation, MHD power generation and so on. The technologies, including solar central power tower technology, parabolic trough solar thermal technology and dish solar thermal technology uses flowing work mediums to convert the solar energy in to thermal energy and then drive the generator by heat engine to convert the heat energy of the medium in to electricity [2].

2) Solar energy $\xrightarrow{\text{Convert}}$ Electrical energy

In the second kind of power generation, the solar energy directly converts in to electric power. Some of the examples are, light induction power generation, photochemical power generation, and biological power generation. In the photovoltaic power generation, the solar energy transforms in to electric power by means of solar battery and is successfully commercialized in nowadays [2]. The solar updraft tower (SUT) is one of the solar power generating technologies which comes under in first category of its kind.

2. Concept of solar updraft tower

Solar updraft tower (SUT) is one of the choices among the various solar technologies for producing power. The idea of SUT technology was initially proposed by Schaich in 1978 [3]. In SUT, the solar radiant energy comes from the sun is converted into electric power with the help of a turbine. It commonly comprises three sections: a solar collector, which absorbs the solar heat flux; a tall tower is called solar chimney which is situated at the centre of the solar collector; final component is wind turbine which is placed at chimney base (CB). The line diagram of a SUT is shown in **Fig. 1.1.**

In a sunny day, solar radiation from the sun falls on the surface of collector cover where a part of energy is reflected back to atmosphere, some amount of energy is absorbed by cover and remains fraction of the energy is transmitted through collector cover and is absorbed by an absorber plate. The air which is near the absorber plate region is heated by greenhouse effect and therefore, the density of air is lowered inside the setup and CB. Hence, the high dense outside air enters into the setup and there is a natural air flow inside the setup. By natural convection mechanism, the heat transfer takes place from hot ground surface to the adjacent air which causes the temperature rise. Now the hot air moves up due to buoyancy effect and enters the solar chimney where heat energy in air gets converted to kinetic energy. The pressure difference between the chimney base and the atmospheric air at the chimney outlet creates the air flow. This pressure difference can be utilized to propel the solar wind turbine which in turn rotates the generator for power generation.

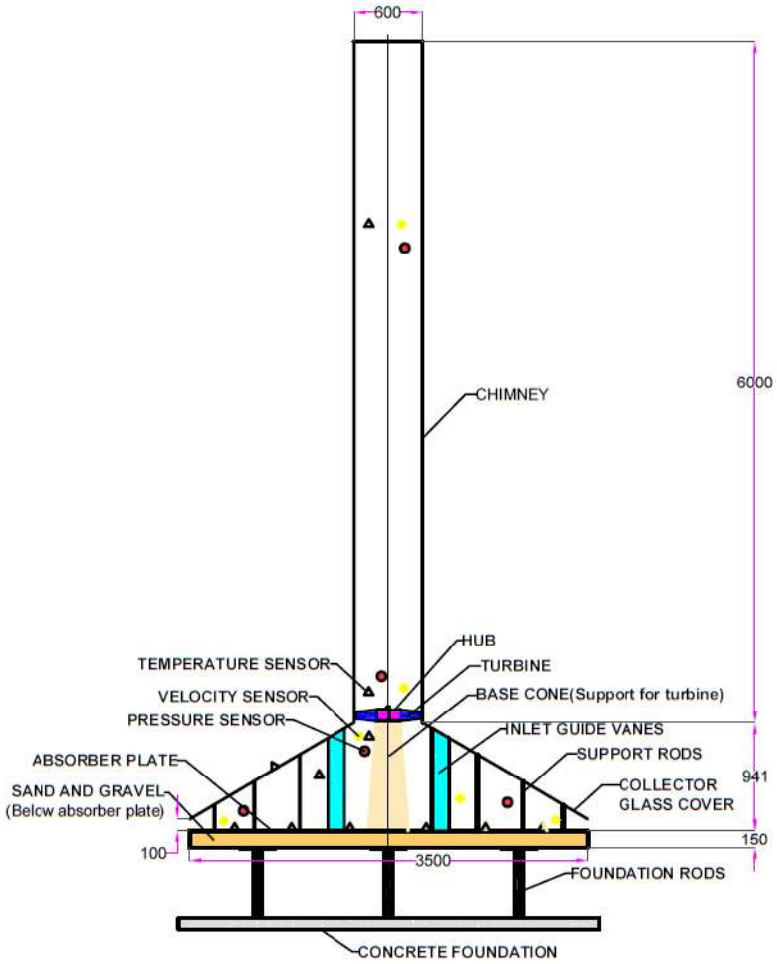

Fig. 1.1. Line diagram of solar updraft tower (SUT) power plant (All dimensions are in mm)

It has various favourable circumstances as it doesn't demand cooling water, no igniting fuel is required and need only a little maintenance. Apart from that, it has some more advantages than other types of solar power generating technologies such as,

- It is easier to design
- Need only simple materials which are easily available in local market
- Operational reliability is high
- No environmental contamination
- Higher operational life time
- Continuous steady running of the plant
- Power generation cost is low

It has very few running components.

3. Literature review

A number of studies noticed in literature on SUT power plant. A 3D CFD model was developed by Kasaeian et al. [4] to describe the fluid flow behaviour through turbine blade of SUT plant. They predicted the effect of angular speed of turbine blade (ω), number of blades, diameter of the collector (D_c) and height of the chimney (H_{ch}) on various thermodynamic parameters such as exit wind velocity, wind mass flow rate through turbine, torque generation and power output. They concluded that air flow rate and electricity production were increased with the increase of H_{ch} and D_c. A 5-blade wind turbine gave much power of approximately 91 kW at a shaft speed of 100 rpm.

A small experimental model was established by Ayadi et al. [5] to bring out the influence of H_{ch} on air flow characteristics inside SUT. Also, CFD simulations were carried out and validated with experimental findings. Finally they came to an agreement that H_{ch} was a crucial parameter to influence the heat transfer characteristics of air inside SUT. Similar study was executed by Ayadi et al. [6]'s another work to examine the impact of collector roof angle on SUT system performance. The various process parameters such as air velocity, temperature, pressure and solar radiation were measured and discussed for different collector roof slope angles.

Tingzhen et al. [7] developed a sophisticated mathematical model which described the complete physical process and estimated the performance of SUT plant. Various performance parameters such as relative static pressure, temperature distribution, power generation and efficiency of the system have been investigated. They concluded that the driving force, maximum power output and efficiency were not only depends on H_{ch} but also depends on solar radiation and other geometric dimensions.

Some studies investigated the design of various collector canopy profiles to get better performance of the system. Steady state mathematical model was formulated by Cottam et al. [8] to analyse the actual physical process of collector very precisely. They suggested that a collector canopy profile with partial slope which minimized various losses such as collector heat loss, heat loss to the ground, heat loss through the chimney wall, pressure loss due to

friction, power losses and recirculation losses. Authors came to a conclusion that segmented canopy profile gave better power output than the flat collector canopy profiles. Sensible thermal energy storage (TES) system (water bags) was used by Bernardes and Zhou [9] to test the enhancement in heat exchange between TES system and working fluid (air). They concluded that the water bags having more thickness were much suitable to enhance the heat transfer behaviour. A comprehensive mathematical model of SUT was developed by Petela [12] to describe the methodology of energy and exergy analysis applied to SUT plant. Using energy balance equations and exergy analysis, the solar flux distributions inside the setup was studied.

The plant efficiency was improved by enhancing the heat transfer coefficient of absorber plate with the help of utilization of corona wind flow [13] which is generated by electrostatic forces linked to corona discharge arising at the tips of some sharp conductors subjected to high voltage to the ground. It was an electro hydrodynamic phenomenon. Heat transfer rate and wind velocity have been increased about 14.5% and 72%, respectively with the application of voltage 15 kV across the setup wire (act as anode) and absorber plate (act as cathode) of experimental setup.

The performance of solar chimney system was assessed by Koonsrisuk and Chitsomboon [14] with the change of fluid flow area. Different types of configurations of collector and chimney such as slopped collector, divergent and convergent chimneys have been investigated. Authors concluded that the ratio of slopped collector roof and divergent chimney must be 16:1 to get more power generation (400 times more than the conventional SUT system).A simple analytical model was developed by Koonsrisuk et al. [15] in order to outline the constructional theory of geometry of SUT. The ratio of height to radius, air flow rate and optimum power output were determined under the constant area of the plant. Finally they concluded that electricity production per unit area was directly proportional to the length scale of the system.

Excess air updraft was created inside SUT system with the help of waste heated water (temperature in between 70 to 100 °C) for enhancing the power generation [16]. They also investigated the effect of various process parameters such as hot water temperature, atmospheric temperature and heat transfer area on the performance of SUT system. They reported that the velocity of air increased up to 8 m/s with the increase of inflow water

temperature from 50 to100°C. The maximum energy conversion efficiency was 0.76% when the temperature of water reached to 100 °C. An unsteady and streamlined model of SUT was proposed by Li et al. [17] to develop correlations between geometric dimensions of system and the power quality factor. By using this factor, they analysed the quality of power generation rate in terms of generation efficiency and power stability. Also they suggested that the optimal thickness of 2m TES layer for a specific plant which has the dimensions of 200m H_{ch} and 368m D_c.

A sensitivity analysis was carried out by Shirvan et al. [18] to acquire the maximum power production from the system. They proved that the maximum power was obtained at zero roof orientation angles. Okoye and Taylan [19] evaluated the performance of SUT by simulating the problem with the hourly weather data of seven specifically chosen regions. They developed an analytical model which was used to predict the electricity generation rate, cost of electricity and carbon emissions. Sustainability assessment showed that the system had great socio-economic and environmental benefits.

A novel design was made by Chan et al. [20] by creating the forced updraft wind inside the chimney with the aid of an air blower. Based on thermodynamic processes, a theoretical model of SUT was developed to examine the force updraft of the system. It is found that the maximum updraft air velocity of 45 m/s was reported when H_{ch} was increased from 15 to 150 m. Sophisticated theoretical and numerical models were developed by Gholamalizadeh and Mansouri [21] to assess the functioning of SUT plant in Kerman, Iran. They introduced a new coefficient called altitude effectiveness for evaluating the impact of site altitude on the performance of SUT. They reported that the power output (P) of plant which was located at 3600 m above the sea level was 9.7% less than the power output of plant at mean sea level.

Maghrebi et al. [22] introduced a new analytical model which described the fluid flow inside the SUT and also predicted the power output of the system. They had chosen five specific regions across the Persian Gulf (in between Iran and Arabian Peninsula) for the investigation. They found that the system can generate power in between 2.98 and 5.91 MW in the selected places on various months of the year 2016.

Zuo et al. [23] introduced a hybrid SUT system for fresh water production and electricity generation. It was reported that fresh water generation and P of plant were possible with an amount of 9.805 ton/h and 46 kW, respectively. Annual power capacity of the conventional

and sloped SUT plants under consideration of maximum solar radiation and maximum power generation was investigated numerically by Cao et al. [24]. The total accumulated power generation of plant was estimated at different collector angles and these ranged up to 8000 MW-h.

The influence of strong atmospheric winds in Orkney Islands, Scotland on the overall performance of SUT was numerically studied by Jafarifar et al. [25]. They reported that ambient cross winds impacted air velocity (15% increase) and efficiency of plant (50% increase). The numerical results were validated with real data of Manzanares plant, Spain. Hassan et al. [26] carried out a numerical study to identify the effect of θ_{cp} and chimney diverging angle on the performance of SUT. The computational results showed that air velocity and temperature increased to a remarkable value of 9.05, 9.34, 9.46 and 9.75 m/s and 316 K, 320 K, 321 K and 323 K when θ_{cp} = 4°, 6°, 8° and 10°, respectively.

The performance of SUT with turbine fan model was investigated numerically (ANSYS FLUENT 16.0) by Rabehi et al. [27]. They estimated the temperature distribution, air velocity, air pressure, pressure drop across the turbine and power output of the system by varying turbine speed. They reported that when the turbine speed was increased, the air pressure and temperature increased, but the air velocity decreased because of drag force generated by the turbine.

The performance assessment of SUT plant was made numerically by Huang et al. [28] using two methods, namely: solar ray trace (SRT) model and discrete ordinates (DO) model. They used ANSYS FLUENT 14.0 package to solve the problem. Ground temperature distributions and collector efficiencies were estimated. The influence of the roughness shape of collector plate, such as triangular, curved and square grooves on the performance of the plant was examined by Elwekeel et al. [29]. They concluded that the air velocity increased 1.5 times with triangular roughness over a plane collector surface at a constant radiation flux of 1000 W/m^2. The enhancement of power output of triangular, curved and square roughnesses were 169%, 96% and 19%, respectively, over plane collector surface.

A simple and more sophisticated cost model was developed by Cottam et al. [30] to predict the optimum configurations of large scale SUT plant in terms of power output per cost. They found that the maximum pressure drop ratio mainly depends on collector and chimney radius

but not on the H_{ch}. Finally they came to a conclusion that it is more beneficial to construct several small SUT's (which are having a collector radius about 3000 m) than the large scale plant. Economically, taller solar chimneys are much beneficial unless until the specific chimney prices enhance more than quadratically with height.

Bouabidi et al. [31] examined the effect of different chimney configurations (such as standard, convergent, divergent and opposing chimney) on the performance of SUT by numerically and experimentally. The results showed that various shapes of chimney definitely affect the behaviour of air velocity inside the canopy. The maximum air velocity is obtained in the case of divergent configuration.

The effect of water vapour film condensate (presents on top and bottom surfaces of collector canopy) on the SUT system performance was assessed by Al-Kayiem et al [32]. It is observed that the presence of condensate film on surface of canopy can reduce the hydrothermal performance of SUT by two ways: by reducing the transmittance of solar heat flux and by absorbing heat from water vapour particles to evaporate.
Asnaghi et al. [33] developed a numerical model for SUT and estimated the velocity and temperature distribution of air. ANSYS FLUENT was used to solve this numerical problem. They found that the chimney diameter of 244 m SUT can generate 25.3 to 43.2 MW power on different months of a year.

A pilot sloped SUT power plant was built by Kalash et al. [34] to investigate the temperature distribution and velocity fluctuations inside the collector. This study concluded that any variation of solar radiation directly impacts the collector outlet temperature and the absorber layer also releases heat to surrounding air immediately when solar radiation starts to decrease in the afternoon. Ghalamchi et al. [35] found the effect of geometrical parameters and climatic effects on the performance of solar chimney power achieved a maximum at an air velocity of 1.3 m/sec and when the temperature difference between ambient and chimney inlet reached to 26.3°C. They recorded and analyzed the temperature distribution and velocity of the air inside the experimental setup.

Optimised process parameters have been achieved by Ghalamchi et al. [36] using experiments in prototype solar chimney power plant. Temperature distribution and air

velocities were reported and compared with different geometrical parameters and collector materials. The optimized dimensions of the system were; H_{ch} = 3 m, D_{ch} = 0.1 m and collector entrance height = 0.06 m. The maximum air velocity obtained was 1.7 m/s and also the maximum air temperature difference between inside and outside of the system was 27°C.

A turbulent numerical model was developed by Sangi et al. [37] for estimating the velocity, temperature and pressure distribution of air inside the chimney. Two distinctive CFD numerical simulations were carried out to examine the fluid flow characteristics of a large scale SUT plant in Manzanares, Spain. Velocity, temperature and pressure distribution of air inside SUT were plotted for three different solar heat fluxes such as 200 W/m^2, 600 W/m^2 and 1000 W/m^2. A mathematical model of SUT was also developed to describe the overall physical process happening inside the system. The predicted values were compared with experimental results and were found good agreement. They proved that 20 K temperature difference between inside and outside air created the air velocity of 15 m/s near the turbine region which was enough to run the wind turbine. Mohiuddin and Uzgoren [38] initiated a CFD model to assess the effect of various geometrical parameters on the vertical flow (swirl flow) of the solar chimney. Parametric study revealed the values of optimum vane width and height. Vertical stability of the device and torque strength was found to increase at vane angles greater than 30°.

The physical process of the solar updraft tower was analysed by Zhou et al. [39]. The temperature distribution inside the collector was measured and the temperature difference between inside and outside the collector was determined. Similarly, the temperature distribution and maximum velocity of air were recorded and analyzed with the help of a reduced scale solar updraft tower by Kasaien et al. [40]. They achieved a maximum temperature difference between inside and outside the collector of about 25°C and a maximum air velocity of 3 m/sec inside the chimney.

The effect of the geometrical parameters of SUT power plant on fluid flow was discussed with the help of numerical and experimental methodologies by Kasaeian et al. [41]. The numerical results of model were compared with the experimental data of a small scale SUT plant (has the dimensions of H_{ch} = 2 m, D_{ch} = 0.2 m and D_c = 6 m) which was built at University of Tehran. The obtained results between the numerical and experimental were

good and comparable. They concluded that the D_{ch} had greater influence on inside air properties than H_{ch}. It is observed that the geometrical dimensions of H_{ch} = 3 m, D_{ch} = 0.3 m and collector entrance height = 0.06 m were the best possible conditions for optimum design of a solar chimney. The maximum air velocity and temperature inside the setup under this optimised design condition were 1.621 m/s and 232.6 K, respectively.

Computational fluid dynamics technology was used to predict the fluid flow behaviour and heat transfer characteristics of real solar updraft tower system by Gholamalizade and Chung [42]. A reverse fan model was used to analyse the temperature, velocity and pressure distributions across the turbine and the study found that it cannot exactly predict the pressure distribution near and through the turbine because of pressure jump across the turbine was 43.7% lower than the system coupled with a real turbine. Dynamic similarity between prototype and its models while using same heat flux was performed by Koonsrisuk and Chitsomboon [43]. They concluded that for achieving the same heat flux, the roof radius between the large scale and its modeled scale should be different and all other geometric parameters of small scale models were similar to prototype. Finally the authors proposed a condition of partial similarity between the prototype and its small scaled models and also validated the same condition by scaling the earlier numerical solutions of fluid flow.

Shiv Lal et al. [44] found the energy and exergy efficiencies of SUT by numerical and experimental techniques. They achieved energy and exergy efficiencies of 3.5% and 8% respectively. They evaluated the effect of the H_{ch}, inlet temperature and solar radiation on the performance of solar chimney power plant. Maximum air temperature and velocity inside the collector zone and outside ambient temperature were noticed as 42.4°C, 12.2 m/s and 42 °C, respectively, at 14:00 h of a sunny day. It is also observed that the recorded maximum solar radiation was 820 W/m^2 at noon. During peak hours of a sunny day, the surface temperature of collector cover was 4 to 6 °C higher than that of air temperature inside the setup.

Schlaich et al. [45] presented the theory, practical experience and economy of SUT power plants. Initially a simplified theory of SUT was described. Finally various technical related problems and economic analysis for future upcoming SUT plants were discussed. The effect of low wind speeds on different turbine blade aerofoil structures was analysed and presented with the help of ANSYS FLUENT [46].

The physical process of a large scale SUT was evaluated by Pretorius and Kröger [47]. This work incorporated the new convective heat transfer coefficient correlation and found that the annual power output of the system reduced up to 11.7%. It was also found that the annual power output increases by 3.4 %by selecting better glass material for collector. Simulations were conducted and it was concluded that the results for energy storage materials such as lime stone and sand stone gave similar results to that obtained for granite.

Tian and Zhao [48] discussed the most recent growths and advancements in solar thermal energy applications. A brief review has been done over solar collectors and various thermal energy storage systems. They concluded that photovoltaic thermal collectors gave the best overall performance among the various non-concentrating type collectors. This work also suggested that the molten salts are the best choice for high temperature thermal energy storage applications because of their wide properties such as density, thermal conductivity and specific heat.

An experimental investigation was carried to check the functioning of a small scale solar tower turbine by von Backström and Gannon [49]. The inlet guide vanes provided in their setup were meant to enhance the pre-whirl of air which reduces the turbine exit kinetic energy at diffuser inlet. The turbine developed in the setup produced 85 to 90 % total-to-total efficiency and 87 to 90% total-to-static efficiency.

A mathematical model for SUT was developed by Gitan et al. [50] and they found the optimized slope angle of a tilted collector and also estimated the hourly solar radiation falls on collector. The mathematical model was compared with an experimental result and good agreement was noticed. Results showed that the SUT with 10° collector slope angle could produce higher electricity over the entire year. It is observed that the tilted solar collector had increased the total power productivity of the system by nearly 3.5 kW than the fixed solar collector. The maximum collector and overall efficiencies of system were, 51% and 0.165%, respectively.

A 3D numerical simulation of SUT plant was carried out by Guo et al. [51] by considering the real turbine, discrete ordinates (DO) radiation model, solar load model and a fan model in

to it. The performance of a turbine was investigated under different rotational speeds. The simulation results of SUT with a real turbine and a fan model were compared to examine the effectiveness of fan model in forecasting the performance of SUT. The results revealed that the fan model approach was the best suitable way to investigate the pressure drop across the turbine and updraft velocity in the chimney. The hourly variation of solar zenith angle was considered for simulation to predict the system performance accurately.

A divergent chimney was proposed for SUT power plant by Hu et al. [52]. A numerical model was developed with different configuration of divergent chimney with other variable parameters of area ratio and divergent angle. They concluded that the performance of the divergent chimney was much higher than the straight chimney. Similarly a mathematical model was developed for the performance analysis of SUT by Maghrebi et al. [53] for a sloped chimney. Various performance parameters such as mass flow rate, collector and system efficiencies of the system were investigated. They concluded that the SUT could produce the electric power in the range of 2.98 – 5.91 MW at selected locations of Iran during different months of a year.

A new solar chimney power plant (floating type) was proposed by Zhou and Yang [54] on barren mountains up to thousands of meters high in northwest China. Outcome of the research reveals that the overall efficiency of the plant is higher compared to conventional solar updraft tower due to larger chimney effect. This plant produced a total power of 25761 TWh per year, can fulfill some of the energy demand of whole world.

Some of the works shows that experimental analysis of wind flow inside the solar chimney. Various process parameters such as temperature, velocity, solar radiation and humidity (inside & outside) were monitored over a period of time, allowing the characterisation of the air flow and evaluation of the optical properties of the materials used. Because of higher thermal losses, a low value (< 5%) of total energy conversion efficiency was achieved [55].

A theoretical model was developed by Zhou et al. [56] to analyze the optimum H_{ch} of SUT to produce maximum electricity. The accuracy of this theoretical model was verified by estimating the optimum H_{ch} at different atmospheric pressure range from 90 kPa to 101.3 kPa. It is noticed that, if the H_{ch} was more than the optimum H_{ch} then negative buoyancy was

created at later part (inside) of the chimney. It came to a conclusion that the optimum H_{ch} was needed to produce maximum power output (102.2 kW) of a SUT was 615 m. The impact of several lapse rates of atmospheric temperatures (γ_{∞}) on optimum H_{ch} was examined. The maximum H_{ch} increases along the increase of γ and reaches to infinity at γ = 0.0098 K/m. Results revealed that construction of higher H_{ch} was possible only at places which have dry atmospheric conditions.

A numerical model was developed by Zxou et al. [57] to assess the physical process of a compressible flow through solar updraft tower. In this paper, CFD FLUENT6.1 software was used to analyse the 3D steady numerical simulation of air flow inside the solar chimney. Finite volume method, second order upwind scheme and SIMPLE algorithm techniques were used to discrete the 3D steady continuity, momentum and energy equations. Results of this 3D model were more accurate when compared to previous developed models such as Boussinesq model and full buoyancy model.

An elaborated experimental study was carried out by Ozgen et al. [58] in order to investigate the thermal performance of three categories of double flow solar air heaters having aluminium cans under different operating conditions. They concluded that the double flow air channels are more efficient than the single flow channel over or under the absorber plate. Similar studies have been performed with artificial neural networks (ANN), wavelet neural network (WNN) [59] and least squares support vector machine (LS-SVM) [60]. Finally it was concluded that WNN was an excellent method for prediction of thermal performance of the system. Similar investigation of greenhouse heating using various renewable energy sources under different climatic conditions was reported by Esen and Yuksel [61].

4. Conclusions from the literature review

From the literature review, it is observed that a couple of small scale models have been built up and investigated [5, 6, 13, 34-36, 39-40, 44, 55, 58, 61]. A real plant was set up by Haaf et al. [3] in 1984, but the plant collapsed after few years. Few studies concentrated on individual components of SUT such as wind turbine [4, 27, 42, 46, 49], TES system [9, 47-48], solar collector [6, 8, 14, 28-29, 47-48, 50] and solar chimney [5, 10, 14, 52]. A lot of studies concentrated on analytical models to analyse SUT system in detail [7, 8, 11, 12, 15, 17, 20-22, 30, 45, 50, 53-54, 56, 59-60].

Remaining studies of SUT contributed based on numerical simulations [4-6, 9-10, 14, 16, 18-19, 21, 23-28, 31, 37-38, 41-44, 47, 51-52, 57]. Few studies investigated [8, 14] the effect of inclined collector plate on SUT system. Few studies have examined the effect of geometrical dimensions of SUT [26, 31] and few on the effect of ambient conditions [23, 25]. Some studies of hybrid models explained water generation from SUT [23]. Many studies were explored by considering 2-D models [23, 25, 28-29, 31, 33], while some used 3-D numerical simulations [26, 27].

5. Literature gaps

Overall, this setup has been enormously reviewed, though there is a dearth of design parameters, as this setup involves a number of process and design parameters, such as turbine blade parameters, solar radiation parameters, quantity and selection of storage materials, materials for solar collector (cover and absorber plate).

- No performance and design details of SUT have been found for the main components such as solar collector, chimney, turbine etc.
- The solar input parameters have not been estimated for this specific application and subsequent energy losses also not found.
- Similarly, the materials needed for the above components have not been discussed.
- There is no solar energy storage facility found as the system has a huge area of solar collector.
- There is always a dearth of information about which position of collector and absorber plates give better flow and performance characteristics. The present numerical investigation analyses this fact by developing three different cases and predicting the parameters, so that better case can be identified.
- No studies have been reported on the overall design of the system and fabrication procedures.
- There are no real models, on measurements and estimating the power output of real systems.
- And also no detailed study has been carried out on a wind turbine of an SUT plant for electricity generation.

- There is no study reported on design procedures of wind turbine of an SUT plant. Also, no study was found on the estimation of the optimized blade angles of SUT plant.

6. Aim and objectives

Aim: To develop an SUT plant and estimate the flow and performance parameters.

The main objectives of the work are;

- To design the solar updraft tower (SUT) power plant with proper components, accessories and materials.
- To estimate theoretically the pressure loss, thermal radiation, heat losses and the performance parameters such as efficiency and power output of SUT plant.
- Numerical investigation of flow parameters and performance characteristics of different solar updraft tower models with a suggested model for better performance.
    1) Case-I: Inclined absorber plate and Inclined collector glass
    2) Case-II: Horizontal absorber plate and Inclined collector glass
    3) Case-III: Horizontal absorber plate and collector glass
- To develop a small scale experimental setup of SUT (with TES system and guide vanes) and to estimate the performance of SUT by doing experiments.
- To design and analyse the wind turbine of a SUT plant to get the optimized power output using blade element momentum (BEM) theory.

The objectives of the work are made by a step by step process as mentioned in the flowchart (**Fig. 1.2**).

7. Work Plan

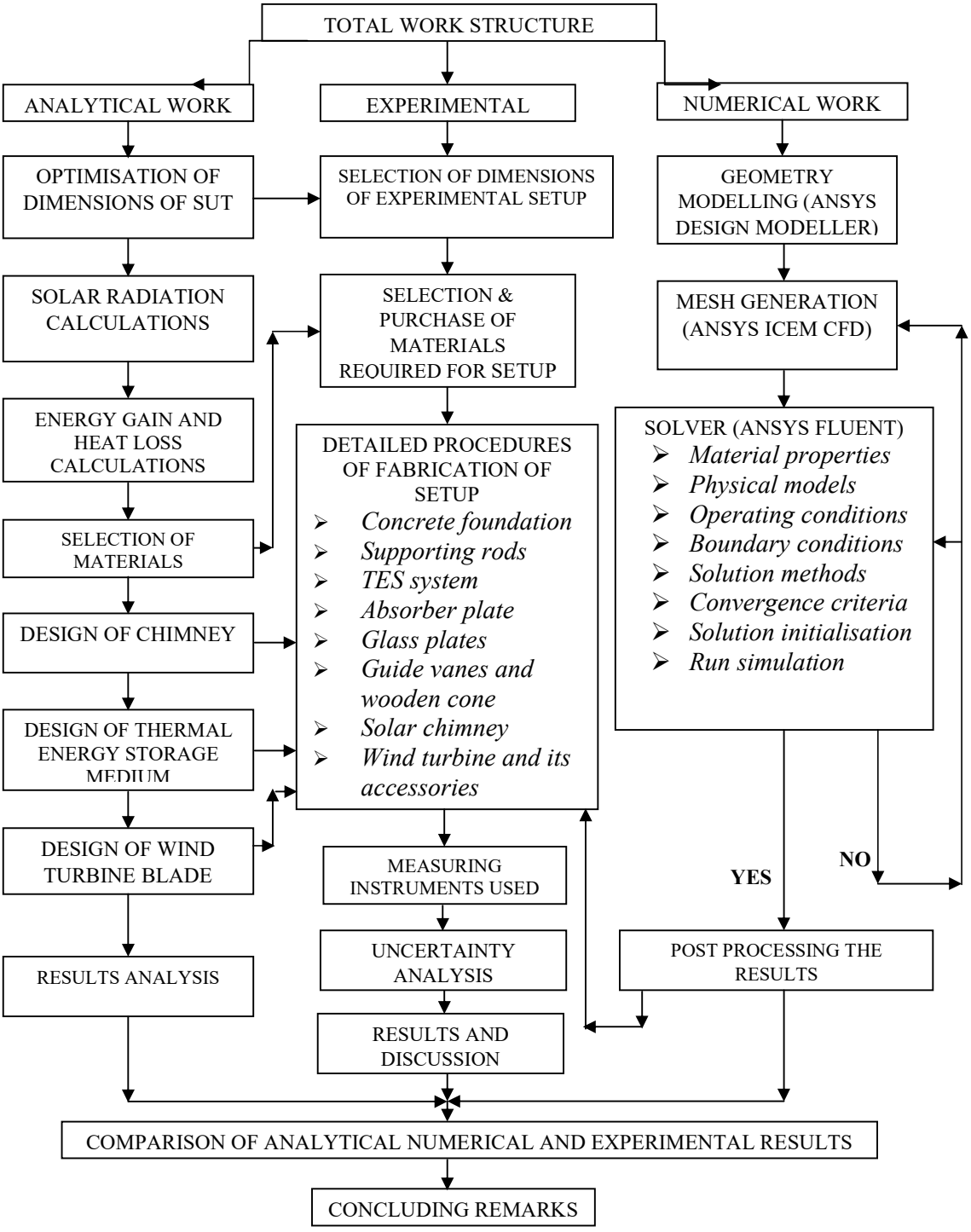

Fig. 1.2. Flowchart mentioning the total work

8. Organization of the thesis

The thesis is organized as follows:

The **first chapter** consists of an introduction cum literature part where the motivation and background of the work are discussed. Different types of solar power generating technologies are discussed and reasons behind the selection of SUT for the detailed analysis are also explained. Various types of literature such as analytical, numerical and experimental studies on SUT are reviewed. Later the important findings and conclusions from the literature review are given. Based on the literature review the objectives of the present studies are given. This chapter also provides the brief details of aim, objectives and work plan of the research work.

The second chapter discusses the methodology of the analytical, numerical work as well as experimental work. Material and method for small scale SUT experimental set-up are discussed. After that, the design and development of the experimental setup are explained in this section. Various instruments used for measuring different parameters are explained followed by the experimental procedure. For the numerical work, the selection of the software for simulation, different operating and geometrical parameters considered are discussed. The domain selection, mesh generation, boundary condition, solution method are discussed. Also the theoretical analysis for performance analysis of the SUT and its components (collector, chimney and turbine) is explained.

The third chapter is related to the results and discussion. Theoretical results obtained for design, development, materials selection of laboratory scale SUT and also for solar radiation calculations, energy gain and loss, collector efficiency, overall efficiency and power output of SUT system. Optimisation of the geometrical dimensions of SUT is explained. Optimisation of the design and performance parameters for various wind turbine blades of a SUT plant using Blade element momentum (BEM) theory is thoroughly clarified.

The fourth and fifth chapters are related to the results and discussion. Results obtained for heat transfer characteristics, flow and performance parameters from the numerical simulation are discussed first and the best shape (collector slope angle) and optimum dimensions of the final shape are finalized which is used for the development of the experimental set-up. After

that, the results and discussions are carried out for the experimental work where the performance of the SUT is estimated. Also, the variation of different parameters such as air velocity, pressure, temperature, mass and volumetric flow rates, relative total pressure (or) pressure drop across the turbine, global solar radiation falls on collector, rotational speed of turbine, temperature of absorber plate and thermal energy storage medium with time is explained. Uncertainty analysis is added in this chapter.

The sixth chapter discusses the conclusions from the numerical and experimental results. Also, the conclusions from the theoretical analysis are added here. The most suitable case for the numerical analysis, in order to find the optimum shape and orientation of the collector is mentioned. Later the overall conclusion of the work is mentioned. And finally, the future scope of the work is given in this chapter.

Chapter 2

Methodology

Chapter 2

2. Methodology

The second chapter discusses the methodology of the analytical, numerical work as well as experimental work. The theoretical analysis for performance analysis of the SUT and its components (collector, chimney and turbine) is explained. For the numerical work, the selection of the software for simulation, different operating and geometrical parameters considered are discussed. The domain selection, mesh generation, boundary condition, solution method are discussed. Also material and method for small scale SUT experimental set-up are discussed. After that, the design and development of the experimental setup are explained in this section. Various instruments used for measuring different parameters are explained followed by the experimental procedure.

2.1 Analytical methodology

The objective of this work is to investigate the performance of SUT and to tabulate all the inputs and estimated parameters with the materials of a SUT power plant. All the three main components' (turbine, solar collector and a chimney) process parameters are estimated and discussed. Appropriate materials are discussed and selected for solar collector, chimney, turbine and heat storage materials. Solar beam, diffuse and global radiation are estimated to analyze the performance of collector cover. Energy losses in solar collector cover and transmissivity estimations are performed to calculate theoretical energy collected in solar collector. Pressure drop inside the chimney is estimated and from that the actual power output of the turbine is calculated. The quantity of heat storage materials needed is evaluated in terms of both mass and volume.

Before going in to design, certain assumptions have to be made for this analysis,

1) Axisymmetric air flow in the collector inlet, that is, non uniform heating of the collector surface in terms of the sun's altitude angle is neglected.
2) Constant environment conditions including ambient temperature and inlet air temperature.
3) Heat losses through the wall of the chimney are neglected.
4) The air follows the ideal gas law.
5) Only the buoyancy force is considered in the chimney.

The setup consists of solar collectors, chimney and an electricity generating turbine as shown in **Fig. 1.1.** The components of the SUT are described below deeply,

2.1.1. Solar air collector

The solar collector plays the important role like heat exchanger which converts the incident solar radiation into useful stored energy in the air. There are essentially two sorts of stationary solar collectors: non-concentrating or stationary and concentrating. A non-concentrating collector has a similar range for capturing and for engrossing solar radiation, though a sun-following concentrating collector has parabolic reflecting surfaces to catch and centre the sun's radiation to a shorter getting region, along these lines expanding the radiation flux. SUT comes under the category of non-concentrating type collector [62].

2.1.1.1 Selection of material

Solar air collector which comprises of the accompanying two main segments is transparent glazing cover and absorbing plate. Different types of the radiation collector cover materials are available and choice of material mostly depends on the transmittance-absorbance ($\tau\alpha$) value, nature and covering of material, sunlight falling angle and cover extinction coefficient. Polymer covers and plastic sheets additionally have high shortwave transmittance range and they receive long wave transmittances as eminent as 0.40. Plastics are additionally by and large restricted in the temperatures they can manage without crumbling or experiencing dimensional changes. Just a couple sorts of plastics can withstand the sun's bright ultraviolet radiation for longer periods [62].

Anti refluxing glazed glass is chosen as collector cover material because of it can transmit as much as 90% of the approaching shortwave sun irradiance while transmitting for all wavelengths. Glass with low iron content has a moderately high transmittance for sun radiation (roughly 0.85–0.91 at typical rate). Normal incidence transmittance values of commercially available Plexi and window glasses are 0.85 and 0.87 respectively. Likewise, the collector glass is tempered to the modern standard which can stand again different climate conditions and most hails or storms. **Table 2.1** gives the transmittance of materials for solar collector cover.

Table 2.1: Solar collectors cover materials [62]

Material	Transmittance
Anti-refluxing glazed glass	0.85 - 0.9
Window glass	0.87
Greenhouse glass	0.85
Polycarbonate	0.844
Fiber glass reinforced polyester	0.831
Corrugated fiber glass	0.78 - 0.79

The objective of the absorber plate is to receive (or) absorb as much solar radiation as is radiated through glazed glass plate. The hot absorber plate transfers the heat to adjacent air, and thus the air is heated. Thermo-physical properties and price details of different absorber plate materials are listed in **Table 2.2**. From **Table 2.2**, it is identified that copper has higher thermal conductivity (393.5 W/m.K) and density (8900 kg/m^3), therefore, its heat capacity is more compared to other materials. The price of copper material is higher than aluminium, brass or steel, but lower than bronze, but its heat capacity is much more compared to all other materials. Therefore, copper was selected as absorber plate materials.

Table 2.2: Properties of absorber plate material [63]

Material	Thermal conductivity (W/m°C)	Density (kg/m^3)	Price (Rs/kg)
Aluminium	220	2700	200
Brass	130	8450	420
Bronze	67	8730	650
Copper	393.5	8900	550
Cast iron	54.5	7250	100
Steel	50.2	7850	210

2.1.1.2 Solar radiation calculations

With a specific end objective to estimate the beam and diffuse radiation on an inclined collector cover surface facing due south, it is very important to convert the estimation of beam flux coming from the origin of the sun to an equal esteem relating to the normal direction to the surface. If θ is the angle between an incident beam of flux (I_{bn}) and the normal to a plane surface, then the equivalent flux failing normal to the surface is given by

$I_{bn}\cos\theta$. The angle θ can be related by a general equation to the latitude (L), the slope (ξ), the declination (δ), and the hour angle (ω). The critical sun angles which are utilized as a part of calculations of the direct and diffuse radiations are shown in **Fig. 2.1.** The collectors ought to be situated specifically towards the equator, facing due south in the northern hemisphere and north in the southern hemisphere. For NIT Warangal, India the longitude is 79°35′ east and latitude (L) = 18°00′ north.

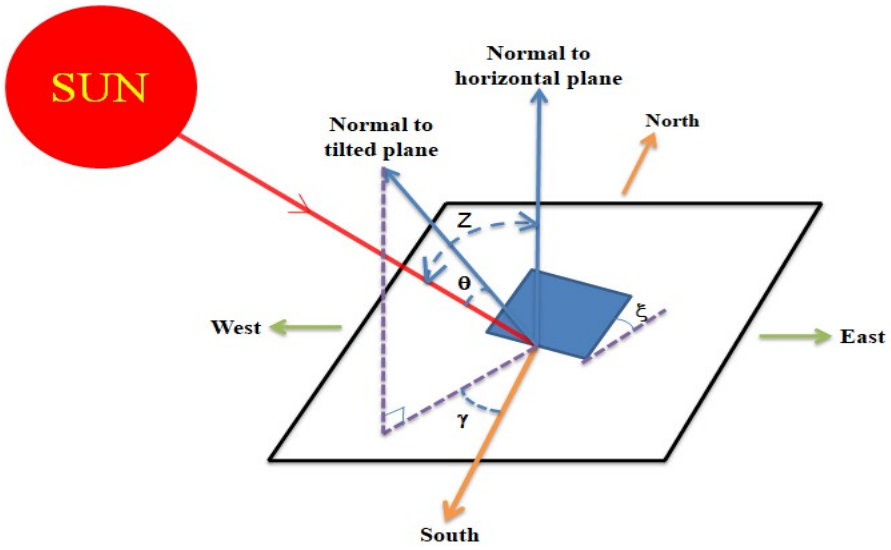

Fig. 2.1. Sun angles on collector surface

The instantaneous hour angles are calculated during day time at sixty minutes of intervals from sunset to sunrise at NIT Warangal, India. These calculated hour angles are used to determine the angle of incidence (θ) and solar zenith angle (Z) on each side of the collector. The direct (or) beam radiation (I_b) and diffuse radiation (I_d) at each interval are calculated from the angle of incidence (θ), zenith angle (Z), tilt factors for both beam and diffuse radiation (r_b and r_d). From the angle of incidence and the calculated beam radiation, the energy transmitted through the glass cover is determined by using Snell's law. The net energy transmitted through the glass cover is the sum of the transmitted beam radiation and the diffuse radiation.

2.1.1.3 Estimation of beam, diffuse and global radiations

The declination (δ) is the angle made by the line joining the centers of the sun and the earth with the projection of this line on the equatorial plane. The declination angle varies from a maximum value of +23.45° on June 21 to a minimum value of -23.45° on December 21. It is zero on the two equinox days of March 21 and September 22.

The solar declination angle (δ) [64] is estimated as,

$$\delta = 23.45 \sin\left[\frac{360(D_Y+284)}{365}\right] \quad (2.1)$$

Where, D_Y is day of the year.

The hour angle (ω_s) is an angular measure of time and is equivalent to 15° per hour. It also varies from -180° to +180°. We adopt the convention of measuring it from noon based on local apparent time (LAT), being positive in the morning and negative in the afternoon.

The hour angle corresponding to sunrise or sunset (ω_{st}) on an inclined surface facing due south (γ=0°) [64], $\omega_{st} = \cos^{-1}[-\tan\delta \tan(L-\xi)]$ (2.2)

Sunrise time: $T_{sunrise} = \frac{\left[\left(-\omega_{st}\left(\frac{60}{15}\right)\right)+720\right]}{60}$ (2.3)

Sunset time: $T_{sunset} = \frac{\left[\left(\omega_{st}\left(\frac{60}{15}\right)\right)+720\right]}{60}$ (2.4)

Here, the time is mentioned as a fraction of an hour instead of hours and minutes and γ is surface azimuthal angle.

The ω_s at any instant during day time is estimated [64],

$$\omega_s = \pm\frac{360^0\ (solar\ time-12)}{24\ hours} \quad (2.5)$$

The ω_s is negative before solar noon and positive after solar noon.

Solar incident angle (θ) on an inclined surface facing due south (γ=0°) [64],

$$\cos\theta = \sin\delta \sin(L-\xi) + \cos\delta \cos\omega_s \cos(L-\xi) \quad (2.6)$$

Solar zenith angle (Z) is estimated from, $\cos Z = \sin\delta \sin L + \cos\delta \cos\omega \cos L$ (2.7)

Where, ξ is the collector slope angle and γ=0° for south facing collector at the northern hemisphere.

ASHRAE [65] has given a method for estimating the hourly global and diffuse radiation falling on horizontal surfaces under cloudless skies (clear days). The equations are based on an exponential decay model in which the beam radiation decreases with increase in the distance traversed through the atmosphere. The global radiation (I_G) reaching a horizontal surface on the earth is given by Sukhatme and Nayak [64],

$$I_G = I_b + I_d \quad (2.8)$$

Where, I_G is hourly global radiation, I_b is hourly beam radiation and I_d is hourly diffuse radiation.

Now, $I_b = I_{bn}\cos Z$ (2.9)

Where, I_{bn} is beam radiation in the direction of the rays.

Thus, $I_G = I_{bn} \cos Z + I_d$ (2.10)

In the ASHRAE model [65], it is postulated that $I_{bn} = A\, e^{\left[-\left(\frac{B}{\cos Z}\right)\right]}$ (2.11)

and diffuse radiation, $I_d = C I_{bn}$ (2.12)

Where, A, B and C are constants whose values have been determined on a month wise basis. These constants change during the year because of seasonal changes in the dust and water vapor content of the atmosphere and also because of the changing earth sun distance. The values of A, B and C were initially given by Threlkeld and Jordan [65] and subsequently revised by Iqbal [66].

The solar collector selected for this analysis is a sloped collector which is tilted at an angle to the horizontal. It therefore becomes necessary to calculate the flux which falls on a tilted surface. Tilt factors should be considered for beam and diffuse radiation calculations. The tilt factor for beam radiation is r_b.

$$r_b = \frac{cos\theta}{\cos Z} = \frac{sin\delta \sin(L-\xi)+cos\delta\ cos\omega \cos(L-\xi)}{sin\delta \sin L+cos\ \ cos\omega \cos L} \quad (2.13)$$

Where, Cosθ is beam radiation flux falling on a tilted surface and CosZ is beam radiation flux falling on a horizontal surface.

The tilt factor r_d for diffuse radiation is the ratio of the diffuse radiation flux falling on the tilted surface to that falling on a horizontal surface. The value of the tilt factor depends up on the distribution of diffuse radiation over the sky and on the portion of the sky dome seen by the tilted surface. Assuming that the sky is an isotropic source of diffuse radiation, we have for a tilted surface with a slope (ξ), $r_d = \frac{1+\cos\xi}{2}$ (2.14)

Since $\frac{1+\cos\xi}{2}$ is the radiation shape factor for a tilted surface with respect to the sky.

Now the beam (or) direct radiation falls on tilted surface is calculated from,

$$I_b = A\,(\cos\theta) e^{\left[-\left(\frac{B}{\cos Z}\right)\right]} \quad (2.15)$$

Similarly the diffuse radiation falls on tilted surface is calculated from,

$$I_d = C I_{bn}\left[\frac{1+\cos\xi}{2}\right] \quad (2.16)$$

The global radiation I_G reaching a sloped (or) tilted surface on the earth is given by [64]

$$I_G = I_{beam} + I_{diffuse} = A\,(\cos\theta) e^{\left[-\left(\frac{B}{\cos Z}\right)\right]} + C I_{bn}\left[\frac{1+\cos\xi}{2}\right] \quad (2.17)$$

2.1.1.4 Energy losses

In this section the energy lost in solar collector cover material due to reflection and heat losses is estimated and discussed.

2.1.1.5 Energy lost due to reflection on collector cover material

When a beam of light travelling through a transparent medium 1 strikes the interface separating it from another transparent medium 2, it is reflected and refracted. The reflected beam has a reduced intensity and has a direction such that the angle of reflection is equal to the angle of incidence (shown in **Fig. 2.2**). On the other hand, the directions of incident and refracted beams are related to each other by Snell's law which states that [64],

$$\text{Angle of refraction, } \theta_2 = \sin^{-1}\left[\frac{\sin\theta_1}{\left(\frac{n_2}{n_1}\right)}\right] \tag{2.18}$$

Where, θ_1 =Angle of incidence, n_1 = refractive index of medium 1, n_2 = refractive index of medium 2.

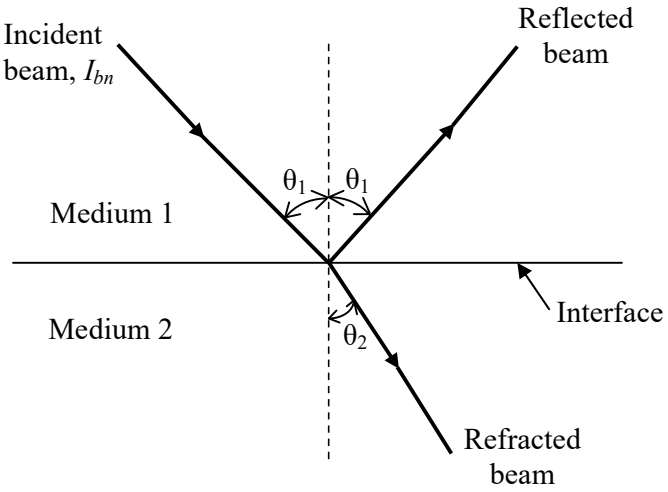

Fig. 2.2. Refraction and reflection at the interface of two mediums

The reflectivity of incident beam (ρ) is given by [64];

$$\rho = \frac{\rho_1+\rho_2}{2} \tag{2.19}$$

Where, ρ_1 and ρ_2 being the reflectivity's of the two components of polarisation [64].

$$\rho_1 = \left(\frac{\sin^2(\theta_2-\theta_1)}{\sin^2(\theta_2+\theta_1)}\right) \tag{2.20}$$

$$\rho_2 = \left(\frac{\tan^2(\theta_2-\theta_1)}{\tan^2(\theta_2+\theta_1)}\right) \tag{2.21}$$

For beam radiation, the transmissivity of the collector cover can be obtained with adequate accuracy by considering reflection-refraction and absorption separately and is given by [64],

$$\tau = \tau_a \tau_r \tag{2.22}$$

Where, τ_r is transmissivity obtained by considering only reflection and refraction and τ_a is transmissivity obtained by considering only absorption.

$$\tau_r = \frac{1}{2}(\tau_{r1} + \tau_{r2}) \tag{2.23}$$

Where, τ_{r1} and τ_{r2} being the transmissivity of the two components of polarisation.

$$\tau_{r1} = \frac{1-\rho_1}{1+\rho_1} \quad (2.24)$$

$$\tau_{r1} = \frac{1-\rho_2}{1+\rho_2} \quad (2.25)$$

Transmissivity obtained by absorption [62], $\tau_a = e^{-C_g \delta_c / cosZ}$ (2.26)

Where, C_g is glass extinction coefficient (m^{-1}) and δ_c is glass cover thickness (m). The net transmissivity of the collector cover material is given by Eq. (2.22). For diffuse radiation, the angle of incidence is taken to be 60°. Therefore, angle of refraction can be estimated from Eq. (2.18), the transmissivity of collector cover is estimated from Eq. (2.22).

Out of the fraction τ transmitted through the cover system, a part is absorbed and a part reflected diffusively. Out of the reflected part, a portion is transmitted through the collector cover and a portion is reflected back to the absorber plate. The process of absorption and reflection at the absorber plate surface goes on indefinitely, the quantities involved being successively smaller. Transmissivity absorptivity product ($\tau\alpha$) indicates that the amount of flux absorbed in the absorber plate with respect to the flux incident on the collector cover.

Transmissivity absorptivity product for beam radiation, $(\tau\alpha)_b = \frac{\tau\alpha}{[1-(1-\alpha)\rho_d]}$ (2.27)

Transmissivity absorptivity product for diffuse radiation, $(\tau\alpha)_d = \frac{\tau\alpha}{[1-(1-\alpha)\rho_d]}$ (2.28)

Where, α is absorptivity of absorber plate and ρ_d is diffuse reflectivity of the collector cover,

$$\rho_d = (\tau_a - \tau_d) \quad (2.29)$$

The net global radiation absorbed per m^2 area of the absorber plate [64] is;

$$I_{A.P} = [(\mathrm{I_b})(\tau\alpha)_\mathrm{b}] + [(I_d)(\tau\alpha)_\mathrm{d}] \quad (2.30)$$

The total surface area of the collector cover is given by:

$$A_c = 4\left(\frac{\pi}{360}\right)\theta_s\,(r/\cos 30)^2 \quad (2.31)$$

Where, r is radius of the collector cover and θ_s is central angle of sector (90^0).

The theoretical radiant energy transmitted through collector cover, $E_{th} = (A_c)(I_G)$ (2.32)

The total incident flux absorbed by the absorber plate, $E_{A.P} = (A_{A.P})(I_{A.P})$ (2.33)

Average sunshine hours available on 21st October 2016, (h_s) = 7.3

The total theoretical energy absorbed by plate on 21st October 2016; $E_A = E_{A.P} h_s$ (2.34)

2.1.1.6 Heat losses

The radiative and convective heat transfer coefficients between the collector cover and the absorber plate are determined to give the resistance between the collector cover and the

absorber plate. The linearized radiative exchange with the sky and wind related losses are determined to evaluate the collector resistance. The collector resistance and the resistance between the collector cover and absorber plate are used to determine the top loss coefficient. From the top loss coefficient, the rate of energy loss per m^2 of collector base area is determined. Useful energy is calculated as the difference between the energy transmitted through the collector and the heat losses. The linearized radiation coefficient is given by Maghrebiet al. [53]:

$$h_L = \frac{\sigma(T_A+T_C)(T_A{}^2+T_C{}^2)}{(\frac{1}{\varepsilon_A}+\frac{1}{\varepsilon_C}-1)} \quad (2.35)$$

Where, σ is Stephan-Boltzmann constant, T_A is absorber plate temperature, T_c is collector cover temperature, ε_A is absorber plate emissivity, ε_c is collector cover emissivity. The collector absorber plate temperature is considered as 80°C and the ambient temperature is 30°C.

The collector cover temperature is chosen as 35°C (i.e. between the ambient and the absorber plate temperatures). The convective heat transfer coefficient h_c [67] is given by,

$$h_c = (0.06 - 0.017)\left(\frac{s}{90}\right) kL\sqrt[3]{\left(\frac{g\Delta T}{T_A \vartheta^2}\right)} \quad (2.36)$$

Where, K is the thermal conductivity of air, L is the distance between the absorber plate and the collector, υ is kinematic viscosity of air, ΔT is temperature difference between plate and air. All the input parameters needed for estimation of heat losses are mentioned in **Table 2.3.**

Resistance between the collector and absorber plate is, $R_1 = \frac{1}{h_L+h_C}$ (2.37)

Wind loss coefficient [64] is given by: $h_w = 5.7 + (3.8\ \mathrm{v})$ (2.38)

Where, v is average wind speed at 1m height in NIT Warangal, India conditions.

Sky temperature is, $T_{SKY} = (0.0552)(T_a)^{\frac{3}{2}}$ (2.39)

The radiative heat transfer coefficient [64] referenced to the air temperature can be estimated from, $h_r = \sigma\epsilon_c\left(T_C + T_{Sky}\right)\left(T_C{}^2 + T_{Sky}{}^2\right)\left[\frac{T_C - T_{Sky}}{T_C - T_a}\right]$ (2.40)

Collector resistance is given by, $R_2 = \frac{1}{h_r+h_W}$ (2.41)

Therefore, the overall loss coefficient can be estimated from,

$$U_t = \frac{1}{R_1+R_2} \quad (2.42)$$

The rate of energy loss is estimated as,

$$Q_L = U_t A_c(T_A - T_a) \quad (2.43)$$

Useful energy available, $Q_U = E_{A.P} - Q_L$ (2.44)

Energy lost per day can be calculated based on the rate of energy loss per hour of a day (7.3 h) and it is, $E_{lost} = h_s Q_L$. (2.45)

The useful energy available during sunshine hours in a day per m^2 of base area,

$E = E_A - E_{lost}$ (2.46)

The efficiency of the collector is, $\eta_c = \frac{Q_U}{E_{th}}$ (2.47)

Table 2.3: Input parameters of heat loss calculation

Given Data	Value
Ambient air temperature, (T_a)	30°C
Absorber plate temperature, (T_A)	80°C
Collector cover temperature, (T_c)	35 °C
Plate emissivity, (ε_A)	0.8
Collector emissivity, (ε_g)	0.9
Stephan-Boltzmann constant, (σ)	5.6 x 10^{-8} W/m^2K^4
Thermal conductivity of air, (K)	0.026 W/m.K
Distance between plate and collector, (L)	0.06 m
kinematic viscosity of air, (υ)	1.5 x 10^{-5} m^2/s
Temperature difference between absorber plate and ambient air, (ΔT)	50 °C
Average wind speed, (v)	2.0 m/s

2.1.2. Solar chimney (or) tower

It is somewhat difficult to find materials for solar chimney. The chimney material should be weather resistant, having light weight, strong in structure, withstand wind and overall loading conditions. The thermal properties and availability of several materials were considered, such as Nylon 66, polycarbonate pipes, polyethylene, polypropylene, polyester, Poly tetra fluroethylene and polyvinylchloride (PVC). **Table 2.4** provides the list of possible chimney materials and their properties. Among the various materials available, the polycarbonate material is selected as chimney material and it can withstand air temperatures of up to 150°C.

Table 2.4: Chimney materials and properties [68]

Thermosetting Plastic Material	T_g (°C)	T_m (°C)	Thermal Conductivity (W/m.K)	Density (kg/m^3)	Specific heat (kJ/kg.K)
Polyvinylchloride (rigid PVC)	87	212	0.14 – 0.28	1467	0.9
Nylon 6,6	100	265	0.24 - 0.3	1140	0.0017
Polycarbonate	150	265	0.19 – 0.22	1200	1.17
Polyester	73	265	-	1370	1.3 – 1.5
Polyethylene	-90	137	-	970	1.25
Polypropylene	-14	176	-	905	1.92
Poly tetra fluroethylene	-90	327	0.25	2200	1.172

With no wind turbine inside the chimney the maximum air velocity [45] is,

$$\mathrm{v}_{max} = \sqrt{2gH_{ch}\left(1 - \frac{T_a}{T_h}\right)} \quad (2.48)$$

Where, g is acceleration due to gravity and T_h is temperature of hot air inside the collector.

Area of the chimney is: $A_{ch} = \left(\frac{\pi}{4}\right) D_{Ch}^2$ (2.49)

The mass flow rate of air is: $m_a = \rho_a \mathrm{v}_{max} A_{ch}$ (2.50)

Where, ρ_a is density of air at chimney base.

Heat flow rate is given by: $Q_a = m_a C_p \Delta T$ (2.51)

Therefore energy required for 12 h operation is,

$$E_{ch} = 12\ Q_a \quad (2.52)$$

Required collector base area is estimated based on the energy required for 12 h and it is,

$$A_{R.C} = \frac{E_{ch}}{E_A} \quad (2.53)$$

Pressure difference between chimney base and surroundings [56] is estimated from,

$$\Delta p = 0.00353\ gH_{ch}\left\{\left(\frac{\pi I_G \eta_c R_c^2}{C_p m_a}\right) - \left(\frac{gH_{ch}}{2C_p}\right) + \left(\frac{\gamma_\infty H_{ch}}{2}\right)\right\} \quad (2.54)$$

Where, γ_∞ is lapse rate of atmospheric temperature.

Volumetric flow rate of air through the chimney [45] is,

$$Q = \mathrm{v}_{max} A_{ch} \quad (2.55)$$

The maximum theoretical power output of SUT system [45] is:

$P_t = (\Delta P)Q$ (2.56)

Chimney efficiency [45] is, $\eta_{ch} = \frac{P_{Total}}{Q_a} = \frac{gH_{ch}}{C_p T}$ (2.57)

The overall efficiency (η_o) of the plant [56] can be calculated from, $\eta_o = \frac{P_{act}}{\pi I_G R_c^2}$ (2.58)

Where, $P_{act} = P_t \eta_t$, actual power output of the turbine, η_t is efficiency of the turbine and R_c is collector radius.

2.1.3. Energy storage materials

In this section, the thermal energy storage (TES) materials are discussed and appropriate materials are selected. TES materials which can store thermal energy in day time and release heat to the surrounding working fluid (air) at night i.e. when there is no solar energy. Therefore, the SUT plant can work even after sunset, so that electrical energy can be generated after sunset. TES materials were placed below the copper absorber plates.

2.3.1.1 Thermal Energy Storage

There are three significant features that are essentially considered for making the design of a solar thermal energy storage system: technical characteristics, price effectiveness and effect on environment. An important element when considering the technical feasibility of a solar thermal energy storage system is a system that shows superior technical properties. The thermal storage capacity should be on the higher side in order to reduce the total volume occupied by the system and to improve the efficiency of the system. Secondly, the rate of heat transfer between the storage material and transfer fluid (air) must be high for the release (or) absorb the thermal energy at uniform speed. Thirdly, the storage material should possess excellent stability to prevent mechanical and chemical deterioration after a finite number of periodic thermal cycles.

2.3.1.2 Sensible heat storage materials

Thermal energy is accumulated in the storage media while there is an increase (or) decrease of temperatures in sensible heat storage processes. **Table 2.5** gives the important properties of solid state thermal energy storage materials. These materials work between the temperature range of 200 to 1200°C. Materials such as fire bricks, sand-rock minerals and concrete have superior thermal conductivities varying from 1.0 to 7 W/m.K [70, 71]. The materials given in Table 9 are less price ranging from 3.35 to 334 Rupees/kg (0.05 US$/kg –

5.00 US$/kg). The main advantage of a sensible thermal energy storage is in low price when compared with the price of latent heat storage materials which normally ranges from 286 to 22310 Rupees/kg (4.186 US$/kg – 326 US$/kg).

Table 2.5: Solid state sensible heat storage materials [48, 72]

Energy storage material	Density (kg/m^3)	Mass Specific Heat (kJ/kg.K)	Volumetric Specific Heat ($MJ/m^3.K$)	Total Mass of the material required, (kg)	Total volume occupied by material, (m^3)	Total price, (INR)
Sand-rock minerals	1700	1.30	2.21	7743.7	4.56	
Reinforced concrete	2200	0.85	1.87	11843.3	5.38	
Cast iron	7200	0.56	4.03	17976.4	2.5	
Cast steel	7800	0.60	4.68	16778	2.15	
Silica fire bricks	1820	1.00	1.82	10066.8	5.53	
Magnesia fire bricks	3000	1.15	3.45	8753.7	2.92	
Dry bricks	1800	0.84	1.51	11984.2	6.66	28285
Soil (gravelly)	2040	1.84	3.75	5471.1	2.68	
Soil (clay)	1450	0.88	1.28	11439.5	7.89	
Rocks	2800	1.18	3.3	8531.2	3.05	25594
Sand (dry)	1602	0.84	1.35	11984.3	7.48	27564
Sand and gravel	1922	1.18	2.27	8531.2	4.44	12797

Among the above mentioned solid state thermal energy storage materials, the sand rock minerals (1.3 kJ/kg.K), magnesia fire bricks (1.15 kJ/kg.K) and soil gravelly (1.84 kJ/kg.K) have large mass specific heat capacities. Cast iron and steel have the highest thermal conductivity (37 to 40 W/m.K) as well as highest volumetric specific heats (4.03 to 4.68 $MJ/m^3.K$) when compared to other storage materials. But in cost point of view, the price of cast iron and steel are more and huge far away from other materials. Sand and gravel have better thermo physical characteristics at a lower cost. Therefore these materials are selected as thermal energy storage materials for making solar chimney power plant. Thermal energy can be stored cheaply in sand and gravel, where the stored energy is given by,

$E_t = m_r C_m \Delta T$(When using the mass specific heat) or (2.59)

$E_t = V C_V \Delta T$(When using the volumetric specific heat) (2.60)

Consider temperature difference as 15°C.

The required energy, $E_t = 12\ Q_U$ (2.61)

Where C_m and C_v are mass and volumetric specific heat of material respectively.

Total mass of the rocks required, $m = \frac{E_t}{C_m \Delta T}$ (2.62)

Total volume of the rocks required: $V = \frac{E_t}{C_V \Delta T}$ (2.63)

The maximum thermal energy required for producing the power of 0.633 W was estimated as 80.64 kWh and it is happened in April 2016.

The stored energy is used for continuous operation during the nights and also for periods of overcast weather conditions.

These sand and gravel are placed in the space below the collector surface. The volume below the absorber plate is given by, $V_{av} = A_b h_g$ (2.64)

Where, A_b is base area $A_b = \left(\frac{\pi}{4}\right) {D_A}^2$ (2.65)

D_A is diameter of absorber plate = 3.5 m.

The height (h_g) of the ground is selected as 150 mm for providing the heat storage materials. The available volume is therefore, $V_{av} = 1.443\ m^3$.

2.1.4. Solar wind turbine

The purpose of this section is to design a wind turbine blade which operates under low speed conditions (2-5 m/s). In the process of design of turbine blade, the first and foremost step is to obtain best power performance by doing aerodynamic analysis of it. The key parameters which influence the blade design includes blade radius (R_B), number of blades (N), type of aerofoil, radial distribution of chord (c) and blade pitch angle (β). The turbine blade material selection and design part are explained in this section.

Wind turbines are devices which can pull out energy from air by applying aerodynamic terminology of lift and drag forces. These forces act on the turbine blade in perpendicular and parallel to the wind flow and these forces are helpful to rotate the blade so that kinetic wind energy is converted to rotational energy. After that the same rotational energy is converted to electrical power by means of a generator/alternator. Wind turbines are generally categorised into two groups on the basis of rotational axis about which it rotates. Horizontal axis turbine (HAT) is one in which the wind flow is parallel to the axis of turbine rotation (most commonly used). In vertical axis turbine (VAT), the wind flow is perpendicular to the axis of

turbine rotation (less frequently used). In the present study, the axis of rotation of turbine is parallel to wind flow i.e. HAT.

A simple model developed by Betz (1926) [73] can be utilized to estimate the electric power generation from an ideal wind turbine, various forces such as lift, drag and axial thrust forces and the effect of rotor blade operation on local wind field. This Betz model works on the principle of conservation of linear momentum theory which originated 100 years back to investigate the performance of ship propellers. In the Betz model [73], no rotation flow is added to the wind. Betz theory can be extrapolated up to a state where the rotating turbine blade produces angular momentum which is directly related to the rotor torque.

2.1.4.1 Schmitz model

For considering the rotational flow in the wind (which was not considered in Betz model [73]), Schmitz [73-74] introduced a small, detailed and advanced model for fluid flow behaviour in the rotor plane (**Fig. 2.3**). Conservation of angular momentum theory and theory of aerodynamic principles have been used to develop this theoretical model. In the case of a rotating wind turbine rotor, the flow behind the rotor rotates in the opposite direction to the rotor, in reaction to the torque exerted by the flow on the rotor. The generation of rotational kinetic energy in the wake results in less energy extraction by the rotor than would be expected without wake rotation. In general, the extra kinetic energy in the wind turbine wake is higher if the generated torque is higher. So that it can be concluded that slow running wind turbines (with a low rotational speed and a high torque) experience more wake rotational losses than high speed wind turbines with low torque.

Three sections are considered in the fluid flow Schmitz model. In **Fig. 2.3,** at the upstream section-1, the wind enters with a velocity V_1 but the turbine blade experiences with a relative wind velocity W at section-2 (rotor plane) and the same relative wind striking on a turbine blade includes two velocity components as mentioned in **Fig. 2.4,** namely, the tangential component of the blade u, which results because of the rotation of the blade in the rotor plane and the axial component of wind V_2 $[(1-a)V_1]$ which acts normal to the plane of rotation. Just before and after the rotor plane, the wind velocity is almost equal ($V_2=V_3$). In the downstream of the blade (section-4), the wind velocity is further reduced and is equal to the V_4 $[(1-2a)V_1]$. Axial interference factor (a) is defined as the ratio of velocity drop in control volume 1-2 (V_1-V_2) to the upstream wind velocity (V_1).

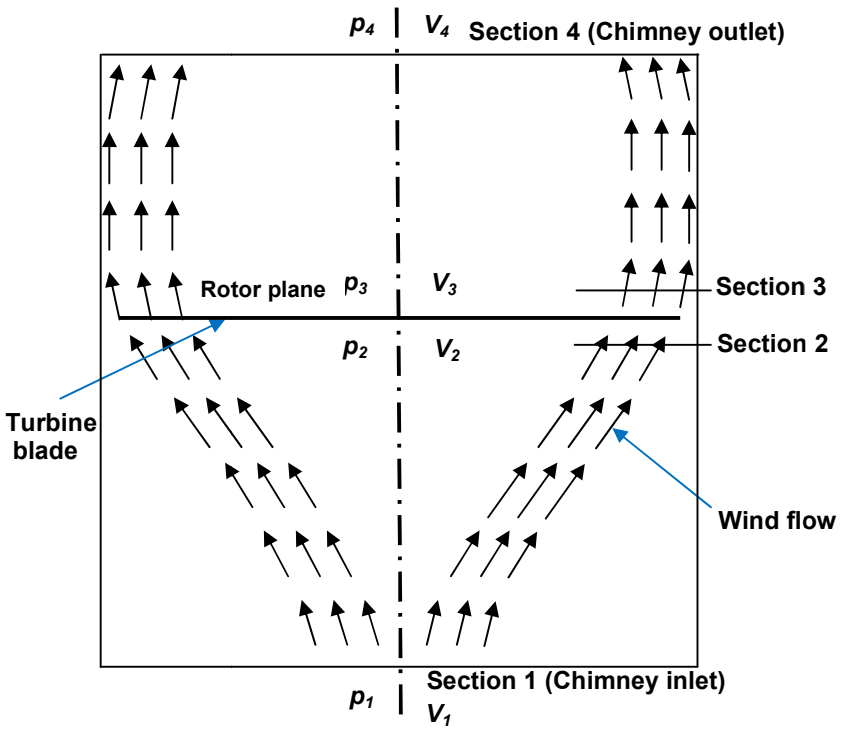

Fig. 2.3. Idealized fluid flow through wind turbine (V_1 – upstream wind, V_2 – air velocity at rotor upwind side, V_3- air velocity at rotor downwind side, V_4 - Downstream wind, p_a - air pressure at entry of control volume 1-2 and air pressure at exit of control volume 3-4, p_2 - air pressure at exit of control volume 1-2 and p_3 - air pressure at entry of control volume 3-4)

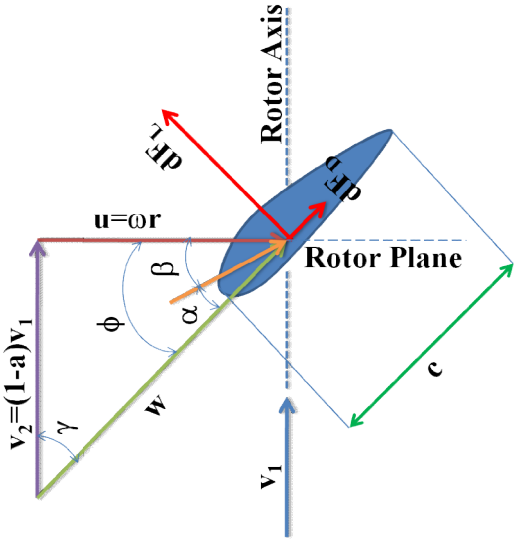

Fig. 2.4. Velocities and blade angles

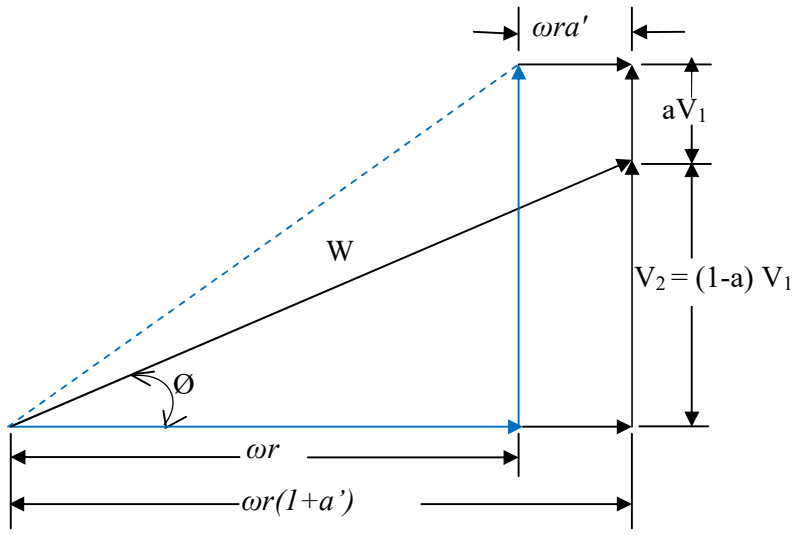

Fig. 2.5. Effect of wake flow at exit of turbine

Figure 2.4 presents the wind and blade velocities and the corresponding angles at a specified distance, *r*, from the rotor axis. In order to design the rotor blade, the β, angle of attack (α), angle of relative wind to rotor axis (γ), angle of relative wind to rotor plane (ϕ) and *c* of the blade should be defined. α is the angle between the blade chord line and the *W*. β is the angle between the blade chord line and plane of rotation. φ is the angle between plane of rotation and *W*.

The tangential blade velocity (u) in terms of the turbine angular velocity 'ω' and the distance 'r' from the turbine hub is expressed in Eq. (2.66) as

$$u = r\omega \tag{2.66}$$

The rotational flow (wake) acts continuously in the downstream section of the blade which causes to add some tangential velocity to the blade. Swirl (or) wake flow does not exist in the upstream section of the blade, so that there is no change in all upstream wind velocity (V_1), *W* and u. The wind strikes the blade with an angle of φ.

But in the plane of rotation, the blade experiences some rotational or wake flow. Conservation of angular momentum theory holds that the generation of the torque or twisting moment in the rotor shaft is possible only with the aid of swirl induction in the downstream flow of the rotor plane. The variation in the tangential velocity of the blade in rotor plane is exactly half of the total change in the rotor plane due to angular rotation of flow. Therefore, u can be written as

$$u = r\omega + \left(\frac{1}{2}\Delta u\right) \quad (2.67)$$

The supplementary tangential velocity of the blade [$\left(\frac{1}{2}\Delta u\right)$ term], is experienced because of wake rotation which can also be expressed in terms of tangential interference factor (*a'*).

$$u = r\omega(1 + a') \quad (2.68)$$

As per **Fig. 2.5,** it is noticed that a small increment in tangential velocity due to wake rotation of flow diminishes in axial wind velocity.

Blade element momentum theory helps to predict the various aerodynamic forces (lift, drag, thrust and tangential) act on turbine blade elements and also to find out the optimum *a* and *a'* for achieving maximum energy extraction from air.

2.1.4.2 Blade element momentum theory

The main objective of this section is to optimise the lift force which acts on the blade and to simultaneously minimise the drag force on it, which causes the force acts in tangential direction can be maximised. The wind turbine blade consists of different aerofoil which can generate lift by virtue of pressure difference between top and bottom surfaces of aerofoil. Momentum theory and blade element theory can help to do this aerodynamic analysis of blade. The results of these two approaches equate together and forms a new theory called blade element momentum (BEM) theory.

- Momentum theory: It refers to a control volume analysis of forces at the blade based on conservation of linear and angular momentum. With the help of this theory, one can estimate the total tangential force which is developed by the blade in the plane of rotation (**Fig. 2.6**) is

  $$dT_a = 4\pi r(dr)\rho V_1(1 - a)\omega r a' \quad (2.69)$$

  And also the total thrust force acted on the turbine by the wind in the axial direction is estimated as

  $$dT_h = 4\pi r(dr)\rho V_1^2(1 - a)a \quad (2.70)$$

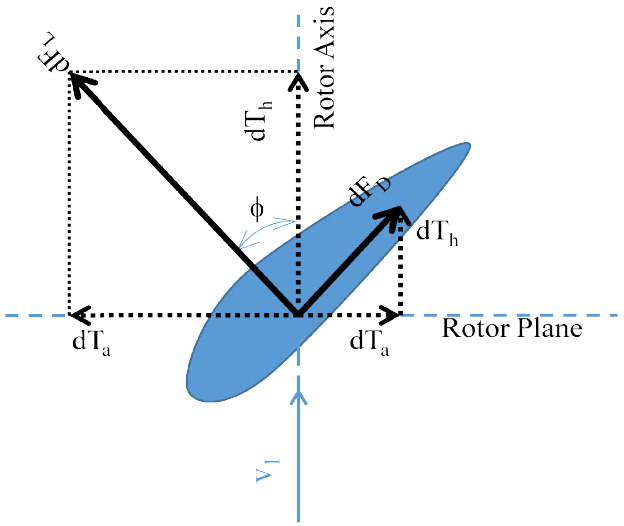

Fig. 2.6. Aerodynamic forces acts at each blade segment of turbine

- Blade element theory: It refers to an analysis of forces at a section of the blade, as a function of blade geometry. In this theory, the blade shown in **Figs. 2.7 and 2.8** is partitioned into a number of independent segments and at each rotation of rotor every segment sweeps an annular area. The elements are considered separately under the assumption that there is no interference between the radial flows in one blade element to its adjacent blade elements. Consider a blade segment (element) with the thickness of *dr* and chord length of *c* at a distance *r* from the axis of rotation.

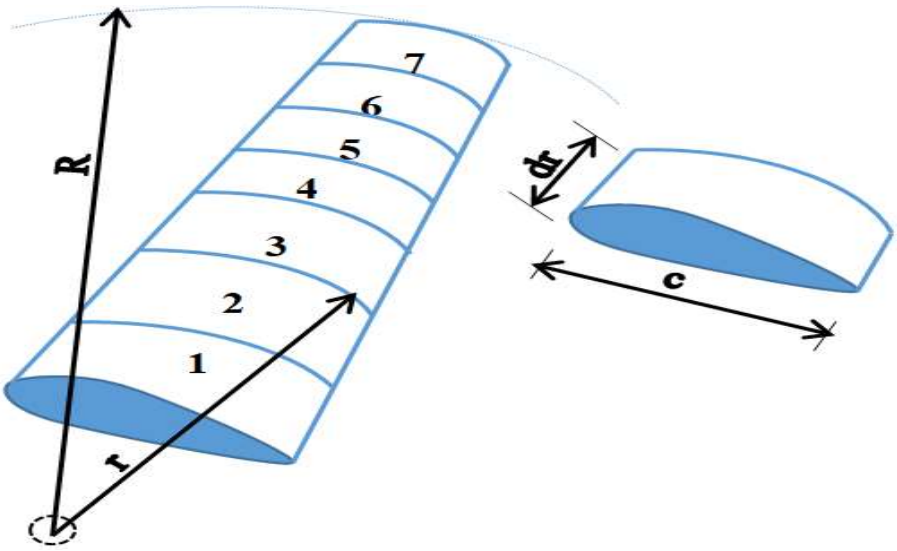

Fig. 2.7. Partition of blade in to number of segments

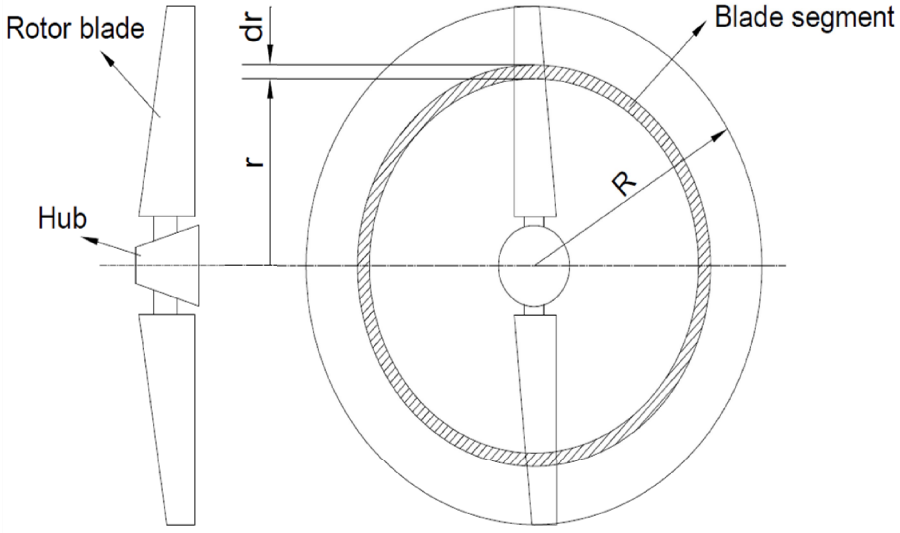

Fig. 2.8. Section of the rotor blade from top view.

After division of the rotor blade into segments, one calculates the power extraction from the wind and various forces acting on wind turbine blade, all of which depend on lift and drag coefficients and blade geometry (chord length and twist angles).

Lift force: $dF_L = \frac{1}{2}\rho w^2 C_L\, dr\, c$ (2.71)

Drag force: $dF_L = \frac{1}{2}\rho w^2 C_D\, dr\, c$ (2.72)

Using the geometric relations found in **Fig. 2.4,** the maximum power generation occurs at relative wind flow angle and it is represented as:

$$\varphi = \left(\frac{2}{3}\right) tan^{-1}\left(\frac{v_1}{\omega r}\right) \quad (2.73)$$

In order to find out the most beneficial relative wind angle with respect to plane of rotation, the α should be subtracted from φ. Then the maximum β can be achieved, which is given by the equation below:

$$\beta = \left(\frac{2}{3}\right) tan^{-1}\left(\frac{v_1}{\omega r}\right) - \alpha \quad (2.74)$$

Total tangential force developed by blade element:

$$dT_a = \frac{N[C_L \sin\emptyset - C_D \cos\emptyset]\rho c\, dr}{2}\left\{\frac{V_1(1-a)}{sin\emptyset}\right\}\left\{\frac{\omega r(1+a')}{\cos\emptyset}\right\} \quad (2.75)$$

The total thrust force acted on the blade element:

$$dT_h = \frac{N[C_L \cos\emptyset + C_D \sin\emptyset]\rho c\, dr}{2}\left\{\frac{V_1^2(1-a)^2}{sin^2\emptyset}\right\} \quad (2.76)$$

As per the BEM theory, the axial interference factor (a) is estimated by equating the Eqs. (2.70) & (2.76) and is,

$$a = \frac{1}{\left[\left\{\frac{8\pi r \sin^2 \emptyset}{(N[C_L \cos \emptyset + C_D \sin \emptyset]c)}\right\}+1\right]} \tag{2.77}$$

The tangential interference factor *a'* is estimated by equating the Eqs. (2.69) and (2.75) and is,

$$a' = \frac{1}{\left[\left\{\frac{8\pi r \sin \emptyset \cos \emptyset}{(N[C_L \sin \emptyset - C_D \cos \emptyset]c)}\right\}+1\right]} \tag{2.78}$$

The power (or) energy extraction rate from the air (or) wind at each segment of the blade is characterised by Eq. (2.79),

$$dP = dT_a\, \omega \tag{2.79}$$

Chord length at each segment of the blade is estimated using Eq. (2.80),

$$c = \left(\frac{1}{N}\right)\left(\frac{16\pi r}{C_L}\right) sin\left\{\frac{1}{3} tan^{-1}\left(\frac{v_1}{\omega r}\right)\right\} \tag{2.80}$$

Calculation procedure: The estimation of various aerodynamic forces and power output of wind turbine are made by a step by step process as mentioned in the flowchart (**Fig. 2.9**).

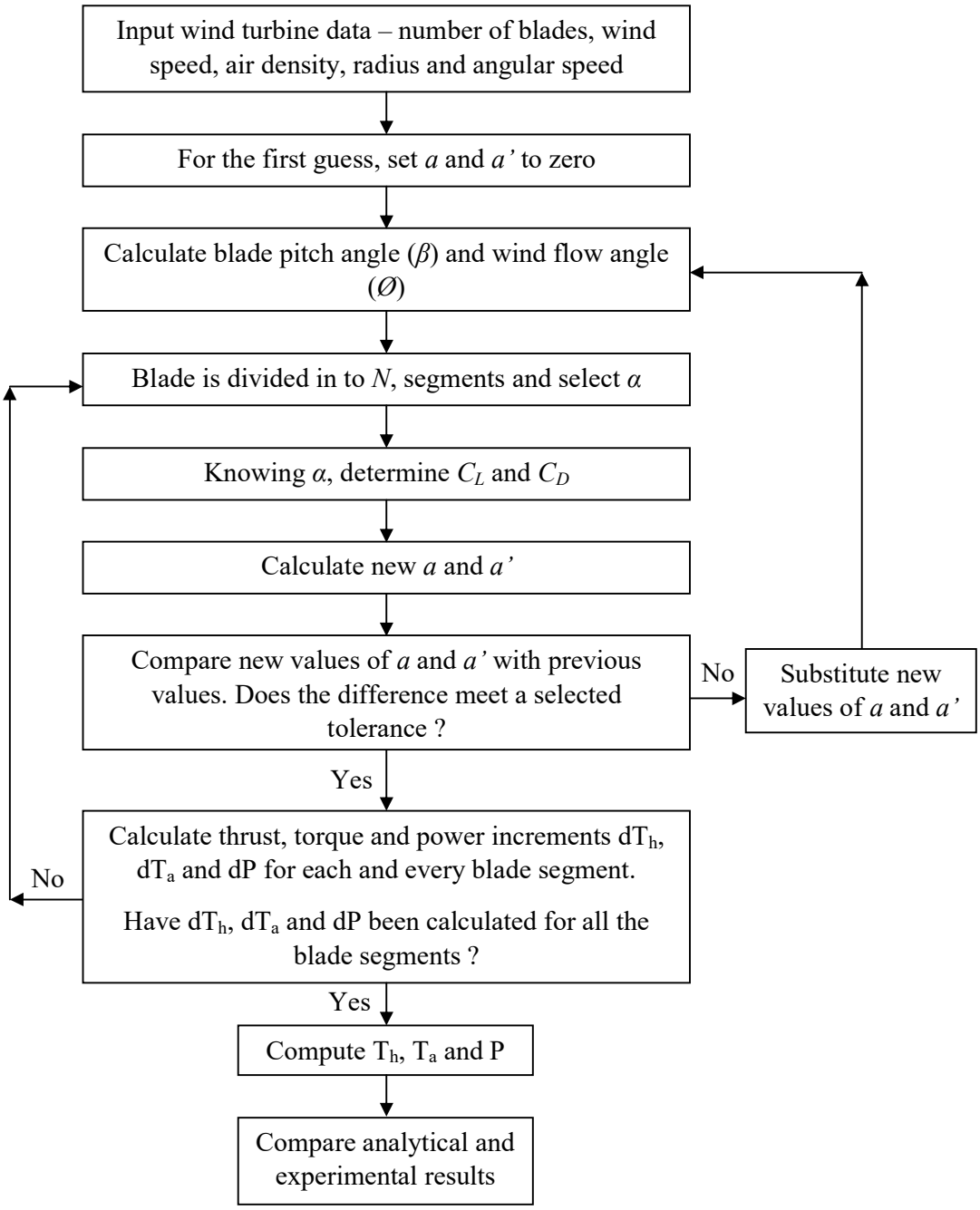

Fig. 2.9. Calculation procedure of power output of wind turbine.

2.2. Numerical methodology

The dimensions of D_{ch} = 0.6 m, D_c = 3.5 m and H_{ch} = 6 m were chosen for all the cases based on the theoretical model. A thickness of absorber plate was 1.5 mm. Thicknesses of chimney wall and collector cover were chosen as 5 mm each. The developed 3D models are mentioned in **Fig. 2.10. Fig. 2.10 (a)** shows the case-I (both inclined collector cover and absorber plates) with the inclination of 30°. **Fig. 2.10 (b)** shows the case-II (inclined collector and horizontal absorber plates) which was made with the collector inclination of 30°. **Fig. 2.10 (c)** shows the case-III (both collector and absorber plates were horizontal). The present numerical investigation analyses these three different models and predicting the parameters, so that a better model can be identified. These models were generated using ANSYS FLUENT 16.0 design modeller.

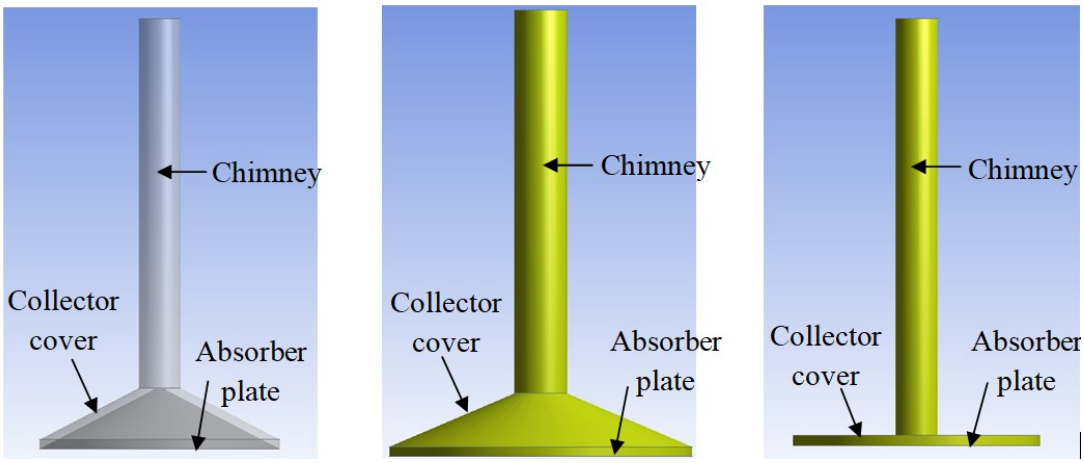

Fig. 2.10. Practical domain generated for (a) Case – I, (b) Case – II and (c) Case – III

2.2.1. Meshing

ANSYSFLUENT16.0 is used for mesh generation of all the three cases because of its capability to create eminent quality of structured and unstructured grid. A hexahedral meshing option is chosen for obtaining much precise solutions in the collector, absorber plate, chimney and fluid flow domain. **Figs. 2.11 (a), (b) and (c)** show the meshes created for case – I, case – II and case – III, respectively.

(a)

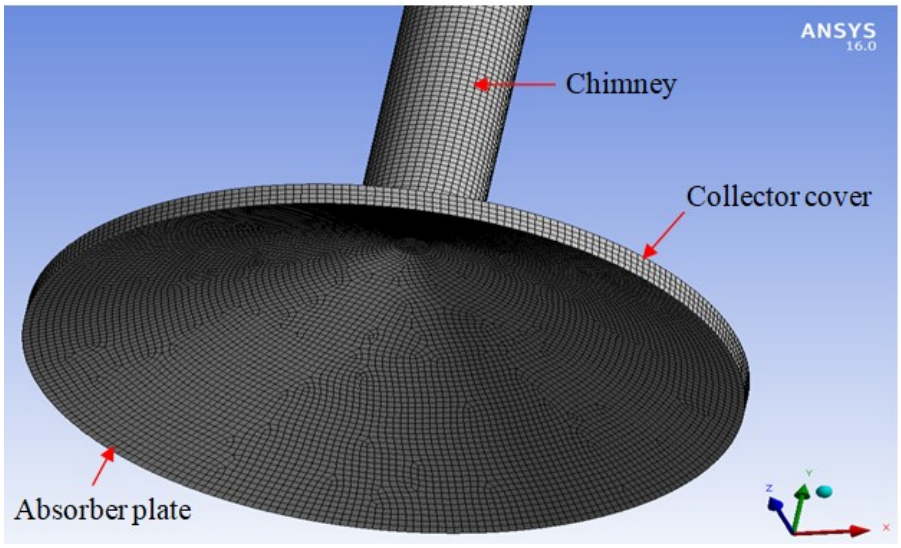
ANSYS
16.0
Chimney
Collector cover
Absorber plate

(b)

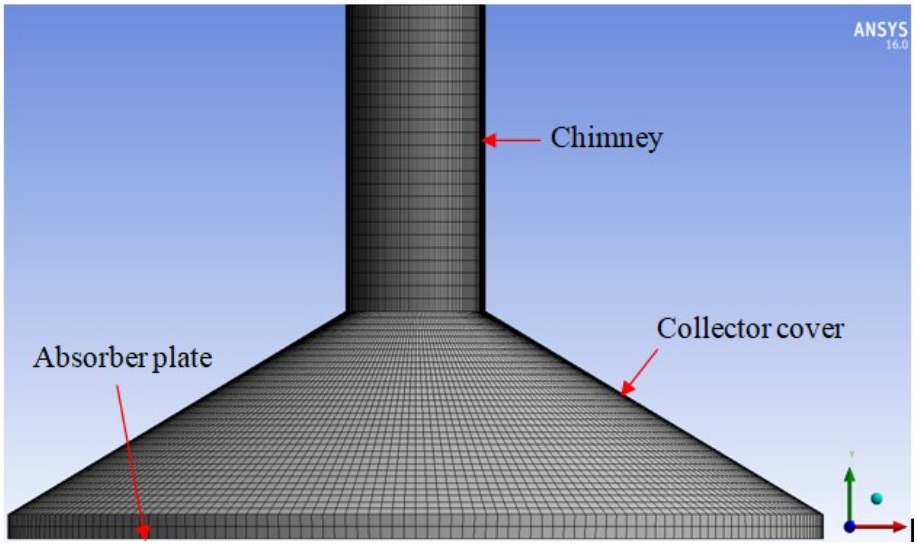
ANSYS
16.0
Chimney
Collector cover
Absorber plate

(c)

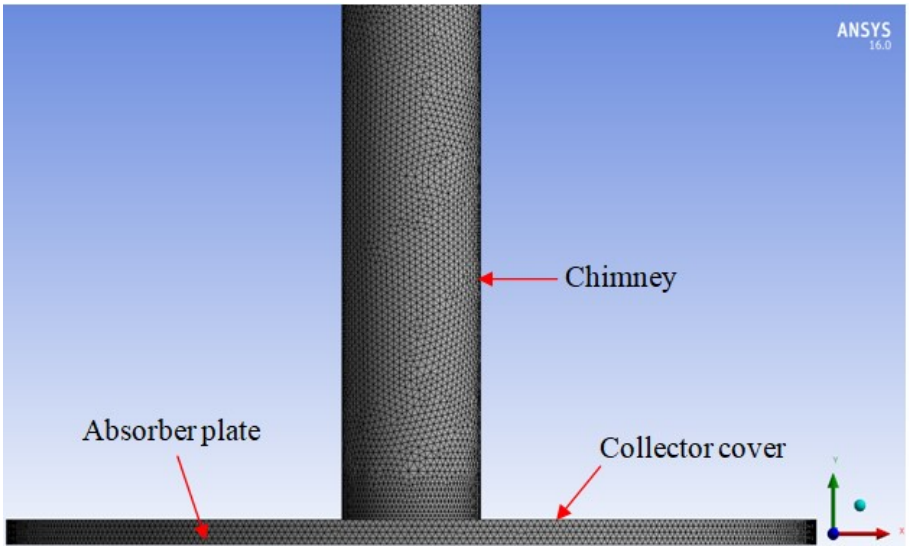

Fig. 2.11. Mesh generated for (a) Case – I, (b) Case – II and (c) Case – III

2.2.2. Grid independence test

Grid independence test was performed with three different grid sizes (2183590, 2439226 and 2741994 elements, respectively) for case-I. The air velocity was estimated and plotted (**Fig. 2.12**) inside the chimney at a height of 0.4 m from CB along the length of D_{ch}. The obtained velocity profiles are in a similar trend with other profiles of different grid sizes. An average error of 0.067% was noticed in the air velocity in between the nodes of 2183590 and 2439226. The error in between the nodes of 2439226 and 2741994 was 0.013%. It is not much beneficial for the simulation work by having an extremely fine meshing of geometry because of higher number of nodes can prolong the computational time and also utilize a lot of computer memory. Therefore, 2439226 nodes were used to run the remaining simulations. Similar tests were performed for case – II and case – III and the grids were finalised (not shown here).

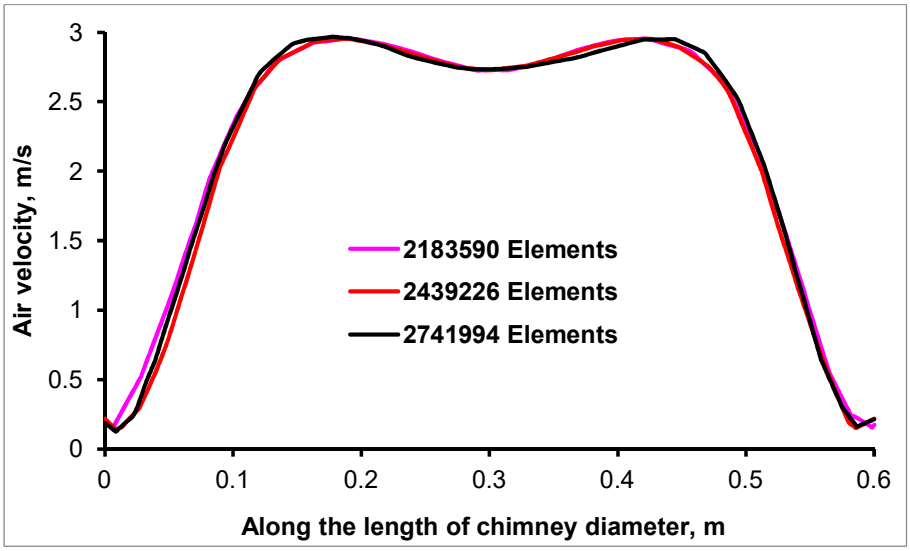

Fig. 2.12. Grid independence test of Case-I (air velocity at 0.4 m height from CB)

2.2.3. Assumptions

The following assumptions were used while solving the numerical problem.

- There is no heat transfer between inner walls of the collector and chimney to ambient air.
- The ambient temperature at inlet and outlet of SUT are assumed as 303 K.
- Steady state and turbulent air flow inside the SUT.
- Air flow is considered as incompressible, as the air velocity range inside the chimney is 2 to 20 m/s (Mach number of 0.006 to 0.06).
- The change in density of air is a function of temperature therefore, Boussinesq approximation is taken in to account in the body force term of momentum equation (y-direction).
- The intensity of solar heat flux (or) solar radiation is varied from 650 to 1150 W/m^2 for all three SUT cases.
- Air pressure is taken as gauge pressure in order to include atmospheric air condition at both entry and exit of SUT.

2.2.4. Governing equations

An SUT plant consists of solar collector, chimney and wind turbine. The flow inside the chimney is caused by buoyancy effect which is expressed in terms of Rayleigh number (*Ra*). If *Ra* is greater than 10^8 then the fluid flow is to be considered as turbulent.

$$Ra = \frac{g\beta\Delta T H^3}{\alpha v} \tag{2.81}$$

Where, g is acceleration due to gravity, β is coefficient of thermal expansion, ΔT is temperature difference inside and outside of the system, H is characteristic length (or) collector inlet gap, $\alpha$is thermal diffusivity and υ is kinematic viscosity of the air. *Ra* is estimated and it is 2.48×10^8. Therefore, the problem is considered as turbulent flow.

The physical principles such as conservation of mass, conservation of momentum and conservation of energy are applied to all the three cases and the resulting governing equations are mentioned as follows;

Continuity equation:

$$\frac{\partial}{\partial r}(\rho u_i) = 0 \tag{2.82}$$

Where, ρ is air density, u is the air velocity.

Momentum equations:

$$\frac{\partial}{\partial x_j}\left(\rho u_i u_j\right) = -\frac{\partial p}{\partial x_i} + \frac{\partial}{\partial x_j}\left[(\mu_t + \mu)\left(\frac{\partial u_i}{\partial x_j} + \frac{\partial u_j}{\partial x_i}\right) - \frac{2}{3}(\mu_t + \mu)\frac{\partial u_l}{\partial x_l}\delta_{ij} + \rho g_i \beta \Delta T\right] \tag{2.83}$$

Where, μ is dynamic viscosity of air, p is the pressure and $\rho g_i \beta \Delta T$ is buoyancy force term.

Air density variation inside the chimney is taken into consideration by Boussinesq approximation model and is represented as,

$$\rho = \rho_0[1 - \beta(T - T_0)] \tag{2.84}$$

Where, ρ_0 is reference air density, T_0 is corresponding temperature at ρ_0.

Energy equation:

$$\frac{\partial}{\partial x_i}(r u_i T) = \frac{\partial}{\partial x_i}\left(\frac{\mu}{Pr} + \frac{\mu_t}{\sigma_t}\right)\frac{\partial T}{\partial x_i} \tag{2.85}$$

Turbulent mathematical model has to be implemented to analyse the fluid flow behaviour within the SUT's.

Turbulent kinetic energy equation *(k)*:

$$\frac{\partial}{\partial x_i}(ru_i k) = \frac{\partial}{\partial x_i}\left(\mu + \frac{\mu_t}{\delta_k}\right)\frac{\partial k}{\partial x_i} + G_k + G_b - \rho\varepsilon \tag{2.86}$$

Turbulent energy dissipation equation *(ε)*:

$$\frac{\partial}{\partial x_i}(ru_i \varepsilon) = \frac{\partial}{\partial x_i}\left(\mu + \frac{\mu_t}{\delta_\varepsilon}\right)\frac{\partial \varepsilon}{\partial x_i} + \left[\left(\frac{\varepsilon}{k}\right)(c_1 G_k + c_1 c_3 G_b)\right] - \frac{C_2 \rho \varepsilon^2}{k} \tag{2.87}$$

Where, δ_k and δ_ε are turbulent Prandtl numbers for k and ε respectively. c_1, c_2, c_3 are constants of k-ε turbulence model. The constants are, c_1 = 1.44, c_2 = 1.9, c_3 = 0.09, δ_k = 1.0 and δ_ε= 1.2.

And G_k is the generation of turbulent kinetic energy due to change of average velocity and G_ε is generation of turbulent kinetic energy because of buoyancy force and is given below:

$$G_b = \beta g_i \frac{\mu_t}{Pr_t}\frac{\partial T}{\partial x} \tag{2.88}$$

$$G_k = \frac{\mu_t}{\rho}\frac{\partial u_i}{\partial x_j}\left[\frac{\partial u_i}{\partial x_j} + \frac{\partial u_i}{\partial x_i}\right] \tag{2.89}$$

Where, μ_t is specific turbulent viscosity (or) eddy viscosity in the flow field and is directly related to the corresponding local parameters of turbulent kinetic energy and its energy dissipation and it is mentioned as,

$$\mu_t = \rho C_\mu \left(\frac{k^2}{\varepsilon}\right) \tag{2.90}$$

Where, C_μ is constant of viscosity and is to be considered as 0.09 [41].

Neglecting the impact of radiation heat transfer inside the solar collector may result to an incorrect temperature distribution in the solar chimney. Thus, to build precision in the prediction of solution for a radiative transfer equation (RTE), a discrete ordinates radiation (DO) model is considered. DO method helps to model different types of semi-transparent

walls and also, evaluation of non-gray radiation is possible by DO model with the help of a gray-band model.

The DO radiation model computes the RTE for a finite number of discrete solid angles and each of these angles related with a directional vector $\vec{s}$ placed in global Cartesian coordinate system.

$$\nabla.(I_\lambda(\vec{r},\vec{s})\vec{s}) + (C_a + C_s)I_\lambda(\vec{r},\vec{s}) = C_a.n^2 I_{b\lambda} + \frac{\sigma_s}{4\pi}\int_0^{4\pi} I_\lambda(\vec{r},\vec{s}')\emptyset(\vec{s}.\vec{s}')\mathrm{d}\Omega' \qquad (2.91)$$

Where, I is solar intensity at a position of $\vec{r}$ in the direction of $\vec{s}$, λ is wave length, C_a is absorption coefficient, C_s is the scattering coefficient, I_b is black body intensity, ϕ is phase function and $d\Omega'$ is discrete solid angle.

According to Planck statement, the black body intensity can be mentioned as,

$$I_{b\lambda} = \frac{\sigma T^4}{\pi} \qquad (2.92)$$

2.2.5. Boundary conditions

The following boundary conditions have been applied at different sections of SUT.

1) Pressure boundary condition is considered at inlet of the collector and outlet of chimney. Pressure of ambient air is 0 Pa (gauge) and ambient temperature is 303 K.

2) Mixed boundary condition (convection as well as radiation) is applied to anti refluxing collector roof glass. This collector roof is considered as semi-transparent wall.

3) No-slip boundary condition is adopted for all the wall surfaces of main elements of SUT such as collector cover, chimney and glass roof joint, chimney wall and ground absorber plate surface.

4) Adiabatic wall boundary condition is selected for wall of the chimney.

5) Absorber plate being conjugated to wall, so that the absorption of solar radiation is to be taken as heat flux boundary condition from plate to its surrounding air flow.

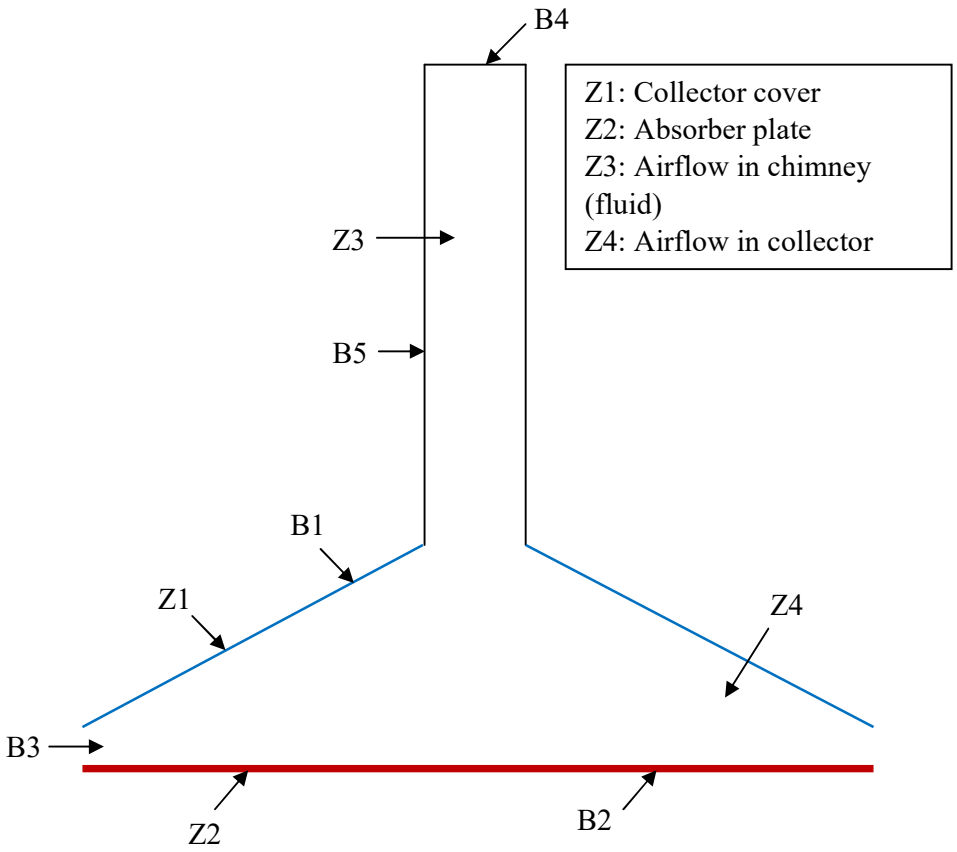

Type	Element	Parameters
B1: Mixed (Semi transparent) (Convection + Radiation)	Collector cover	DO Radiation, thickness = 5 mm
B2: Heat flux	Absorber plate	Thickness = 2 mm
B3: Pressure inlet	Collector inlet	$P_i = 0$ N/m^2 (gauge), $T_i = 303$ K
B4: Pressure outlet	Chimney outlet	$P_o = 0$ N/m^2 (gauge), $T_o = 303$ K
B5: Adiabatic	Chimney surface	$q = 0$ W/m^2, thickness = 5 mm

Fig. 2.13. Boundary conditions applied at different places of SUT

2.2.6. Numerical solution and methods

~~A finite volume method (FVM) is applied to discretize the governing equations of flow model.~~ A steady state, absolute velocity formulations and pressure based solver is selected for simulation of fluid flow and SIMPLE algorithm is chosen for pressure velocity coupling. Gravitational acceleration (-9.81m/s^2 in Y-direction) is to be considered for more precise and appropriate response of results.

In spatial discretization scheme, least square cell based method is applied to gradients. Gradients are required for building values of a scalar at control volume faces and also for estimating secondary diffusion terms and velocity gradients. PRESTO algorithm is strongly recommended for flows with high swirl numbers, natural convection with high Rayleigh numbers, high speed rotating flows and flows in strongly curved domains [6]. So that it is chosen for pressure interpolation scheme.

Momentum, energy, turbulent kinetic energy, turbulence dissipation energy and radiation heat transfer equations are discretized with the help of second order upwind scheme. Realizable k-ε model with wall treatment as standard wall functions and buoyancy effect is considered for turbulence predictions. Discrete ordinates (DO) method is used to solve RTE equation as it allows RTE equation for semi-transparent wall materials such as glass. The convergence criterion for continuity, momentum and other velocity terms were given as10^{-4} and the energy and radiation terms were 10^{-6}.

2.3 Experimental methodology

Based on the preliminary analytical calculations, numerical simulations and space constraints, the setup dimensions were finalized thus: D_c of 3.5 m, D_{ch} is 0.6 m and H_{ch} is 6 m (**Fig. 2.13**).

Fig. 2.14. A SUT setup developed at CAM Building, NIT Warangal, Telangana state, India.

2.3.1. Detailed procedure of fabrication of setup

The setup is installed in the middle of the floor to avoid possible shadows of trees around the building.

2.3.1.1 Concrete foundation

The total mass of the system was estimated and according to that a concrete foundation (made up of mixture of cement, rock gravel and sand) was made with a diameter of 4 m and thickness of 10 cm. There were eight foundation rods (material: SA36) clamped on the concrete foundation using proper bolt and nuts.

2.3.1.2 Supporting rods, TES system and absorber plate

There were 16 hollow rectangular support rods (length of 1500 mm, width of 76.2 mm and thickness of 38.1 mm, made up of low carbon steel (SA36) which were fixed appropriately with eight foundation rods.

A TES bottom plate was fitted on the support rods. It is circular in shape with a diameter of 3.5 m and made up of plywood with a thickness of 10 mm. The peripheral outer surface of TES system was covered with polycarbonate sheet (thickness 5 mm) for accommodating TES material inside it. Thermocol sheets (25 mm thickness) were provided on the wooden panel in order to avoid heat losses from the bottom of TES plate to the atmosphere. A calculated quantity of TES material was provided on the thermocol sheets. It was a mixture of sand and gravel (50:50 ratio) and they were tightly packed within 3.5 m diameter TES plate. The total thickness of TES device (including wooden panel, thermocol and mixture of sand and gravel) was 150 mm as shown in **Fig. 2.14.** The top surface was covered by copper absorber plate as explained in next paragraph.

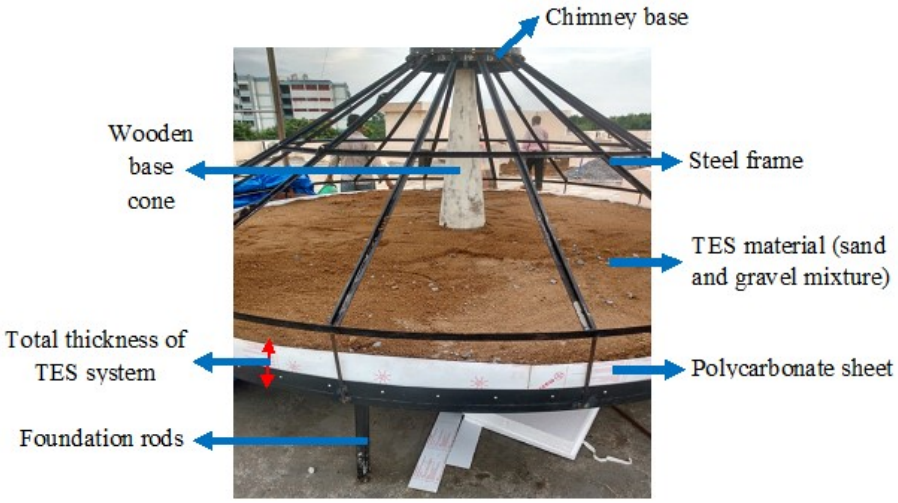

Fig. 2.15. TES wooden plate filled with a layer of thermocol and TES material (sand and gravel mixture)

An absorber plate made up of copper was placed on top of TES system to absorb maximum amount of solar radiation. A number of rectangular copper plates (length of 1220 mm, width of 356 mm, and thickness of 1.5 mm) were purchased from Hyderabad, India and cut and riveted into a circular piece of 3.5 m diameter. Black paint was applied on it to increase its absorption capacity. Temperature sensors are fixed on the surface of absorber plate in all four directions (East, West, North and South) at a distance of 300 mm, 800 mm and 1300 mm from the entrance of collector.

2.3.1.3 L-Shaped structural steel frame (SA36) and glass plates (canopy or collector cover)

A collector cover was placed on top of TES plate after keeping a collector inlet distance of 0.1 m. A strong frame was fabricated to place the collector cover (glass) and chimney on top

of it. It was made up of structural steel material (SA36) in order to withstand the strong wind forces and heavy rains. It was made into two halves: L – shaped rods (thickness of 5 mm) were welded together to make each circular half piece. The framework was divided into two halves along its circular surface leads to upper and bottom halves. Rectangular anti-refluxing glazed glass plates (length of 1 m, width of 1 m, and thickness of 0.005 m) were purchased as per the availability of size in the local market, cut into pieces according to the dimensions and filled on bottom and top halves.

The correctly cut glass pieces were placed on the structural steel frame (SA36). A rubber gasket was provided between the frame and glasses to make a tight seal between glass and frame. Silica gel was applied on top and bottom surfaces of collector cover to fill the side gap between the steel frames and glass, so that there was no leakage of hot air. The shape of the collector cover looks like a frustum of cone shape. This assembly of the frame and glass cover is called canopy. The top end of the canopy (collector cover top) is connected with a circular flange and is welded to the chimney base plate. A solar chimney is fitted on top of the chimney base plate, which will be discussed in section 2.3.1.6.

2.3.1.4 Guide vanes and wooden cone

Guide vanes are placed vertically from the absorber plate base to the collector cover top. It is used to generate the nozzle effect near the chimney base and to direct the air towards the chimney base. These plates (12 nos) are made up of galvanized iron sheet (IS 277) material and cut as per the requisite dimensions (length of 900 mm, width of 200 mm, and thickness of 1.5 mm). Top end of guide vanes are permanantly welded to steel frames of collector cover. Each set of guide vanes creates a nozzle effect with a divergent distance of 250 mm and converged part distance of 40 mm.

A central base cone was placed in the middle of the collector. The purpose of a base cone is to guide the flow (in swirl motion) in upward direction towards the turbine blades. It produces turbulence effect and hence the air flow velocity increases further and hence, there is increase in kinetic energy. It is also used to hold various sensing instruments such as pressure, temperature and velocity sensors in fixed position by clamping to it. Wood is considered as base cone material because it is light weight. A truncated cone shape was made (height of 0.98 m, bottom and top diameters of 0.45 m and 0.1 m, respectively) from raw wood (0.5 m in diameter and 1.1 m in height).

2.3.1.5 Solar chimney or tower and strings

At the chimney base, a steel flange with nuts and bolts was fitted to accommodate the chimney cylinders. The chimney tower was made of light weight polycarbonate sheets. Rectangular plates (length of 2 m, width of 1.2 m, and thickness of 0.005 m) of polycarbonate sheets were purchased and made into cylinders by bending them as per requisite D_{ch} of 0.6 m. Riveted joints were used to connect two ends of plates, so that the final shape looks like a cylinder. Similarly, five cylinders were made with height of each cylinder of 1.2 m. Mild steel straps (**Fig. 2.15**) with rivet joints were used to couple five circular parts to make a chimney with H_{ch} of 6 m (**Fig. 2.15**). Supportive wires (low carbon iron strings) were used to tie at six locations (from middle and top of the chimney, **Fig. 2.15**) and nailed at different locations of the roof top to improve the stability of chimney and setup during heavy storms. The chimney outlet was covered by a conical cap to prevent rain water entering into the setup and enough space was provided (between the cap and chimney outlet) for the free flow of hot air at chimney outlet as mentioned in **Fig. 2.15.**

Fig. 2.16. Solar chimney (or) tower and strings

A turbine fan made of plastic is fitted in a shaft and placed near the chimney base. Therefore, it can absorb the wind flow and can generate mechanical energy to produce electric power. It has dimensions as follows: shroud diameter of 580 mm, hub diameter of 80 mm and blade thickness of 1.5 mm. A plastic shaft (polycarbonate) was used to connect the fan and roller bearing. One end of the shaft is fitted with turbine and the other end has central rotary

bearing. This bearing is positioned at the center of chimney base and is permanently welded to the inner wall of chimney with the help of steel rods (low carbon steel material).

2.3.2. Cost analysis of used materials

The price details of main components/materials used to construct a small scale SUT power plant are mentioned in below **Table 2.6.**

Table 2.6: Cost analysis of used materials

S.No	Equipment / material used	Quantity (No's)	Unit Price in INR	Total Price in INR
1	Chimney (Polycarbonate)	1	30000	30000
2	Turbine and its accessories (bearings and shaft)	1 Set	500	500
3	Collector cover (Glass)	As per the dimension	30000	30000
4	Absorber plate (Copper)	As per the dimension	250000	250000
5	Insulation Material (wood and thermocol sheet)	1 Set		7000
6	Thermal energy storage material (Sand & gravel)	2500 kg	1.5	6000
7	Supporting strips, strings, flange, guide vanes, bolts, nuts, rivets etc.	As per the requirement		8000
8	Base supporting and foundation rods	100 kg		20000
9	Concrete foundation	As per the dimension		5000
10	Transportation, man power, fabrication and installation cost			120000
	Total expenditure to build a small scale SUT power plant =			**476500 ($ 6636)**

2.3.3. Measuring instruments used and uncertainty analysis

2.3.3.1 Measuring instruments used

Table 2.7 provides a list of instruments was used to perform different measurements such as velocity, temperature, pressure, speed and solar intensity. The sensor output signal is converted to a digital signal by transmitting it to the multichannel data logger where it stored all the data each minute for the whole day.

Table 2.7: List of instruments and their specifications

Instruments	Make, Model, Country	Range	Accuracy
Cup type Velocity sensor	Sivara Systems and Solutions, WS9838, India	0 – 20 m/s	< 0.1 m/s + 5% from reading
Velocity sensor	Aerosense, AVT-D, Singapore	0 – 20 m/s	< 0.1 m/s + 5% from reading
Temperature sensor	ABN Engineering Services, PT100, India	0 – 100 °C	±0.3°C to ±0.8°C of full scale reading
Pressure sensor	Sivara Systems and Solutions, SB100, India	0-115000 N/m^2 (absolute)	±0.3% of full scale reading
Radiation Pyranometer		0 - 2000 W/m^2	±2% of full scale reading
Speed Sensor	Pioneer Instruments, Hyderabad, India	0 – 5000 rpm	±0.05% of full scale reading

2.3.3.2 Uncertainty analysis

Uncertainty analysis was performed to check the accuracy of the obtained primary and secondary parameters. When a set of readings of a particular instrument is considered, the individual readings may vary somewhat each other. The experimenter thus needs to take the mean of all the readings for calculations. If each and every reading is denoted by x_i, and there are n readings, then arithmetic mean (x_m) is estimated by,

$$x_m = \frac{1}{n}\sum_{i=0}^{n} x_i \tag{2.93}$$

The deviation for each reading is defined by, $d_i = x_i - x_m$

The standard deviation (σ) is,

$$\sigma = \sqrt{\frac{1}{n}\sum_{i=0}^{n}(x_i - x_m)^2} \tag{2.94}$$

The standard deviation of the mean (σ_m) is defined as,

$$\sigma_m = \frac{\sigma}{\sqrt{n}} \tag{2.95}$$

The uncertainty (or) error of recorded data is $\pm \sigma_m$.

Chapter 3

Results and discussion based on theoretical analysis

Chapter 3

3. Results and discussion based on theoretical analysis

In this section, the obtained theoretical results are discussed. The results obtained for design, development and materials selection of laboratory scale SUT are discussed. The solar radiation calculations, energy gain and loss, collector efficiency, overall efficiency and power output of SUT system are also explained. Optimisation of the geometrical dimensions of SUT is explained. Optimisation of the design and performance parameters for various wind turbine blades of a SUT plant using blade element momentum (BEM) theory is discussed.

3.1. Solar radiation calculation

As per the ASHRAE model [27], beam and diffuse radiations were calculated on 21st of every month of the year 2016, at NIT Warangal. **Figs. 3.1 and 3.2** show that the comparison between the availability of solar radiation on 21st of every month of the year 2016. From both **Figs. 3.1 and 3.2** the maximum solar global radiation was observed in summer (April/May). In the primary time frame; both daylight hour and temperature are high. The second peak happens in August (harvest time) which is not so noticeable, because of a high temperature but rather short sun shining period (**Fig. 3.2**). In the winter (November/December), again sufficient sun shining periods are available but the temperature is low (**Fig. 3.2**). Subsequently, it brings about low global sun radiation. These theoretically estimated global radiation values were compared with India's Meteorological department values, 2016 [75]. The most extreme estimation of global radiation is 1059.38 W/m^2 at the time of April when the bright sunshine hour and normal temperature are 9.17 hours and 31.5˚C respectively [75]. The base estimation of global radiation is 851.22 W/m2 at the time of December when the bright sunshine hour and normal temperature are 8.39 hours and 21.6˚C [75] respectively.

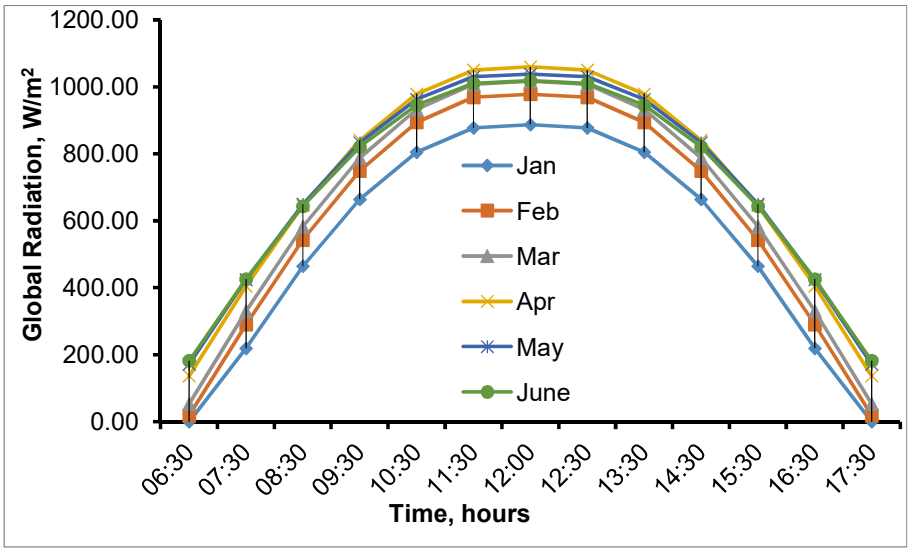

Fig. 3.1. Monthly average daily global radiation for first six months of 2016

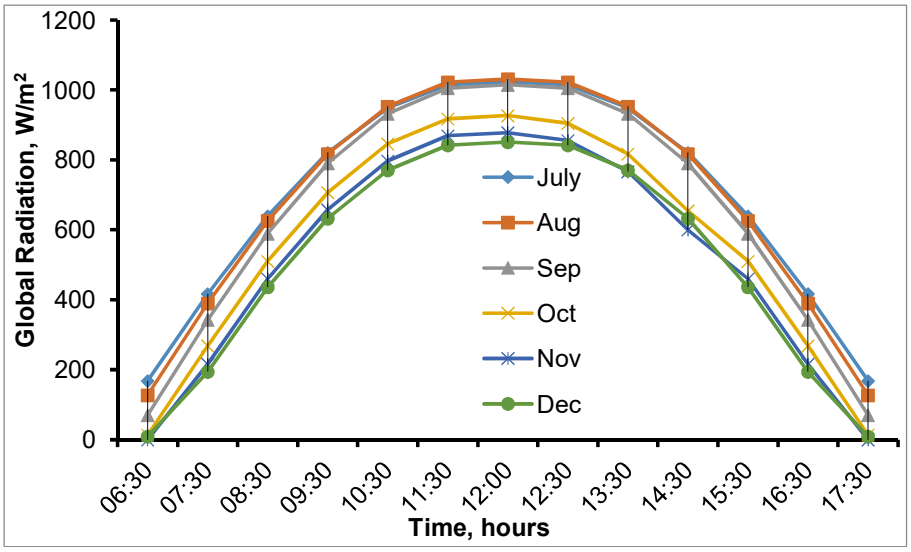

Fig. 3.2. Monthly average daily global radiation for last six months of 2016

The estimated beam radiation values were compared with experimental data of same location (Warangal, India). Instantaneous beam radiation was measured using a solar power meter (Tenmar TM 207). The experimental average value of beam radiation from February to June, 2016 was 833 W/m^2 [76] and the same by theoretical estimation is 897.41 W/m^2. The percentage difference noticed is 7.7 %. The average beam radiation throughout the year 2016 is estimated and it is 985 W/m^2. The same estimated beam radiation for the year of 2016 is compared with the India Meteorological department [75] and the maximum percentage variation is noticed as 6%.

Solar radiation parameters are estimated from Eqs. (2.1-2.17) and are listed in **Table 3.1** and **Table 3.2**. The parameters are estimated at noon time of 21st of each month of 2016. Therefore, instantaneous hour angle at solar noon (ω) is zero. The collector slope angle (ξ) and surface azimuthal angle (γ) are considered as 30° and 0° respectively [64]. Results shows that direct radiation is higher in intensity to the global radiation during the summer, post monsoonal and winter months due to clear sky conditions and variations in altitude angle. The average value of global radiation for 1st 6 month is 984.5 W/m^2 and 2nd 6 month is 985.5 W/m^2.

Table 3.1: Calculated parameters of solar beam, diffuse and global radiation for 1st six months of year 2016

Parameters	Value					
Day of the year, D_Y	21	52	70	111	141	172
Solar declination, δ	-20.14°	-11.23°	-4.41°	11.58°	20.14°	23.45°
hour angle at sunrise and sunset, ω_{st}	94.48°	90.83°	92.24°	97.8°	125.4°	130.3°
Solar zenith angle, Z	38.12°	29.21°	22.4°	6.4°	2.15°	5.47°
Solar incident angle at noon, θ	8.12°	0.79°	7.6°	23.6°	32.15°	35.47°
Constant, A (W/m^2)	1202	1187	1164	1130	1106	1092
Constant, B	0.141	0.142	0.149	0.164	0.177	0.185
Constant, C	0.103	0.103	0.104	0.109	0.12	0.13
Beam radiation, I_b (W/m^2)	790.45	790.45	916	952.1	925.8	902.7
Diffuse radiation, I_d (W/m^2)	96.55	96.55	100.75	107.27	112.4	115.9
Global radiation, I_G (W/m^2)	887.01	887.01	1016.76	1059.4	1038.2	1018.6

Table 3.2: Calculated parameters of solar beam, diffuse and global radiation for last six months of year 2016

Parameters	Value					
Day of the year, D_Y	202	233	264	294	325	355
Solar declination, δ	-20.44°	11.75°	-0.2°	-11.75°	-20.44°	-23.45°
hour angle at sunrise and sunset, ω_{st}	129.2°	125.9°	102.1°	90.3°	80.8°	77.2°
Solar zenith angle, Z	2.46°	6.23°	18.2°	29.75°	38.43°	5.47°
Solar incident angle at noon, θ	32.46°	23.77°	11.81°	0.26°	8.43°	35.47°
Constant, A (W/m^2)	1202	1187	1164	1130	1106	1092
Constant, B	0.141	0.142	0.149	0.164	0.177	0.185
Constant, C	0.103	0.103	0.104	0.109	0.12	0.13
Beam radiation, I_b (W/m^2)	906.5	916.35	907.2	828	925.8	725.7
Diffuse radiation, I_d (W/m^2)	116.9	115.25	107.8	98.75	112.4	102.55
Global radiation, I_G (W/m^2)	1023.3	1031.6	1015	926.74	1038.2	878.3

3.2. Energy losses

Transmissivity estimations of solar collector cover are performed using Eqs. (2.18-2.34) and are tabulated in **Table 3.3**.

Table 3.3: Transmissivity estimations of solar collector cover

Parameter	Value	
Hourly beam (or)direct radiation, (I_b)	827.99 W/m^2	
Hourly diffuse radiation, (I_d)	98.75 W/m^2	
Hourly global radiation, (I_G)	926.74 W/m^2	
Refractive index of glass relative to the air, (n_2/n_1)	1.526	
Glass extinction coefficient, (C_g)	15 m^{-1}	
Glass cover thickness, (δ_c)	5 mm	
	Beam	Diffuse
Reflectivity of first component of polarisation, (ρ_1)	0.043	0.185
Reflectivity of second component of polarisation, (ρ_2)	0.043	0.001
Angle of incidence, (θ_1)	0.26°	60°
Angle of refraction,(θ_2)	0.17°	34.58°
Reflectivity, (ρ)	0.043	0.093
Transmitivity of first component of polarisation, (τ_{r1})	0.917	0.687
Transmitivity of second component of polarisation, (τ_{r2})	0.917	0.997
Transmissivity by considering reflection and refraction,(τ_r)	0.917	0.842
Transmissivity by considering absorption,(τ_a)	0.999	0.999
Transmissivity, (τ)	0.917	0.842
Absorptivity of copper plate (α)	0.94	
Diffuse reflectivity of the cover system (ρ_d)	0.1579	
Transmitivity absorptivity product for beam radiation $(\tau\alpha)_b$	0.870	
Transmitivity absorptivity product for diffuse radiation $(\tau\alpha)_d$	0.799	
Net global radiation absorbed by the absorber plate, ($I_{A.P}$)	799.29 W/m^2	
Total surface area of the collector cover, (A_c)	12.831 m^2	
The theoretical radiant energy transmitted through collector cover (E_{th})	11891 W	
The incident flux absorbed by absorber plate, ($E_{A.P}$)	7690.05 W	
Average sunshine hours available on 21-October-2016 in Hyderabad. (nearest weather station to NIT Warangal) [66]	7.3 h	
The total theoretical energy absorbed by plate on 21-October-2016 (E_A)	56137.36Wh (or) 5834.88 Wh/m^2	

3.3. Heat losses

The heat loss estimations are performed using Eqs. (2.35-2.47) and are tabulated in Table 6. The efficiency of the collector (η_c) for 21st October 2016 is estimated and it is 43.82% (**Table 3.4**). The variation of η_c on entire year 2016 is estimated and shown in **Fig. 3.3**. Similar collector efficiency is noticed in the study of Guo et al. [52]. In their numerical work, the collector efficiency varied from 35 to 43 %. Kalogirou [62]'s collector efficiency is 45%. A

solar tracking system was used in the study of Gitan et al. [50], therefore their collector efficiency increased up to 51%. Maghrebi et al. [53] developed a sloped SUT plant and their collector efficiency was 56%.

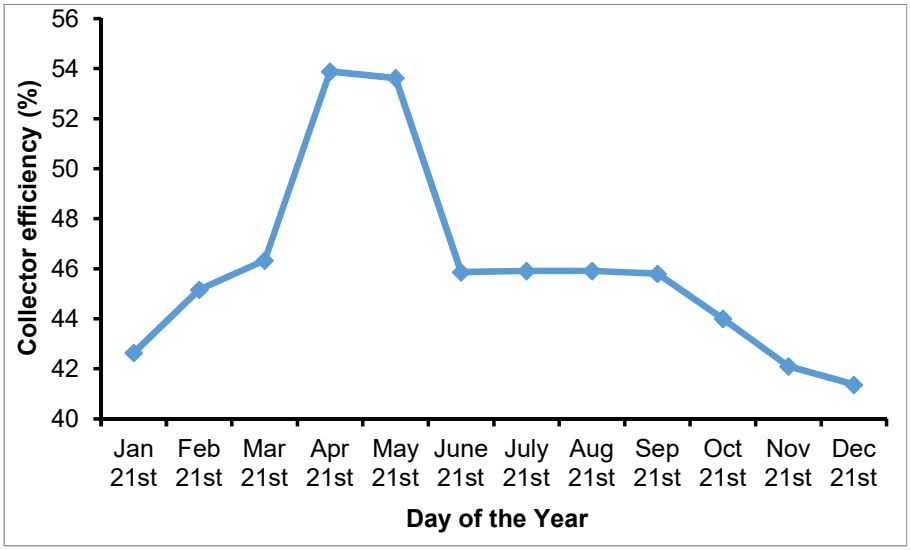

Fig. 3.3. Variation of collector efficiency (η_c) in the year 2016.

Table 3.4: Estimated parameters of heat loss calculations

Parameter	Value
Linearised radiation coefficient, (h_L)	6.04 W/m^2.K
Convective heat transfer coefficient, (h_c)	0.04 W/m^2.K
Wind loss coefficient, (h_w)	15.2 W/m^2.K
Radiative heat transfer coefficient, (h_r)	21.32 W/m^2.K
Resistance between the collector and absorber plate, (R_1)	0.16 K/W
Sky temperature, (T_{sky})	18.14°C
Collector resistance, (R_2)	0.03 K/W
Overall heat loss coefficient, (U_t)	5.15 W/m^2.K
Rate of energy loss, (Q_L)	2479.5 W
Useful energy available, (Q_U)	5210.6 W
Efficiency of the collector, (η_c)	43.82 %

The total theoretical energy absorbed by plate on 21-October-2016 (E_A)	56137.36 Wh
Energy lost through the collector during sunshine hours in a day, (E_{lost})	18100.4 Wh
Useful energy (E)	38037.01 Wh

3.4. Solar chimney

Maximum air velocity inside the chimney is estimated using Eq. (2.48). In the present study, it was estimated and varies between 1.82 to 2 m/s. The maximum velocity values of existing studies of Zhou et al. [69] and Kasaeian et al. [40] are 3 m/s and 2.9 m/s respectively. It is presented in **Fig. 3.4.**

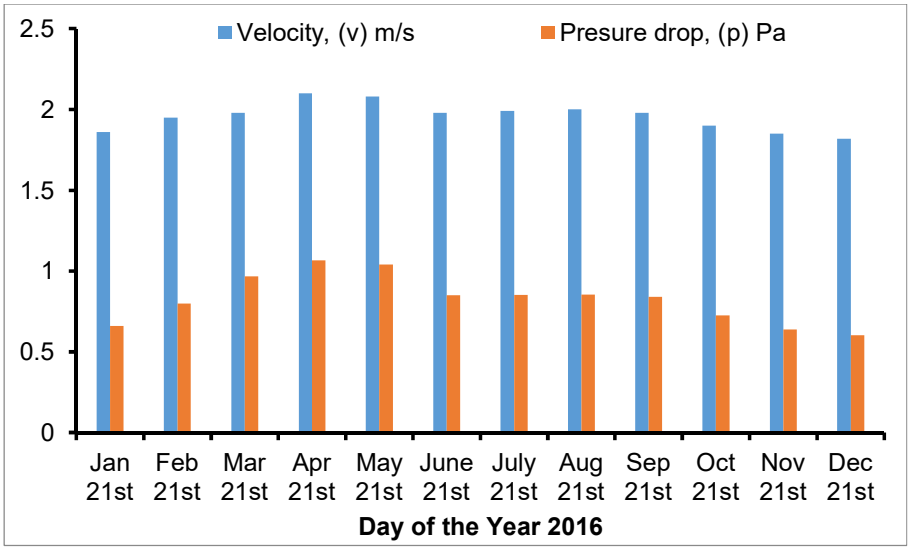

Fig. 3.4. Variation of velocity and pressure drop in the year 2016.

Temperature of hot air is calculated from Eq. (2.43 and 2.51) and it is shown in **Fig. 3.5**. Where, C_p is specific heat of air, ΔT is temperature difference of air inside and outside collector. This temperature difference is estimated and it varies in between 9 to 15 °C and it is mentioned in **Table 3.5**. This value is quite comparable with Pasumarthi and Sherif [77]'s value of 13.9 °C. Haaf et al. [3] and Haaf [78]'s pilot plant in Manzanares, Spain gave 17.5 °C temperature difference. Zhou et al. [69] and Gitan et al. [50]'s system developed 15 and 17 °C, respectively. Depends upon the geographical location the temperature difference was varied from 11 to 28 °C in different studies [7, 47, 48, 69, 73].

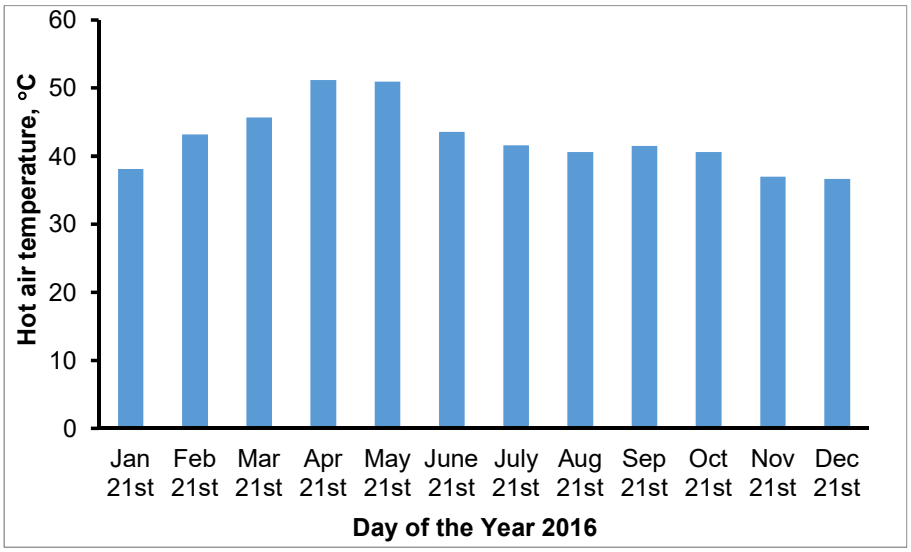

Fig. 3.5. Variation of hot air (T_h) temperature in the year 2016.

The variation of pressure drop across the turbine is shown in **Fig. 3.4.** Pressure drop is evaluated from Eq. (2.54) and it varies in between 0.602 to 1.065 N/m^2. The pressure drop value was experimentally evaluated by Ahmed et al. [6] and it is 2.0 N/m^2. Theoretical power output of the system is in between 0.31 to 0.633 W and is shown in **Fig. 3.6.** The power generation was experimentally evaluated by Ahmed et al. [6] and it is 0.1 W. Maximum power generation is noticed in the month of April due to high amount of global radiation.

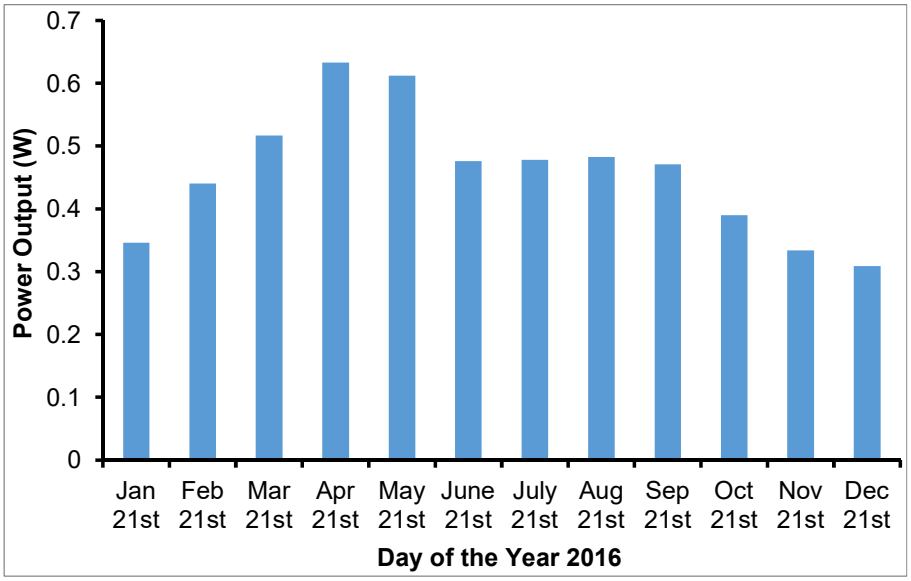

Fig. 3.6. Theoretical power output (P_t) of the system in the year 2016.

The chimney efficiency (η_{ch}) is estimated using Eq. (2.57) and is shown in **Fig. 3.7**. The η_{ch} is dependent on height and temperature. Specific heat (C_p) is in the order of 1.005 kJ/kg.K and T_h will always be above 273 K (i.e. the denominator of the efficiency equation is in the order of 273000 or above). For the efficiency to be increased to a maximum (or) optimum, the chimney height must be in the order of 273000/9.81 = 27828 m. This is three times the height of Mount Everest! Increasing the chimney height to produce reasonable velocity is too expensive and will present major engineering challenges. η_{ch} varies with height at constant chimney temperature of 353 K. The analysis shows that although the chimney temperature is above the ambient temperature, it should be kept as low as possible as T_h appears on the denominator of the efficiency equation.

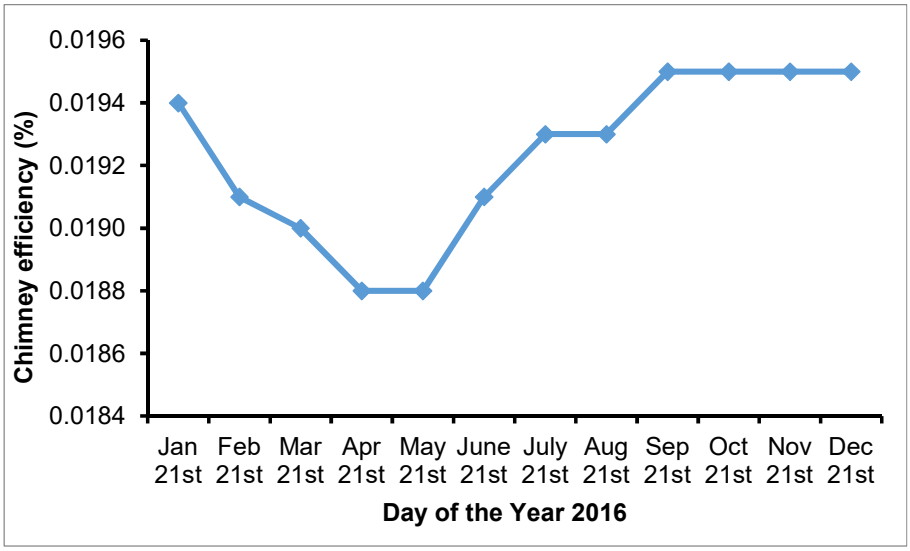

Fig. 3.7. Chimney efficiency (η_{ch}) of the system in the year 2016.

Maximum efficiency of the turbine (η_t) is considered as 66.67% [49]. The overall efficiency (η_o) of the plant throughout the year 2016 is estimated using Eq. (2.58) and it is presented in **Fig. 3.8**. It is in the range between 0.0017 to 0.0028 % and this value range is almost similar of Pasumarthi and Sherif [77]'s value of 0.0013 to 0.0023 %. The maximum η_o (0.0028%) is noticed in the month of April 2016. All the input and estimated parameters of chimney are mentioned in **Table 3.5**.

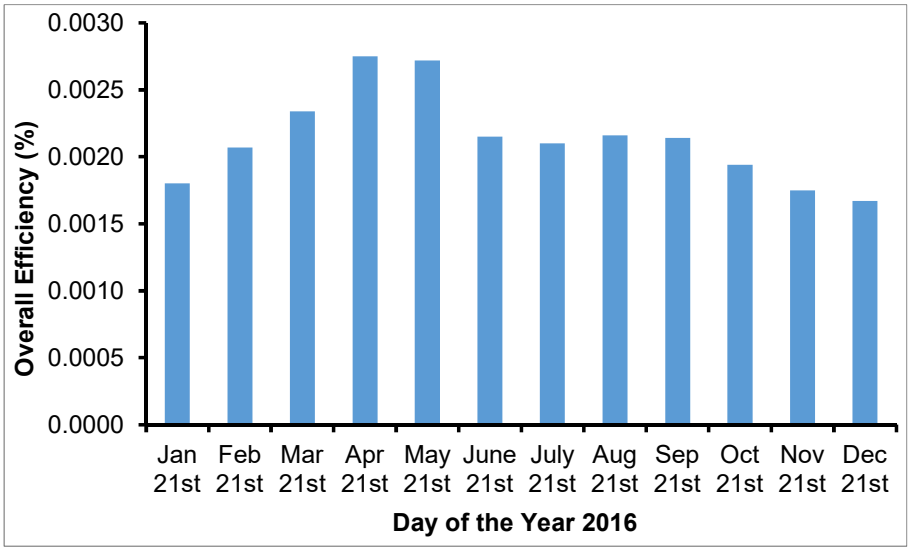

Fig. 3.8. Variation of overall efficiency in the year 2016.

Table 3.5: Input and estimated parameters of chimney

Parameter	Value
Absorber plate temperature, (T_A)	80 °C
Ambient or air temperature, (T_a)	30 °C
Temperature difference of absorber plate (T_A) and hot air (T_h)	50° C
Diameter of chimney, (D_{ch})	0.6 m
Height of the chimney, (H_{ch})	6 m
Density of air at chimney base	1.005 kg/m^3
Maximum air velocity, (v_{max})	1.94 m/s
Area of the chimney, (A_{ch})	0.2827 m^2
Mass flow rate of air, (m_a)	0.55 kg/s
Air heat transfer rate, (Q_a)	5.56 kW
Energy required for 12 h operation (E_{ch})	66.72 kWh
Required collector base area ($A_{R.C}$)	8.92 m^2
Pressure drop inside the chimney, (ΔP)	0.55 N/m^2
Maximum theoretical power output of a turbine (P_t)	0.37 W
Efficiency of the turbine (η_t) [49]	66.6 %

Actual power output of a turbine (P_{act})	0.25 W
Efficiency of the chimney (η_{ch})	0.0193 %
Overall efficiency of the plant (η_o)	0.15 %

3.5. Wind turbine

3.5.1. Optimization of angle of attack (α)

The coefficient of lift (C_L) and drag (C_D) were selected for different types of turbine blade aerofoil (NACA 0012, 4412 and 23012) under a particular Reynolds number (Re) and α, from NACA aerofoil data sheet are shown in **Figs. 3.9** and **3.10.** The maximum power output of the turbine is obtained when the glide ratio (C_L / C_D) is to be highest. The highest value of (C_L / C_D) for the different turbine blade aerofoil (NACA 0012, 4412 and 23012) are 5.5°, 5° and 7° respectively, which indicates that optimum angle of attack of respective blade aerofoil's (**Fig. 3.11**).

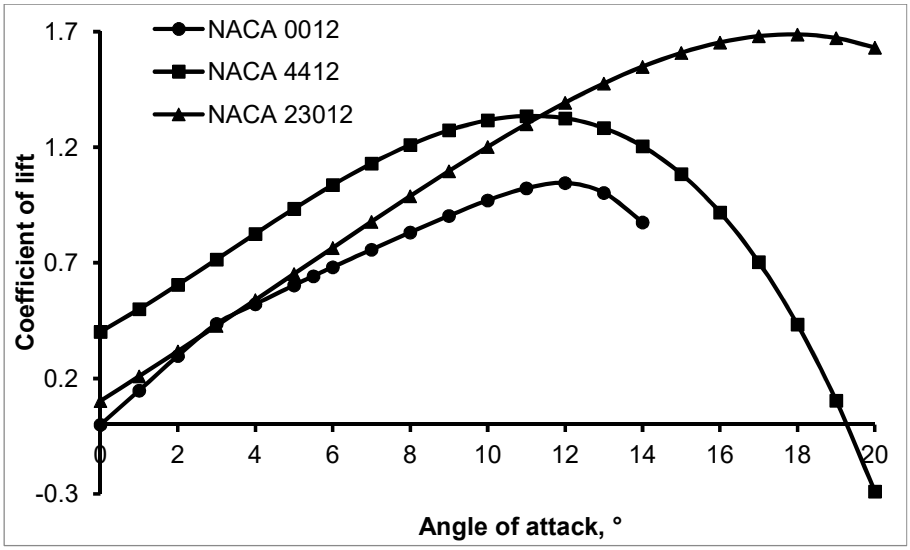

Fig. 3.9. Variation of coefficient of lift for different α

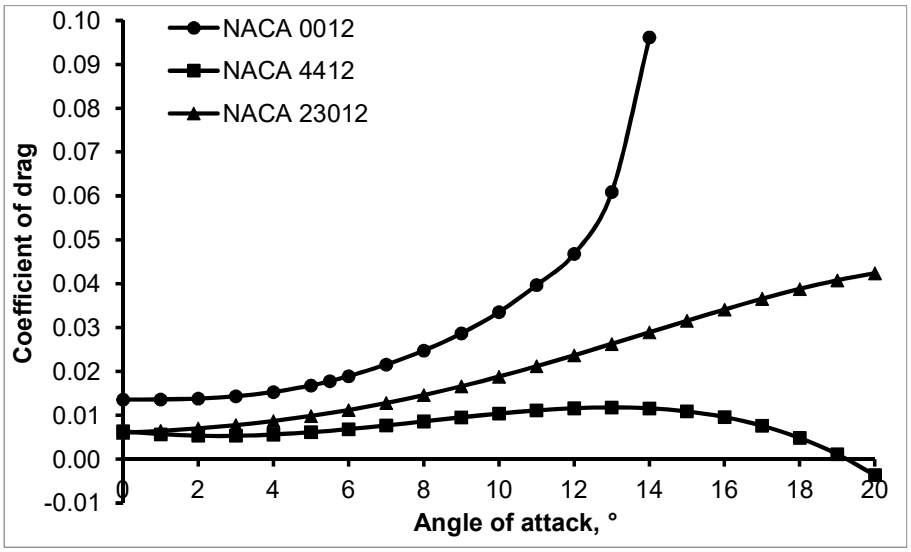

Fig. 3.10. Variation of coefficient of drag for different α

The power produced by different blade segments was estimated by Eq. (2.79) for various α and is shown in **Fig. 3.11.** Optimised power production of different blade aerofoil is shown in **Fig. 3.11.** NACA 0012, NACA 4412 and NACA 23012 turbine blades produce maximum power of 0.59 W, 0.624 W and 0.61 W at $\alpha = 5.5°$, $\alpha = 5°$ and $\alpha = 7°$ respectively.

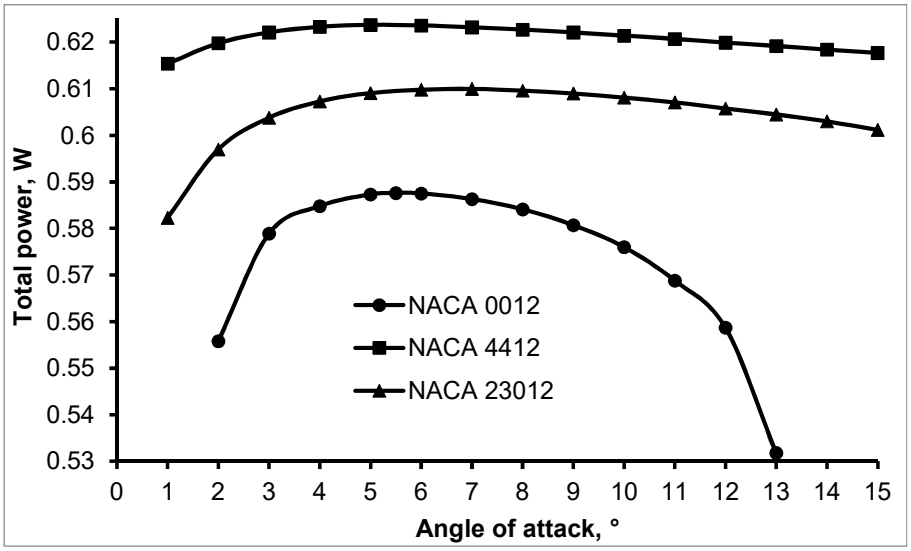

Fig. 3.11. Optimisation of angle of attack (α) for different blades

3.5.2. Optimization of number of blades (*N*)

The power output is evaluated at each blade segment (*r/R*) of turbine by varying numbers of blades (*N*) under the consideration of a constant α (5°). The kinetic energy extraction rate (*dP*) increases with the increase of *N* and is presented in **Fig. 3.12**. It is very difficult to balance the wind turbine by choosing two number of blades. If the number of rotor blades is more (greater than four) the weight of the rotor system increases followed by decreasing speed of shaft. And it is also observed that a very less quantity of air passing through the rotor plane when turbine having more than four number of blades. So that, turbine with four number of blades is considered as optimised one for effective energy extraction from wind.

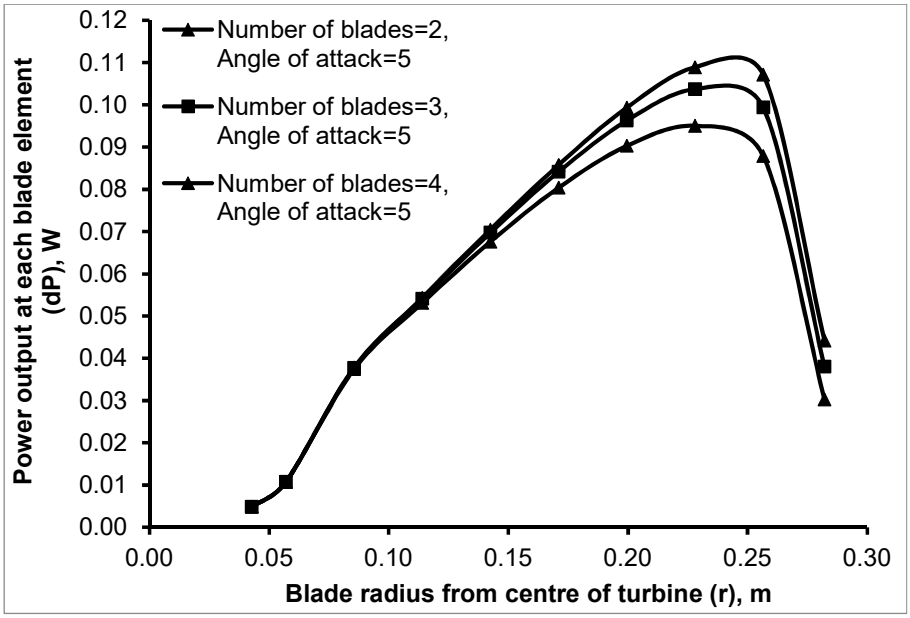

Fig. 3.12. Optimisation of number of turbine blades

3.5.3. Estimation of wind flow angle ($\emptyset$) and blade pitch angle (β)

The wind flow angle ($\emptyset$) and blade pitch angle (β) are evaluated for each sectional segment of blade and the results are shown in **Fig. 3.13.** It was clear that β is greater than 30° near the blade root section because maximum wind velocity occurs at the axis of the turbine (nearer to blade root section). So that, the blade is twisted more at root section than at tip section for withstand incoming wind forces. Similarly φ also maximum at the root of blade and decreases linearly along *R* for the same reason explained above. β and φ decrease with increased radius (in **Fig. 3.13**) because of decrease of relative wind velocity along the radius of the blade (from root to tip) and sufficient time is available for wind to reach and strike the

tip of the blade. Same trend of profile is observed for all three types of NACA series turbine blades.

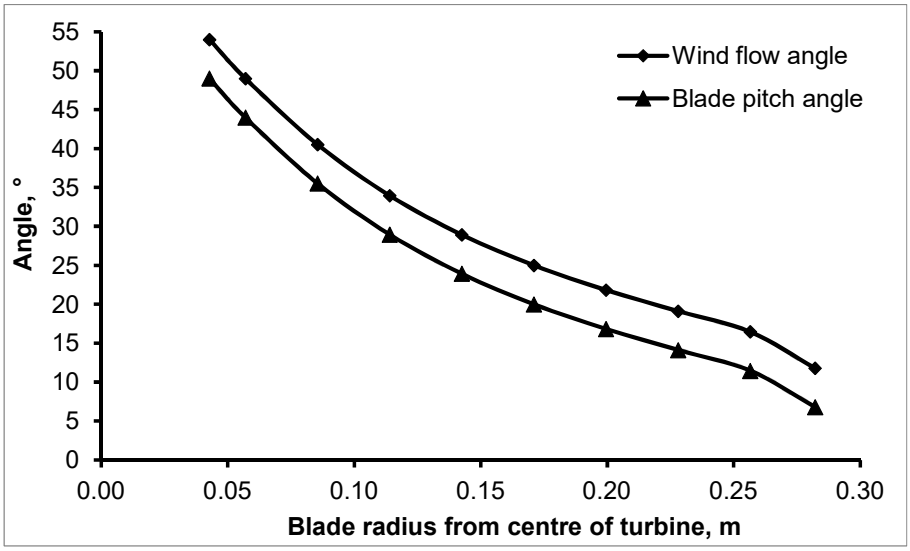

Fig. 3.13. Variation of φ and β with different blade segment radius.

3.5.4. Estimation of chord length distribution (*c*) of blade at each segment

Chord length distribution (*c*) at each segment of turbine blade for various aerofoils is shown in **Fig. 3.14**. In **Fig. 3.14,** the maximum *c* is achieved at first segment of the blade because the chord length of the blade is directly related to *sine* function (from Eq. 2.80) and also the maximum bending and shear stresses are developed at this section only. This *c* is maximum at root of the blade and is minimum at the tip of the blade which leads to narrow blade profiles. This leads to minimum material usage and lower production costs. Out of all the three types of turbine blades, the NACA 0012 has more *c* (0.09 m) at root section due to symmetric aerofoil nature.

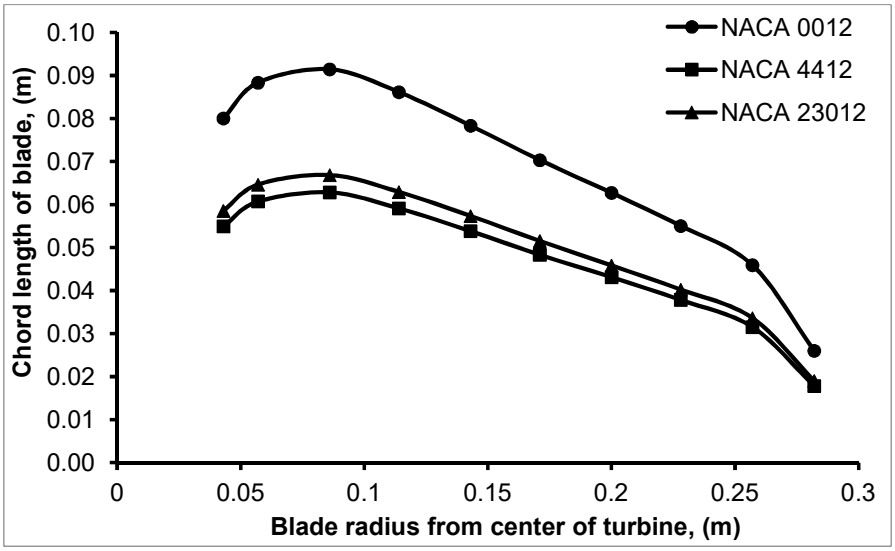

Fig. 3.14. Chord length of blade at each segment

3.6. Summary

A modest attempt was made to estimate the performance parameters of an SUT with the chimney and solar collector plate diameter of 0.6 m and 3.5 m respectively. From the theoretical analysis, the following conclusions were made:

- The average global radiation of year 2016 was estimated as 985 W/m^2.
- Inside the chimney, the air velocity was found in between 1.82 to 2 m/s.
- Maximum pressure drop inside the chimney was 1.065 N/m^2.
- The maximum theoretical power output of SUT was 0.633 W.
- The energy required for producing the power of 0.633 W was estimated as 80.64 kWh.
- As per the design of this present system, the maximum overall efficiency of the plant was estimated as 0.0028 %.
- If we need to achieve optimum efficiency of the plant, then the chimney height should be 27 km, which is impossible for all practical purposes.
- Maximum collector efficiency is obtained for the month of April and is 53.9 %.
- Optimised angle of attack for various turbine blades (NACA 0012, NACA 4412 and NACA 23012) was estimated as 5.5°, 5° and 7°, respectively.
- In order to extract maximum kinetic energy from wind, the required number of blades of a wind turbine was optimised as four.

- The wind flow angle ($\emptyset$), blade pitch angle (β) and chord length distribution (c) of blade at each segment were estimated. The maximum values of $\emptyset$, β and c of NACA 4412 turbine blade were estimated as 54°, 49° and 0.063 m. The minimum values of $\emptyset$, β and c of NACA 4412 turbine blade were estimated as 11.8°, 6.8° and 0.019 m. Similar kinds of values were noticed for remaining two turbine blades (NACA 0012 and NACA 23012).
- The maximum power produced by various wind turbines (NACA 0012, NACA 4412 and NACA 23012) was estimated as 0.59 W, 0.624 W and 0.61 W respectively.

Chapter 4

Results and discussion based on numerical analysis

Chapter 4

4. Results and discussion based on numerical analysis

This chapter is related to the results and discussion. Results obtained for heat transfer characteristics, flow and performance parameters from the numerical simulation are discussed first and the best shape (collector slope angle) and optimum dimensions of the final shape are finalized which is used for the development of the experimental set-up.

Numerical simulations were performed for all the three cases of SUT (case-I - both inclined collector cover and absorber plates with the inclination of 30°, case-II - inclined collector and horizontal absorber plates which was made with the collector inclination of 30° and case-III - both collector and absorber plates were horizontal). The governing equations such as continuity, momentum, energy, and radiation equations were solved and velocity, temperature, pressure and turbulent kinetic energy were estimated. The results are discussed in further sub-sections.

4.1. Results of case-I (both absorber plate and collector glass were inclined)

The contours of air velocity, temperature and turbulent kinetic energy were estimated for case-I and shown in **Figs. 4.1 to 4.3**. The profiles were plotted in X-Y plane and at the middle of the domain in z direction (z = 0). **Fig. 4.1 (a)** shows the velocity distribution of case-I. From **Fig. 4.1 (a),** it is observed that air velocity is gradually increased from the collector inlet to CB because of solar updraft effect. It is also observed that the velocity profile is almost symmetrical because of the symmetrical setup and constant inlet conditions. The maximum air velocity obtained at CB and is 3.06 m/s (with an average of 1.63 m/s). Air velocity nearer to the inner surface of the chimney is observed as minimum when compared to the centre of the chimney because, the air particles in contact with the surface of the chimney is almost zero (no slip condition). Average air velocity in the entire setup is 1.63 m/s and the average near the turbine region is 2.15 m/s.

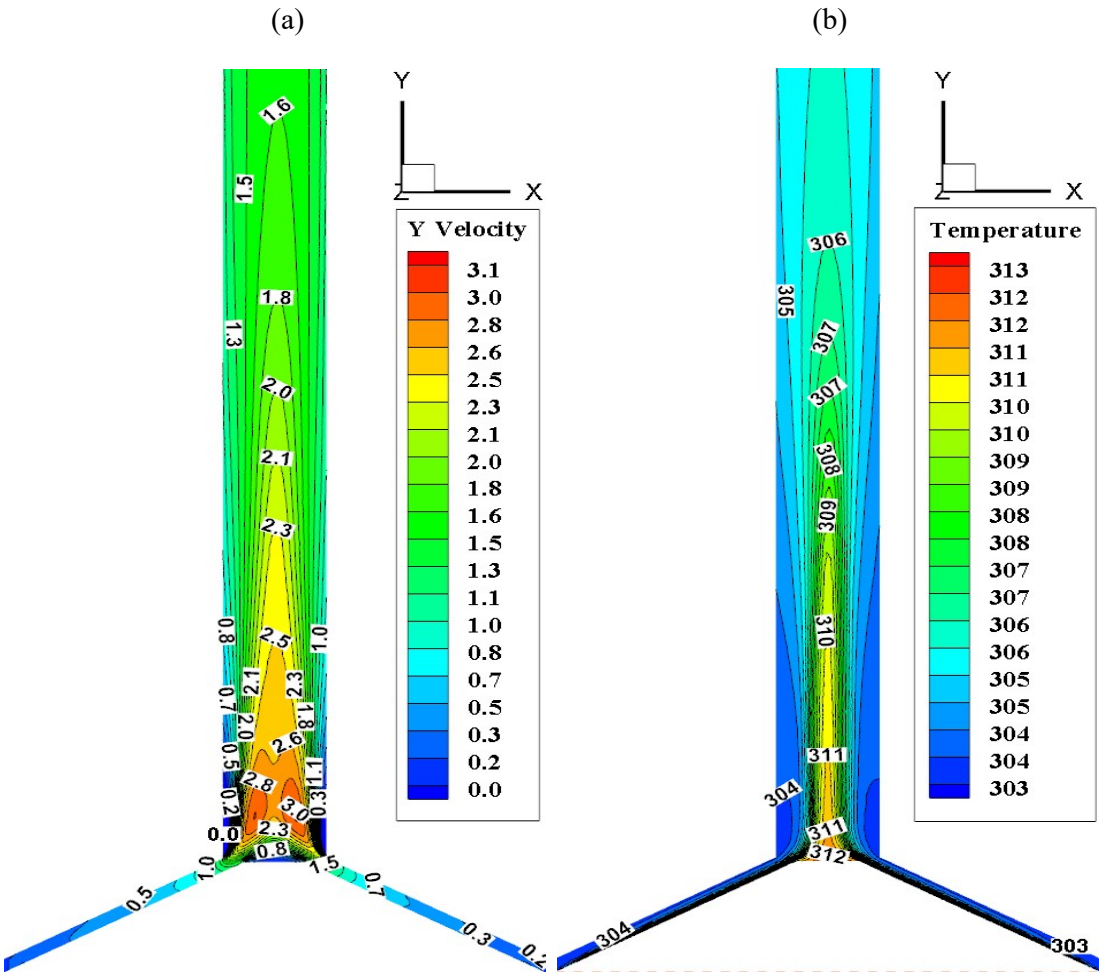

Fig. 4.1 (a) Velocity contour (m/s) and **(b)** temperature contour (K) inside the case-I

The air temperature inside the case-I is shown in **Fig. 4.1 (b).** From the collector inlet, the temperature increases gradually towards CB, because of absorber plate heats the air. Air temperature at inlet is assumed as 303 K and it is increased at CB with a maximum of 312 K. It is noticed that the air temperature is always maximum near central regions of chimney and minimum at boundary regions. A significant temperature drop occurs in air temperature near exit of chimney (305 K) because the chimney outlet is open to ambient air, so that heat transfer takes place from inside the chimney to outside air. Average air temperature inside SUT is 306 K. Temperature profile also looks symmetrical profiles as same as velocity profile (**Fig. 4.1 a**).

The variation of air velocity inside the chimney (in terms of line plot) at different heights with respect to the radial length of D_{ch} is estimated and plotted in **Fig. 4.2**. It is drawn to identify the height where the maximum velocity is achieved, so that the location of turbine

can be confirmed. It is seen that the air velocity reached a maximum and started to decrease at centre of the chimney at a height of 0 (on CB) and 0.1 m from CB. The air flows from all the directions from collector inlet to chimney through the inclined passage (in between absorber and collector plates) and reaches the middle of CB where the velocity is minimum as seen in the contour plot (**Fig. 4.1 a**). A similar nature was observed for the height of 0.2, 0.3 and 0.4 m (from CB, not shown in **Fig. 4.2**). In the height of 0.5 m, most of the chimney centre region (70% of region, **Fig. 4.2**) was occupied with more air velocity (approx. 2.7 m/s, with a maximum of 2.87 m/s and an average of 2.16 m/s). The height is increased beyond 0.5 m, the maximum velocity decreases as shown in **Fig. 4.2** because of decreased velocity gradient towards chimney height. Therefore, it is proved that a height of 0.5 m from CB is better for fixing the turbine to capture more kinetic energy from air inside the case-I.

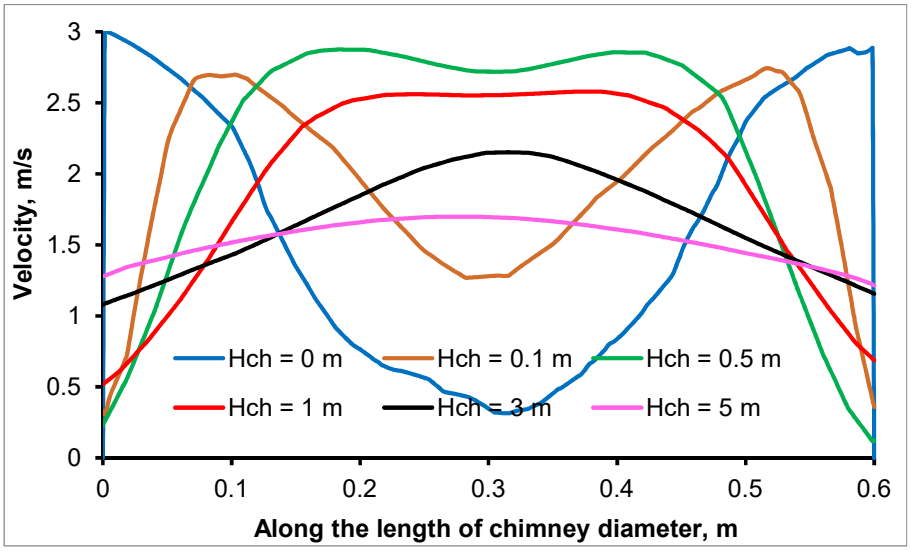

Fig. 4.2. Air velocity profiles along the radial length of D_{ch} for various heights of chimney (case-I).

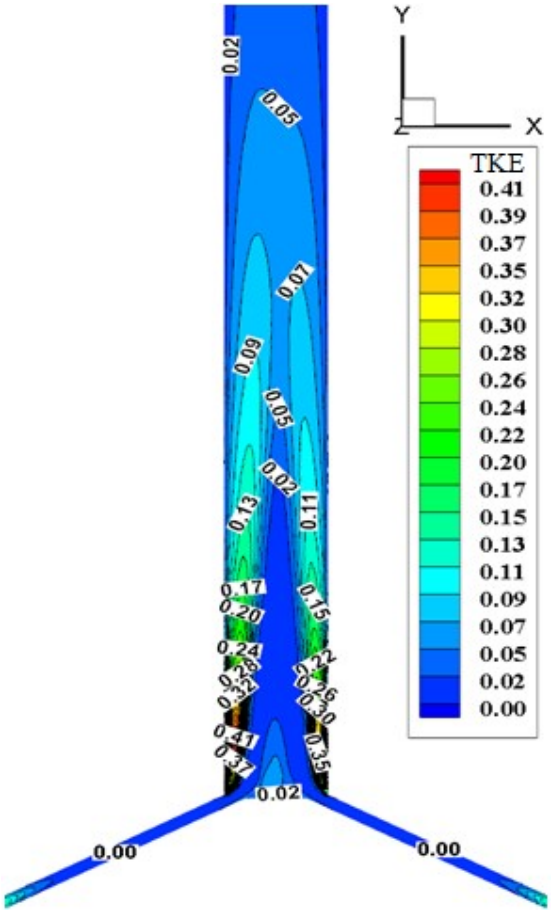

Fig. 4.3. Turbulent kinetic energy (m^2/s^2) of air inside case-I

Figure 4.3 shows the turbulent kinetic energy (TKE) distribution inside the case-I. TKE is a measure of strength of turbulence generation in air flow. It is noticed that a minimum TKE (0.0001 m^2/s^2) at the inlet of collector and a maximum (0.41 m^2/s^2) is on CB. The average TKE inside is 0.064 m^2/s^2 (for case-I).

Temperature distribution on the surface of absorber plate (for case-I) is estimated and shown in **Fig. 4.4** (top view of absorber plate). From **Fig. 4.4**, it is noticed that the majority portion of absorber plate (300 to 800 mm from the circumference) has experienced the maximum temperature range of 327 to 329 K because of continuous absorption of the radiant energy available inside the collector. Minimum temperature (314 K) is observed at centre of the absorber plate because it cannot absorb direct solar radiation as the shadow of chimney is fallen at centre of the absorber plate. Mean temperature of the plate is 326.2 K for case-I.

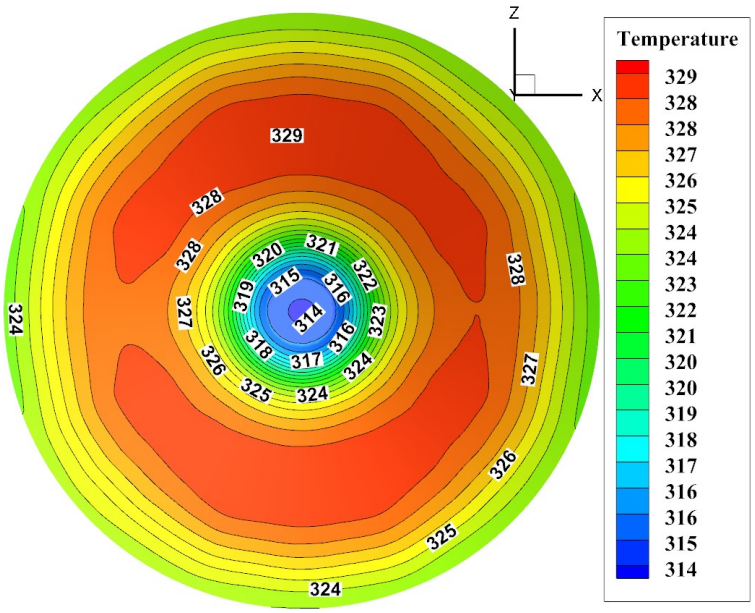

Fig. 4.4. Temperature distribution (in K) of absorber plate for case-I

4.2. Results of Case-II (inclined collector glass and horizontal absorber plate)

Velocity, temperature, pressure and TKE were estimated for case-II and the results are explained in this section. The contour plots were drawn at XY plane and at the centre of domain (z = 0).

Figure 4.5 (a) shows the velocity distribution inside the case-II. The velocity profile looks symmetrical near the canopy air region, but it deviates slightly from its symmetrical nature inside the chimney. The air velocity near CB is higher (with a maximum of 2.4 m/s) compared to other locations. Similarly, the air velocity at the centre of chimney is maximum compared to other locations. A similar maximum air velocity (2.2 m/s) is noticed at experimental and numerical study of AL-Kayeim et al. [80]. Ahmed and Patel [80]'s experimental setup also produced a similar maximum air velocity of 2.5 m/s. The average air velocity achieved inside SUT (case-II) is 1.34 m/s.

(a) (b)

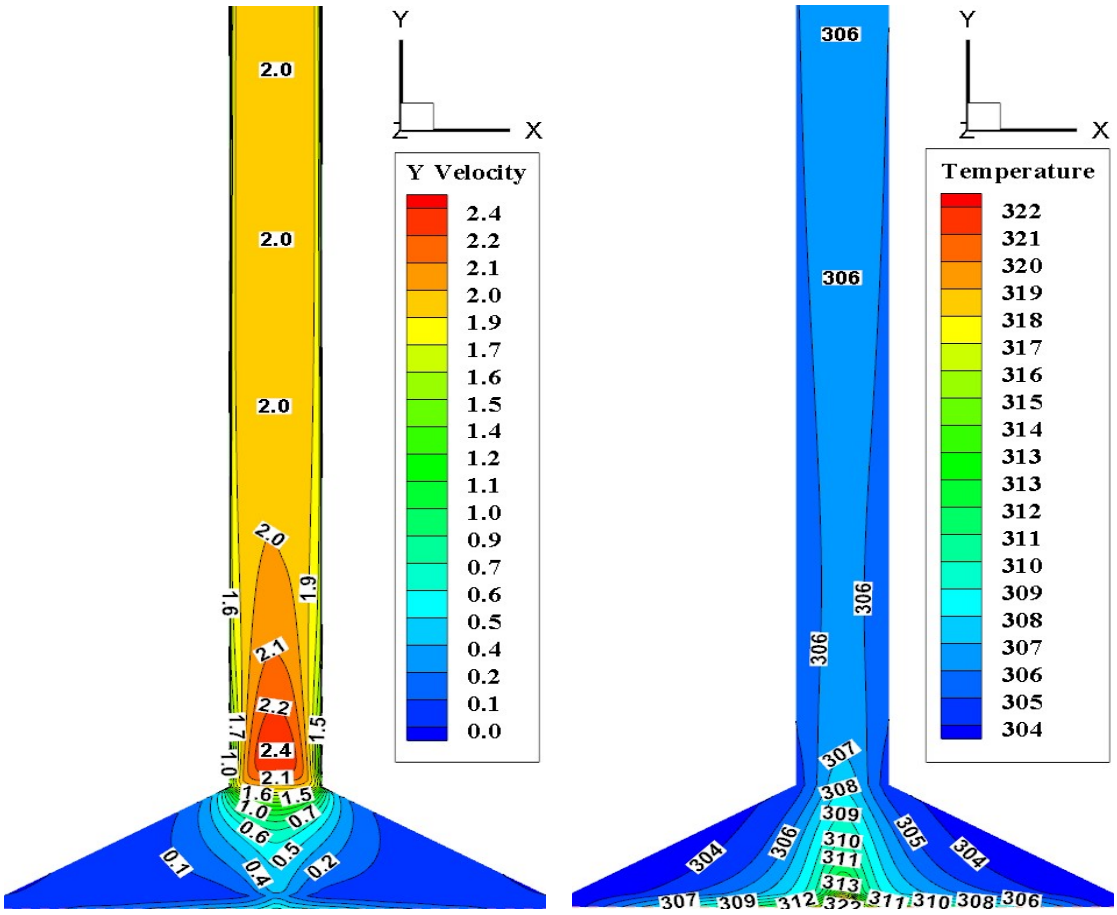

Fig. 4.5. (a) Air velocity (m/s) and **(b)** temperature (K) inside the case-II

The temperature contour of air inside the case-II is presented in **Fig. 4.5 (b)**. The temperature profile is also symmetrical in nature inside the canopy region and the symmetricity slightly varies inside the chimney region (**Fig. 4.5 b**) as same like velocity profile (**Fig. 4.5 a**). The temperature is lower at inner surfaces of the collector roof and chimney due to no slip condition. But temperatures of air at interior regions are gradually increasing because of solar radiation and subsequent heat transfer from absorber plate to air. Maximum temperature of air (322 K) is attained near the centre of absorber plate because inclined collector cover transmits more solar radiation near the centre of absorber plate and therefore, the absorber plate transfer the heat to air which surrounds the centre of absorber plate. The air temperature reduces to 307 K (approximately) when it rises up from the absorber plate to CB because fresh air enters inside the setup. A significant reduction in air temperature (from 322 K to 306 K) is noticed when the location moves towards H_{ch} because at chimney outlet, the air temperature is ambient condition (300 K). At CB a rise in air temperature (ΔT) of 19 K is noticed. A similar difference of air temperature is observed (15 K) in the study of AL-

Kayeim et al. [80] at the solar radiation of 850 W/m^2. A similar nature of air temperature contours are noticed at Lal et al. [44] with the minimum and maximum temperatures 300 K and 320 K.

Figure 4.6 shows the air velocity inside the chimney at different local heights along the length of D_{ch} (case-II). It is found that the air velocity is maximum at centre of the chimney for the cases of H_{ch} of 0.2, 0.5 and 1 m. The average velocity at different heights of H_{ch} = 0, 0.2, 0.5, 1, 2 and 5 m are 1.88, 2.03, 2, 1.92, 1.87 and 1.86 m/s, respectively. The maximum air velocity (2.34 m/s) is found in H_{ch} of 0.2 m. Also, the maximum velocity range of 2.2 to 2.34 m/s is found in H_{ch} range of 0.1 to 0.5 m. Almost 75% of chimney cross section area has the maximum air velocity at the location of H_{ch} of 0.1 to 0.5 m and hence, the turbine can absorb more kinetic energy from the air in this location. Therefore, H_{ch} range of 0.1 to 0.5 m is the preferable location for turbine location in case-II.

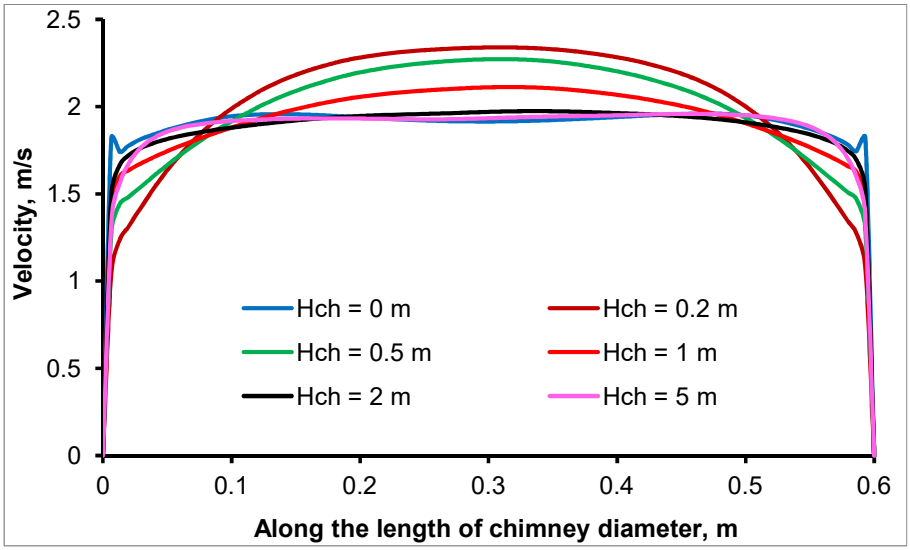

Fig. 4.6. Air velocity profiles along the radial length of D_{ch} for various local heights of chimney (for case-II)

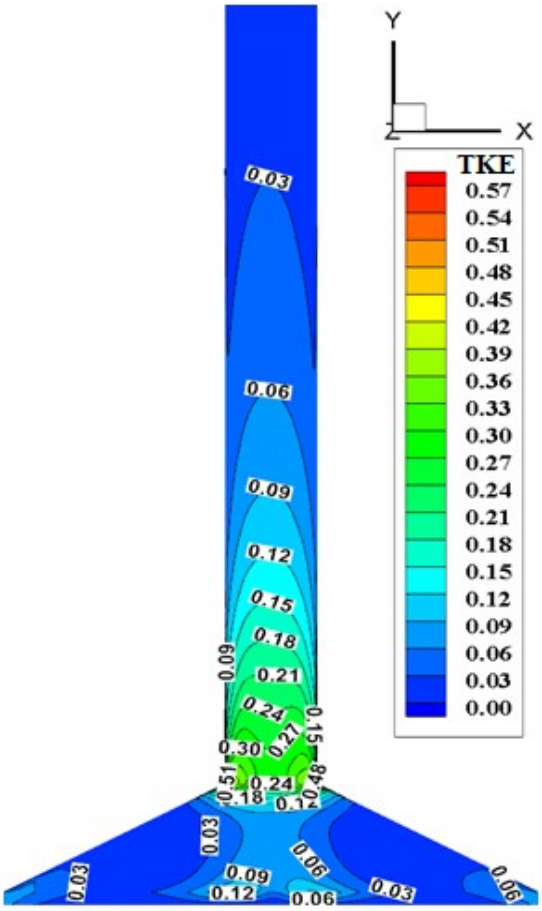

Fig. 4.7. Turbulent kinetic energy (m^2/s^2) of air in case-II

Figure 4.7 shows that TKE inside case-II. TKE is in the range of 0.002 to 0.574m^2/s^2. A higher TKE is noticed at CB region because of higher air flow velocity near this region as discussed in **Fig. 4.5 (a)**. The average TKE inside the case-II is 0.074m^2/s^2.

Temperature distribution on the surface of absorber plate (for case-II) is shown in **Fig. 4.8**. The absorber plate temperature is minimum (331 K) on the outer periphery region because of fresh air enters inside the setup and the temperature is gradually increasing towards the centre of setup. The maximum temperature of 335.7 K is noticed at the centre. The average temperature of the absorber plate is 332.7 K.

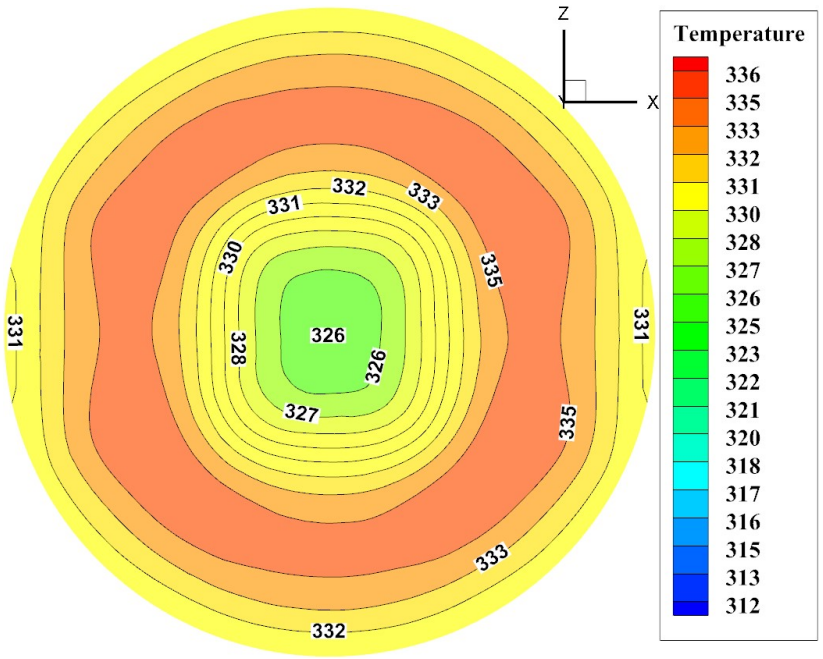

Fig. 4.8. Temperature of absorber plate for case-II

4.3. Results of Case-III (both collector glass and absorber plate are horizontal)

The results of case-III is presented in this section. All the contour plots were drawn in the XY plane and at middle of the setup.

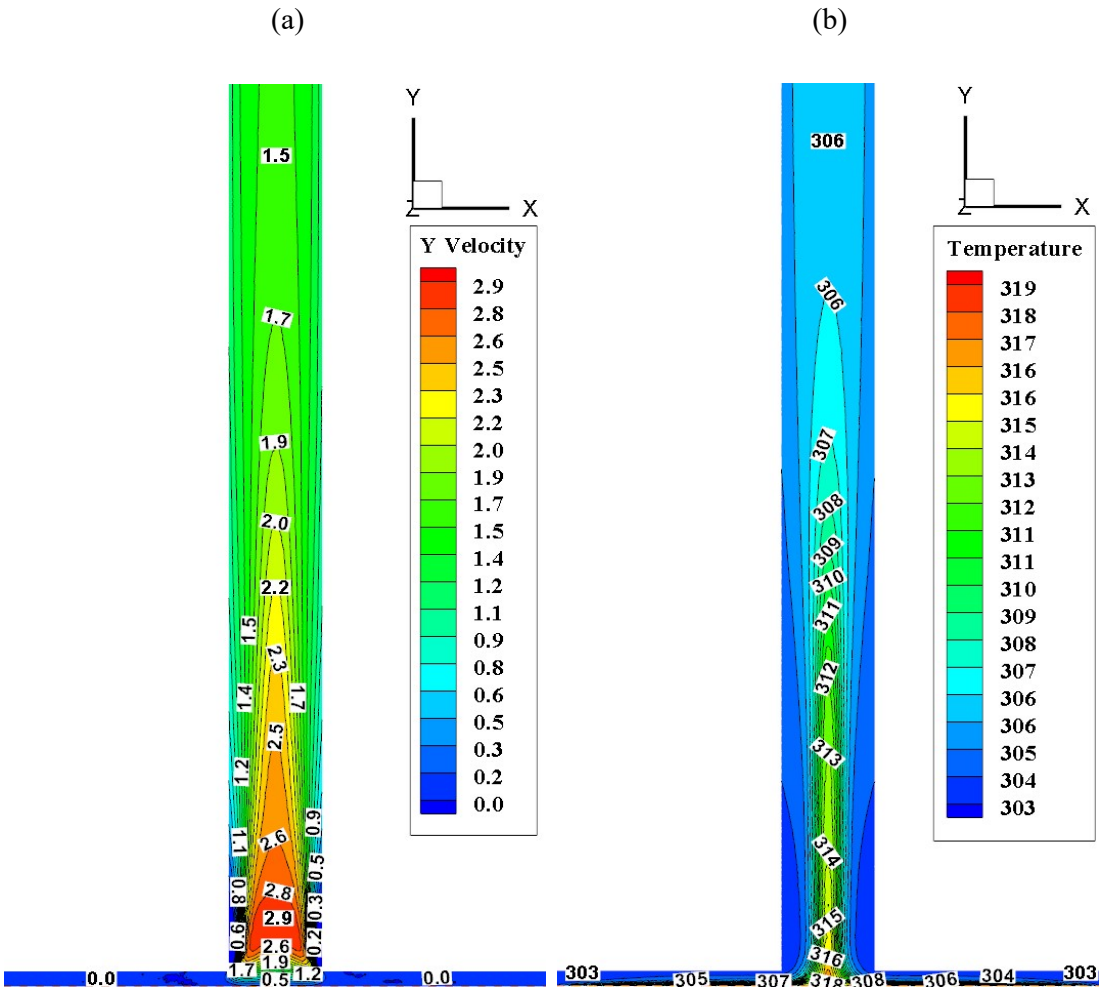

Fig. 4.9. (a) Velocity (m/s) and **(b)** temperature (K) contours of case-III

The velocity contour for case-III is estimated and shown in **Fig. 4.9 (a)**. The velocity profile almost looks like a symmetrical profile as the setup is also symmetry. The air velocity is maximum (2.9 m/s) near to CB because of more nozzle effect as the distance between the surface of absorber plate and CB is 0.1 m. The average air velocity inside the case-III is estimated using area weighted average method and is 1.57 m/s. A similar type of horizontal collector and absorber plate setup was developed by Ayadi et al. [6] and found the velocity distribution. They reported that the air velocity was in the range of 0 to 2.13 m/s.

Similarly, the temperature distribution inside the case-III is estimated and shown in **Fig. 4.9 (b)**. It can be seen that the air temperature is higher (318 K) at the centre region of the absorber plate. The average air temperature is 306.3 K inside the case-III. Air temperature inside the setup of Nasraoui et al. [82] was in the range of 308 to 326.74 K. Also, the maximum air temperature of Ayadi et al. [6] was 322 K. The maximum air temperature of

present study's case-III is 321 K which is almost equivalent to above studies of Nasraoui et al. [82] and Ayadi et al. [6].

The air velocity inside the setup of case-III at different heights were estimated and plotted in **Fig. 4.10**. It is observed that the air velocity increases when H_{ch} increases from 0 to 0.3 m because of nozzle effect near CB as already explained in **Fig. 4.9 (a).** It decreases for further increase of H_{ch}. The air velocities are almost same at H_{ch} of 0.4 m (not shown here) and 0.5 m. The average air velocity of 1.83 m/s is noticed at H_{ch} of 0.3 and 0.4 m, respectively. The maximum air velocities are 2.92 and 2.87 m/s at H_{ch} of 0.3 and 0.4 m, respectively. Therefore, in this region (H_{ch} of 0.3 and 0.4 m), the turbine can be fitted for extracting more kinetic energy from air flow.

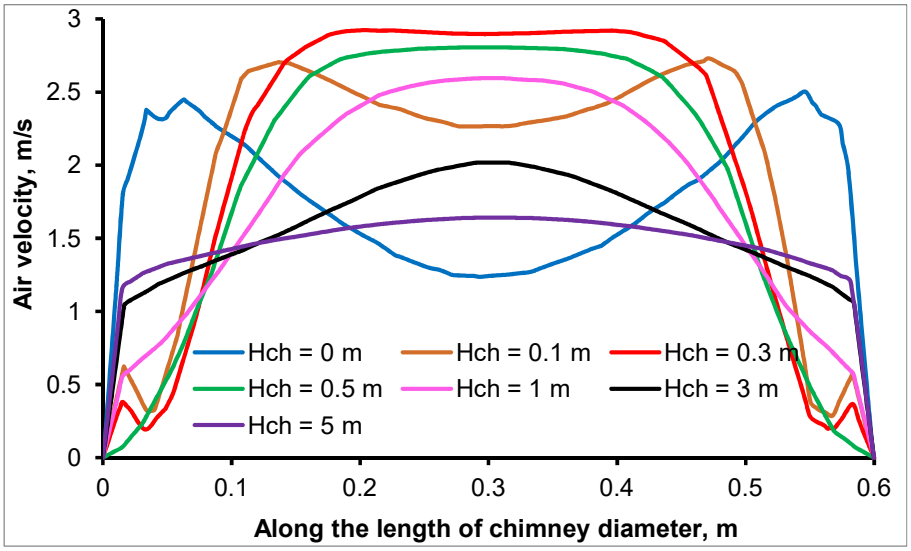

Fig. 4.10. Air velocity profiles along the radial length of D_{ch} for various heights of chimney (for case-III)

(a) (b)

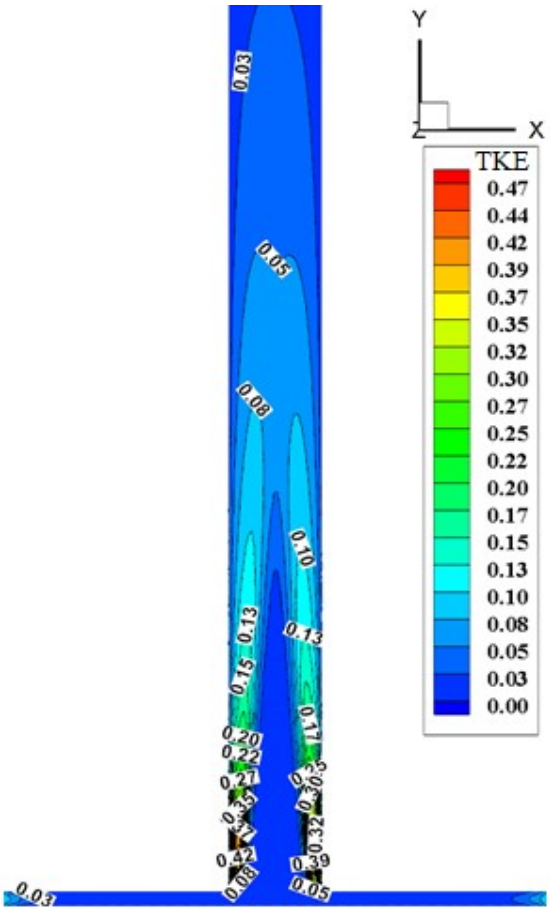

Fig. 4.11. Turbulent kinetic energy (m^2/s^2) of air inside case-III

The TKE contour of case-III is shown in **Figs. 4.11**. It is observed that a minimum of TKE (0.003 m^2/s^2) is at the inlet of collector and a maximum (0.47 m^2/s^2) is at CB with an average of 0.06 m^2/s^2. The contours of TKE inside the setup of Ayadi et al. [6] were noticed in the range of 0.00012 to 0.4 m^2/s^2.

Temperature distribution on the absorber plate for case-III is estimated and is shown in **Fig. 4.12**. A maximum temperature (335 K) of absorber plate is noticed at a location from 500 to 1150 mm away from the outer periphery. A minimum temperature of absorber plate (326 K) is observed at the outer periphery because of fresh air enters inside the system. Mean temperature of the plate is 331.1 K. Fadaei et al. [83] reported a similar absorber temperature (maximum of 343 K) and they used concrete cement as absorbing material.

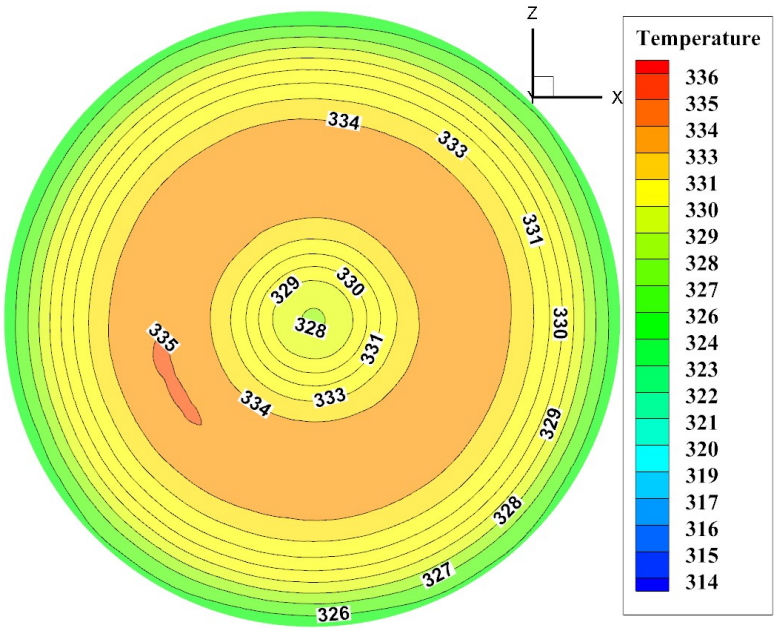

Fig. 4.12. Temperature of absorber plate for case-III

4.4. Results comparison of model – I, model – II and model - III

The minimum, maximum and average flow properties of case-I (both inclined collector and absorber plates), case-II (inclined collector plate and horizontal absorber plate) and case-III (both horizontal collector and absorber plates) were estimated and mentioned in **Table 4.1.** Also, the performance parameters are estimated for all the three cases and tabulated in **Table 4.2.** It is seen from **Table 4.1** that the maximum air velocity of 3.06 m/s (average of 1.63 m/s) is noticed for case-I, followed by case-III (2.9 m/s, average of 1.57 m/s) and case-II (2.4 m/s, average of 1.34 m/s). The maximum velocity of case-II is low (2.4 m/s) because higher volume of air is available in case-II (refer **Table 4.2**) below the collector plate compared to case-III and case-III, therefore, residence time of air flow is more, so that it freely expands inside the canopy.

Maximum air temperature inside case-I is low (312 K, average is 305.8 K) compared to other case-II (322 K, average is 306 K) and case-III (318K, average is 306.3 K) because of less air stagnant time when the air flows through the collector and chimney.

Maximum turbulence kinetic energy (TKE) of case-II is higher (0.574 m^2/s^2, with an average of 0.074 m^2/s^2) compared to case-I (0.41 m^2/s^2, with an average of 0.064 m^2/s^2) and case-III (0.47 m^2/s^2, with an average of 0.06 m^2/s^2). The hot air enters through all the 360° outer periphery of collector inlet and flows through the horizontal passage and merges near the

region of CB, therefore, the average TKE is more for case-II compared to other two models. TKE is one of the essential parameter inside the chimney. If TKE is more, the turbine can absorb more kinetic energy, so that power output of the system would increase. The average absorber plate temperature is higher in case-II (332.7 K) because of 30° collector angle inclination (as per Warangal, India's latitude). Mass flow rate of air is low in case-III (0.45 kg/s, as mentioned in **Table 4.1**) compared to case-I (0.554 kg/s) and case-II (0.59 kg/s). The heat which is trapped in the absorber plate is not carried frequently because of low mass flow rate in case-I and case-III and difficulties in air flow in between the absorber and collector plates, therefore, average absorber plate temperature is more in case-II. It shows that the chimney drags more quantity air through the inlet gap of case-II than other two models.

Table 4.1: Flow parameters and heat transfer characteristics of SUT

Parameters	case-I			case-II			case-III		
	Min	Max	Av.	Min	Max	Av.	Min	Max	Av.
Air velocity, (m/s)	0	3.06	1.63	0	2.4	1.34	0	2.9	1.57
Temperature of air inside the setup (K)	303	312	305.8	303	322	306	303	318	306.3
Turbulent kinetic energy, (m^2/s^2)	0.0	0.41	0.064	0.002	0.574	0.074	0.003	0.47	0.06
Temperature of absorber plate, (K)	314	329.2	326.2	325.6	335.7	332.7	325	335	331.1
Average mass flow rate of air at collector inlet (kg/s)	0.554			0.59			0.45		
Average volumetric flow rate of air at collector inlet (m^3/s)	0.492			0.52			0.4		

From **Table 4.2**, it is observed that the maximum power output of case-II is higher (0.51 W) than case-I (0.4 W) and case-III (0.22 W). Similarly, the maximum overall efficiency of case-II is higher (0.006 %) than other two models (0.005% for case-I and 0.003% for case-III).

Table 4.2: Estimated output parameters (maximum) of different models of SUT

	Case-I	**Case-II**	**Case-III**
Air velocity near turbine (m/s)	2.98	2.4	2.82
Volumetric flow rate of air inside chimney (m^3/s)	0.843	0.68	0.796
Relative total pressure at chimney base (P_a)	0.47	0.75	0.27
Power output (W)	0.4	0.51	0.22
Chimney efficiency (%)	0.0187	0.0182	0.0184
Overall SUT efficiency (%)	0.005	0.006	0.003

4.5. Results validation

The numerical results are compared with existing literature of various small scale SUT's and mentioned in **Fig. 4.13** and **Tables 4.3 and 4.4.** The temperature profile of air (10 mm above absorber plate surface) inside the case-III is compared with that of Ayadi et al. [6] model as this model also made with horizontal absorber and collector plates. The temperature range of case-III (303.04 to 318.05 K) is matching with Ayadi et al. [6] result (305.2 to 318.6 K) as presented in **Fig. 4.13.** Also, the trend of temperature profile of the present model is same as Ayadi et al. [6] model.

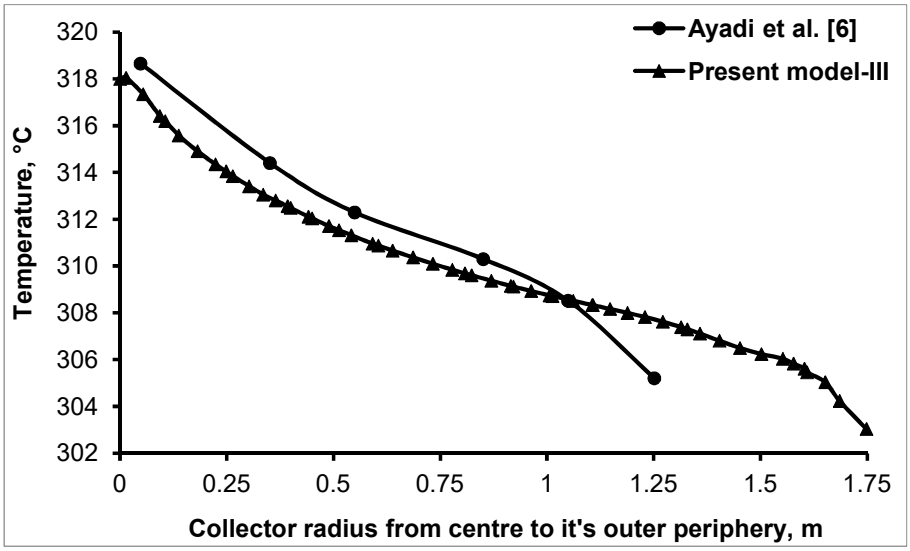

Fig. 4.13. Air temperature inside collector (10 mm above absorber plate surface)

Few of the available parameters from literature are compared with the present results of case-II (**Table 4.3**). The maximum velocity of case-II (2.4 m/s) is almost similar in the studies of Ahmed and Patel [81] (2.5 m/s) and Al-Kayeim et al. [80] (1.8 m/s). The chimney efficiency (η_{ch}) of Lal et al. [44] was 0.025% as its H_{ch} was 8 m, whereas η_{ch} of present case-II is 0.0182 %. The power developed by case-II is 0.51 W whereas, Ahmed and Patel [81] model gave 0.15 W [81] as H_{ch} of the setup was 4 m.

Table 4.3: Comparison of simulated and estimated parameters of model-II with existing literature.

	D_{ch} (m)	H_{ch} (m)	D_c (m)	Maximum temperature (K)	Maximum velocity (m/s)	Chimney efficiency (%)	Power (W)
Al-Kayeim et al. [80]	0.15	6	6	324	1.8	--	--
Ahmed and Patel [81]	0.37	4	3.2	321.3	2.5	--	0.15
Lal et al. [44]	0.2	8	12	318	--	0.01	-
Present model-II	0.6	6	3.5	322	2.4	0.0182	0.51
Present theoretical model	0.6	6	3.5	324.2	2.1	0.0195	0.63

The maximum temperature, maximum velocity and TKE range of case-III were compared with existing studies and mentioned in **Table 4.4.** The maximum temperature inside the setup of case-III (323 K) is almost same with the studies of Ayadi et al. [6] (322 K) and Nasraoui et al. [82] (326.7 K). The maximum velocity of Nasraoui et al. [82] was 2.41 m/s (with H_{ch} of 2.95 m) whereas the present case-III has 3.2 m/s as H_{ch} of case-III is 6 m. Overall, the results of present model is quite convincing with existing results.

Table 4.4: Comparison of estimated parameters of model-III with existing literature.

Studies	D_{ch} (m)	H_{ch} (m)	D_c (m)	Maximum temperature (K)	Maximum velocity (m/s)	Turbulent kinetic energy range (m^2/s^2)
Ayadi et al. [6]	0.16	3	2.75	321	2.13	0.00012 to 0.4
Nasraoui et al. [82]	0.154	2.95	3.7	326.7	2.41	0 - 0.8
Present case-III	0.6	6	3.5	318	2.9	0.003 – 0.47

4.6. Summary

A numerical investigation was carried out for the computation of flow and heat transfer characteristics of various SUT models (case-I - inclined absorber and collector plates, case-II– inclined collector and horizontal absorber plates and case-III– horizontal absorber and collector plates). All the three cases were generated using ANSYS FLUENT 16.0 design modeller. Each and every cases, the flow and performance parameters were studied. The following conclusions were drawn.

- The maximum air velocities were obtained at chimney base (CB) and these were 3.06, 2.4 and 2.9 m/s for case-I, case-II and case-III, respectively.
- The maximum air velocity is found at 0.5 m above CB for case-I. For case-II, it is found in the range of 0.1 to 0.5 m from CB and for case-III, it is from 0.3 to 0.4 m. Therefore, these are the preferred locations for fixing the turbine.

- The maximum air temperatures were estimated and these were 312 K for case-I (near CB), 322 K for case-II and 318 K for case-III (just above the absorber plate).
- The maximum power output of case-II is higher (0.51 W) than case-I (0.4 W) and case-III (0.22 W).
- Similarly, the maximum overall efficiency of case-II is higher (0.006 %) than other two models (0.005% for case-I and 0.003% for case-III).

Comparing all aspects, the case-II could produce maximum average TKE, average volumetric flow rate and relative total pressure than other two models. Power output and overall system efficiency are also higher in case-II. Therefore, it is suggested that case-II can be preferred while erecting SUT setup as it gives better performance.

Chapter 5

Results and discussion based on experimental analysis

Chapter 5

5. Results and discussion – Experimental part

The results and discussions are carried out for the experimental work where the performance of the SUT is estimated. Also, the variation of different parameters such as air velocity, pressure, temperature, mass and volumetric flow rates, relative total pressure (or) pressure drop across the turbine, global solar radiation falls on collector, rotational speed of turbine, temperature of absorber plate and thermal energy storage medium with time is explained. Uncertainty analysis is added in this chapter.

Solar intensity, temperature of air, absorber plate and TES system, air pressure, and velocities at different locations were measured and all the results are discussed in this section. These parameters were measured for 24 h and saved in multi-channel data logger. The experiments were carried out for a period of 10 days (16th to 25th Mar. 2019). Almost similar ranges of parameters were observed on all these days. A brief analysis of the experimental data collected on 23rd March 2019 (from 6:00 AM to 6:00 PM) is presented in this paper.

5.1. Variation of solar radiation with time

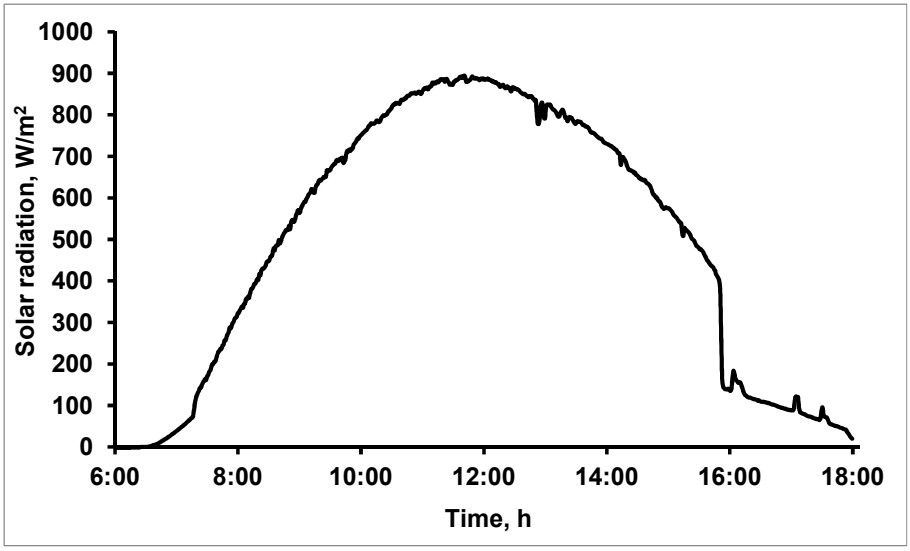

Fig. 5.1. Variation of global solar radiation with respect to time

Figure 5.1 shows that the variations of solar heat flux which falls on collector cover with respect to time from 6:00 AM to 6:00 PM on 23rd March 2019. The maximum solar radiation

was obtained just before the noon and was 894 W/m^2. The average solar radiation from 7:00 AM to 6:00 PM was 534.5 W/m^2.

5.2. Temperature distribution on absorber plate

The temperature distribution on absorber plate (on south side) is taken and mentioned in **Fig. 5.2.** Variation on temperature of absorber plate is directly proportional to solar radiation, therefore, the temperature of the absorber plate is gradually increasing and reaches a maximum value and again starts decreasing when solar intensity reduces during afternoon session. These readings were taken at three locations - 300, 800 and 1300 mm from the collector inlet. The temperature readings at 300 mm from collector plate are lower because interaction of fresh air from collector inlet and it increases when the location moves away from the collector inlet. The maximum temperatures of 64.5°C, 68.8°C and 67.4°C were noticed at 300, 800 and 1300 mm, respectively, from collector inlet. Similarly, the average temperatures are 43.98°C, 46.93°C and 47.78°C at the same locations (6.00 AM to 6.00 PM).

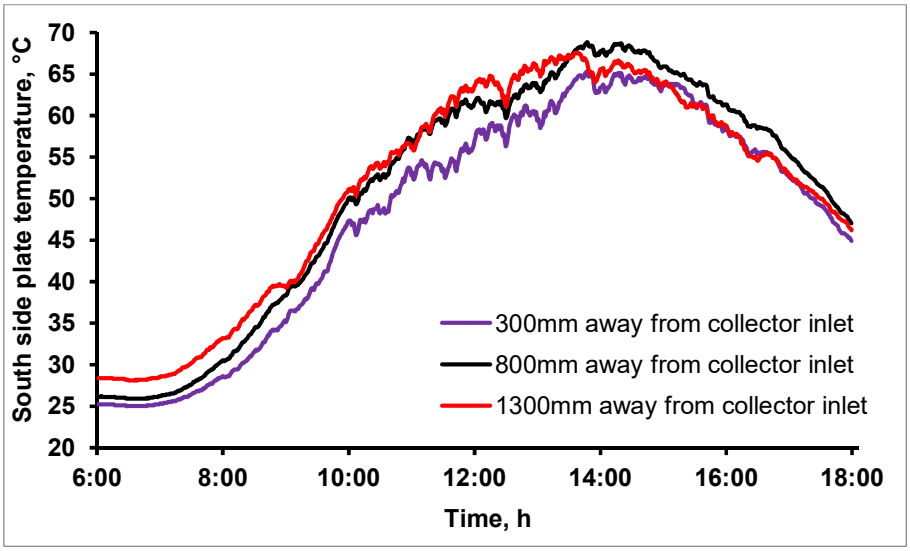

Fig. 5.2. Temperature of absorber plate (in south side)

Similarly temperature distributions of absorber plate at north, west, east sides were measured and mentioned in **Figs. 5.3-5.5**, respectively. **Fig. 5.3** shows the north side of absorber plate temperature. A similar variation as already explained in **Fig. 5.2** is noticed here also. But a gradient is noticed from 300 to 800 mm location because air flow direction on 23rd March 2019 was from north to south. The maximum temperatures of the plate at north were 48.7°C,

65.1°C and 66.3°C at 300, 800 and 1300 mm from the collector inlet, respectively. There is a small temperature drop from noon to 1.15 PM at 800 and 1300 mm locations (**Fig. 5.3**) because the shadow of the wooden cone falls on these locations.

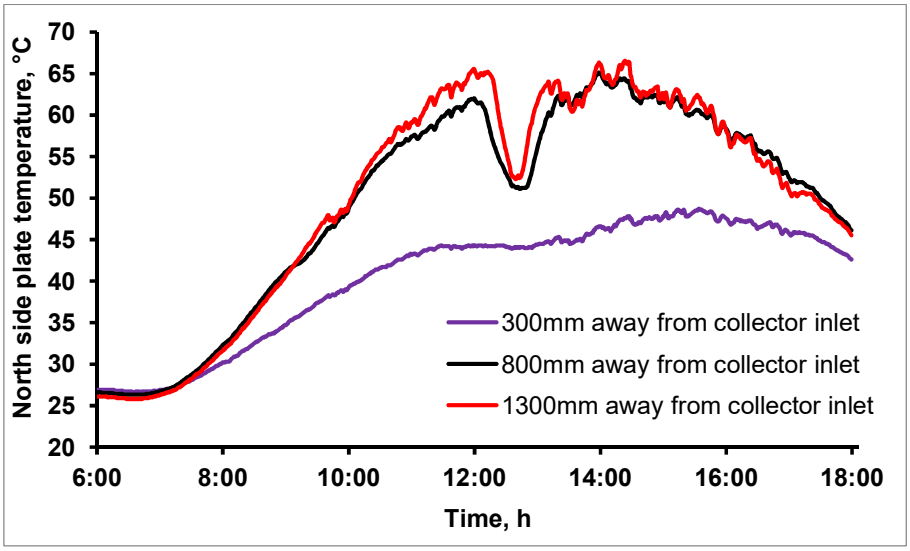

Fig. 5.3. Temperature of absorber plate (in north side)

Figure 5.4 shows the temperature data recorded along the radius of west side absorber plate with respect to time. The results are slightly different in **Fig. 5.4** than **Figs. 5.2** and **5.3**. The maximum temperature is obtained at 800 mm at noon. The temperature at 1300 mm is lower than at two other locations (300 and 800 mm) because the west side plate absorbs lower solar radiation during morning session as the sun rises in the East. The shadow of wooden cone and guide vanes also are reasons for low temperature at this location. At afternoon, the temperature of the plate increases and reaches to peak value 74.8°C because of conduction heat transfer on this copper plate.

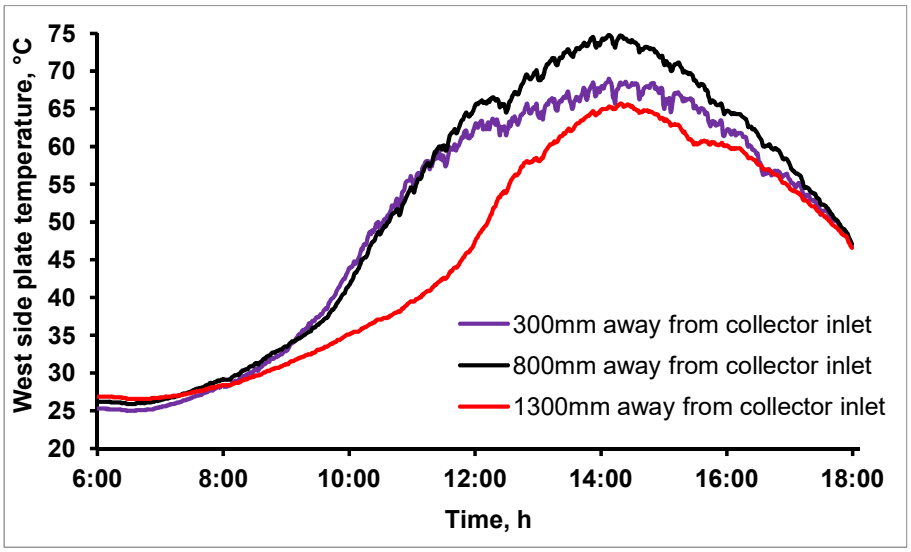

Fig. 5.4. Temperature of absorber plate (in west side)

Figure 5.5 shows the temperature measured at east side of absorber plate. The temperature at the outer periphery of the collector (300 mm away from collector inlet) is lower than the temperature of plate 800 mm away from the collector inlet because of exposure to fresh air. The maximum temperature of the absorber plate at east side is 67.7°C, 70.2°C and 66.9°C at 300, 800 and 1300 mm from collector inlet, respectively.

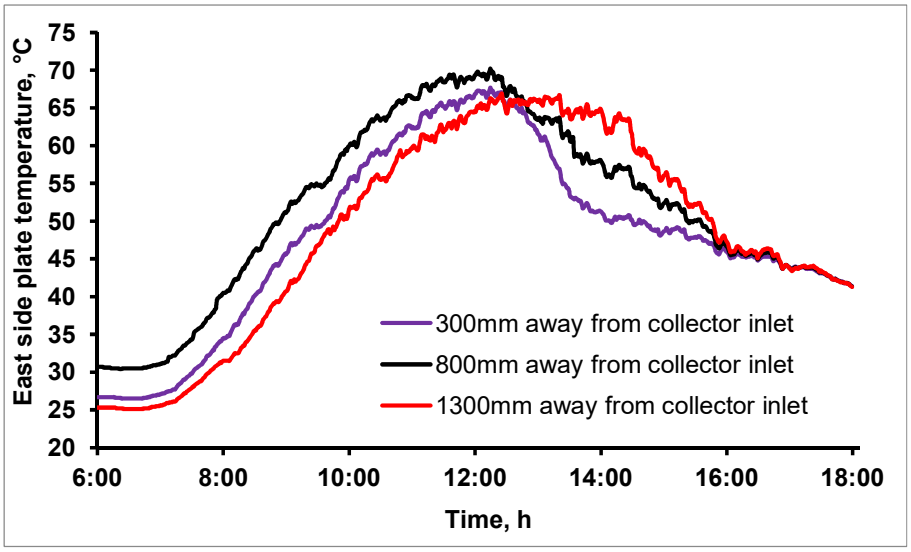

Fig. 5.5. Temperature of absorber plate (in east side)

Absorber plate temperatures in all the four directions were drawn at a distance of 300 mm (**Fig. 5.6),** 600 mm (**Fig. 5.7**) and 1300 mm from collector inlet (**Fig. 5.8**). At morning, the

north side absorber plate absorbs very little radiation compared to south and east side plates (**Figs. 5.6-5.8**). The temperatures on the south side plate are a little higher than the north side plate because the plant is located in northern hemisphere. The west side absorber plate temperature 1300 mm away from the collector inlet is lower than temperatures at other three sides of the same location (**Fig. 5.8**) because it absorbs little solar radiation during morning due to sun rises in the East. The shadows of the wooden cone and the guide vanes also are the reason for low temperature in this location. During the second half of day time, the plate temperatures on the east side (all three locations) starts to decrease because sun moves from east to west in the second half.

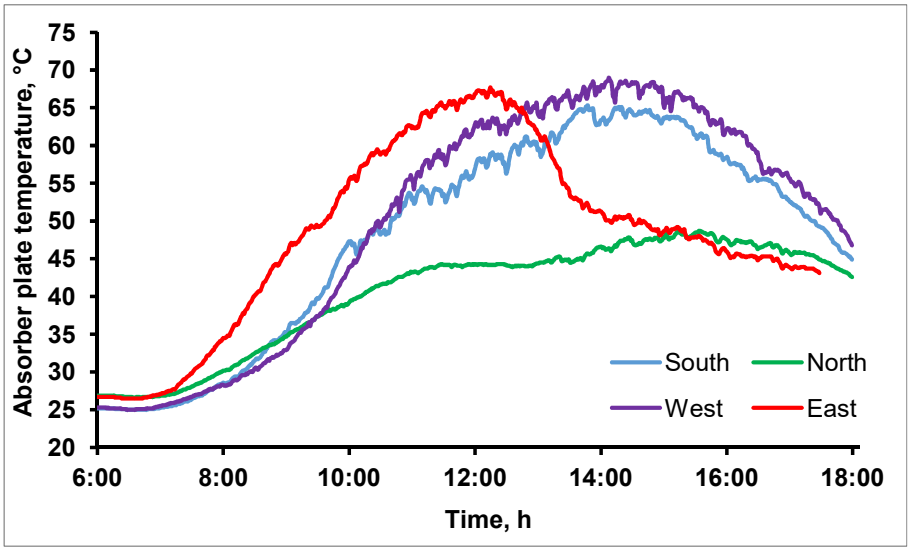

Fig. 5.6. Temperature of absorber plate at 300 mm away from collector inlet (all sides)

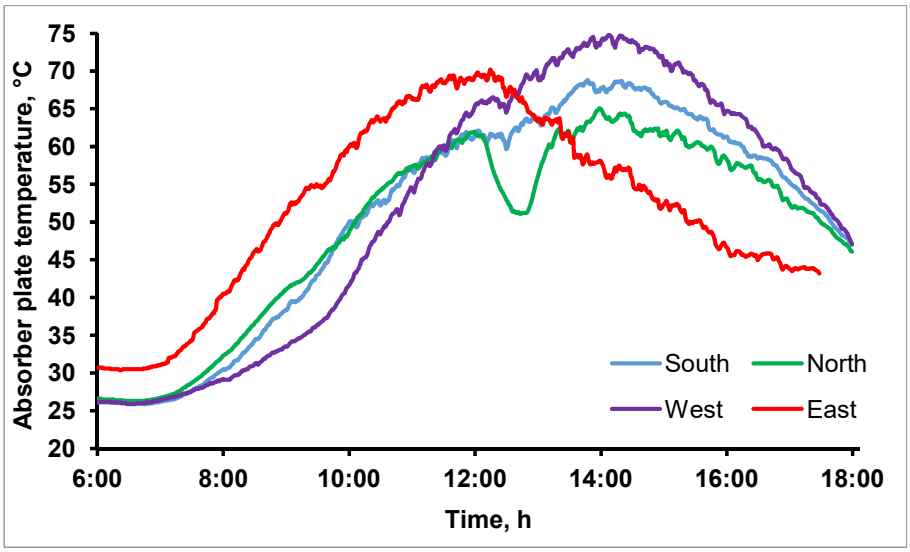

Fig. 5.7. Temperature of absorber plate at 800 mm away from collector inlet (all sides)

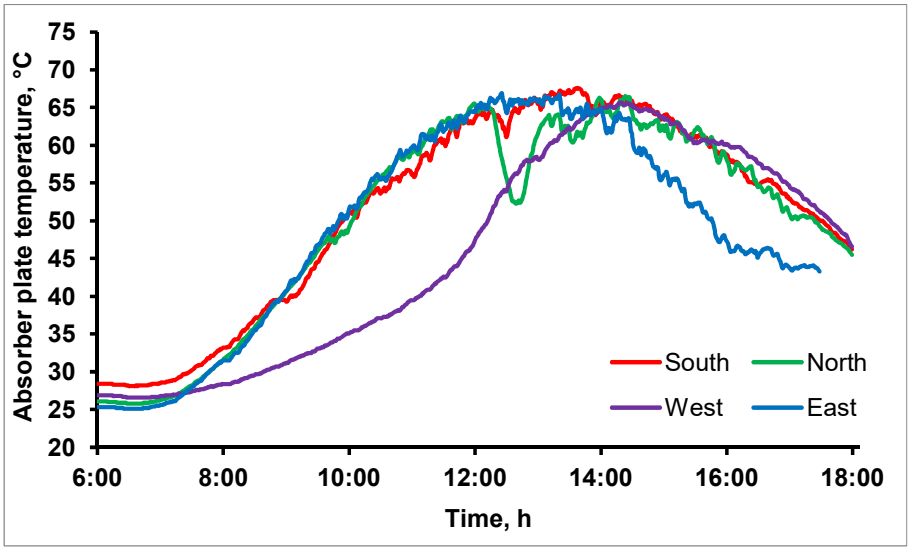

Fig. 5.8. Temperature of absorber plate at 1300 mm away from collector inlet (all sides)

5.3. Air temperature variation inside the plant, collector glass and TES system

Figure 5.9 shows the air temperature inside the chimney at different location such as below and above the turbine (200 mm from the turbine rotation plane) and near the chimney outlet. There is not much variation in air temperature below and above the turbine rotational plane in the first half of day. In the second half of the day, a marginal air temperature difference is observed at below and above the turbine. The maximum air temperature noticed was 45.6 °C

and 46.2 °C below and above the turbine at 14:18 h (2.18 PM) and 15:14 h (3.14 PM). The average air temperatures at the above locations were 38.86°C and 39.5°C from 7.00 AM to 6.00 PM. The air temperature at the exit of chimney can be considered as an ambient temperature because this location is very near to open air on top of chimney. This temperature is lower than air temperatures below and above the turbine because air near the turbine is heated because of absorber plate and solar radiation. The maximum air temperature difference between ambient and inside chimney (200 mm above turbine) is 12°C at noon.

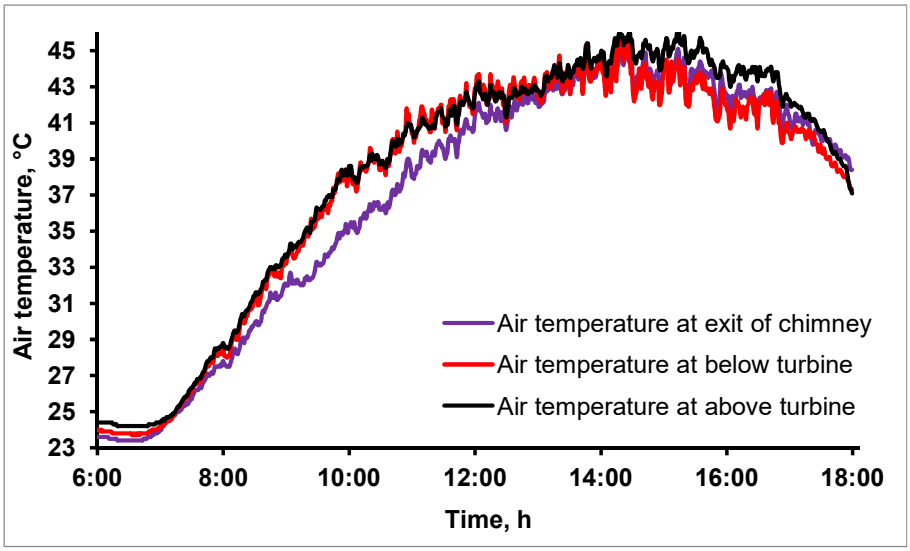

Fig. 5.9. Air temperature variation inside SUT with respect to time

Figure 5.10 shows the collector surface temperature and air temperature inside the collector at two different locations such as west and east side and at the middle of collector. The collector plate temperature is increasing and reaches maximum value and then decreases because of solar intensity. The maximum range of temperature (49.9 to 53.3°C) of collector glass plate is almost maintained from 10.30 AM to 2.15 PM. The average glass plate temperature is 43.28°C from 7.00 AM to 6.00 PM. A similar nature of variation is found in air temperature in the west and east sides. Also, it is observed that both temperature profiles are almost equal in the two sides. It proves that the air inside the SUT plant is uniformly heated for a particular instant of time. The maximum air temperature difference between ambient and inside collector is noticed as 11.4°C, which proves that the absorber plate and solar radiation heat the air inside the setup.

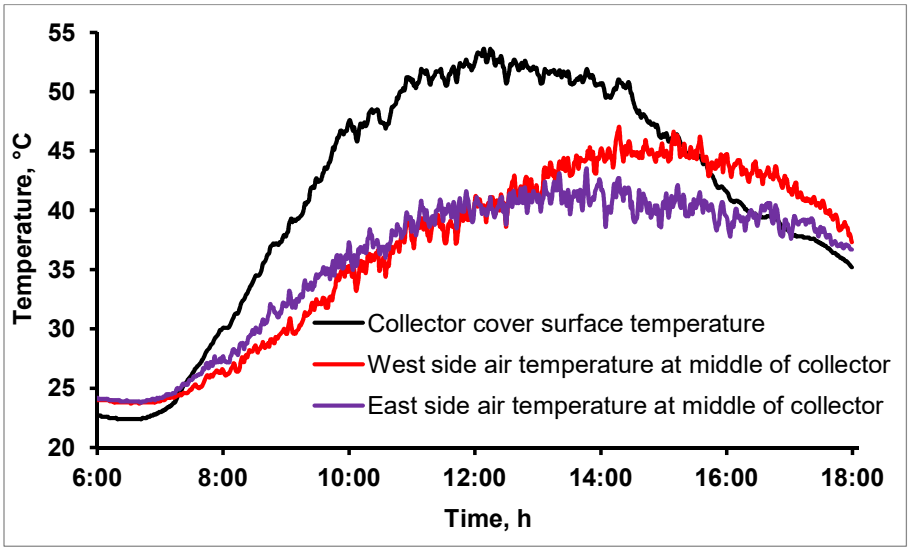

Fig. 5.10. Temperature variation with respect to time

Figure 5.11 shows the temperature data recorded on TES material (mixture of sand and gravel) round-the-clock. It is noticed that the temperature of TES system in the east side is higher than the west side because of more solar radiation in the east side in the morning. The maximum temperature of TES system was 65.8 °C. Also, the temperature was more than 60 °C from 10.45 AM to 2.30 PM. The average temperature of TES system from 6.00 PM to 7.00 AM of next day (no sunlight time region) was 39.95°C (in west side) and 32.54°C (in east side) which is more than the average temperature of ambient air (24°C) on the above mentioned days when there was no sunlight. Also, the average air temperature inside the canopy at the above mentioned time (no sunlight time) is 28.74°C (in west side) and 29°C (in east side). It proves that TES system stores heat energy in day time and liberates the heat during no sunlight time region. Therefore, the system can work round-the-clock.

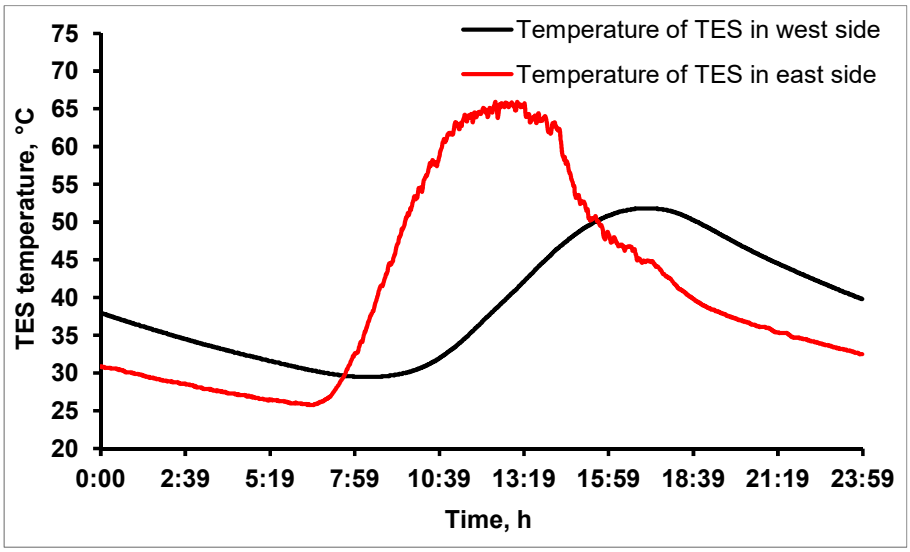

Fig. 5.11. Temperature variation of TES with respect to time

5.4. Air velocity distribution in the setup

Air velocities were measured in different locations inside the setup and the air velocities just below and above the turbine were plotted and shown in **Fig. 5.12**. These readings were taken for 10 days and round the clock. Each minute, air velocity was recorded and velocities from 6.00 AM to 6.00 PM are presented in this plot (**Fig. 5.12**). The temperature difference between the air inside the collector and ambient temperature creates a density difference inside the setup. Air density inside the canopy is low, therefore, high density fresh air enters the setup which creates a buoyancy effect; hence, the air flow starts naturally inside the setup. From **Fig. 5.12**, it is noticed that the air velocities below and above turbine plane slowly increase from early morning and reach peak value at noon. Afterwards, the air velocity decreases with the fall of solar radiation by evening. Early in the morning (6.00 to 8.00 AM) and late in the evening (4.00 to 6.00 PM) solar intensity is less; therefore, air temperature inside the setup is also low. Hence, the air flow velocity is also low. From 8.00 AM to 4.00 PM, solar intensity is more (as explained in **Fig. 5.1**) – absorber plate temperature is also more, which creates a higher temperature difference inside the setup. Buoyancy effect is also more during this region and therefore air velocity is more in this region. It is also observed that air velocity above the turbine is more compared to below the turbine. This is because velocity sensor was placed 200 mm above the turbine, so that when the turbine rotates, the air flow velocity near the region is more.

The minimum air velocity is 0.5 and 1 m/s at turbine below and above, respectively. Similarly the maximum air velocity is 4.7 and 5.5 m/s in the same locations, respectively. The average air velocity below the turbine is 2.18 m/s and above the turbine is 3 m/s. The maximum air velocities were 1.8 and 1.3 m/s just below and above the turbine, respectively, for the table top model developed by Al-Kayiem et al. [80] in Malaysia. In that model, the guide vanes were not provided, but in this present setup, guide vanes were placed vertically near the chimney base.

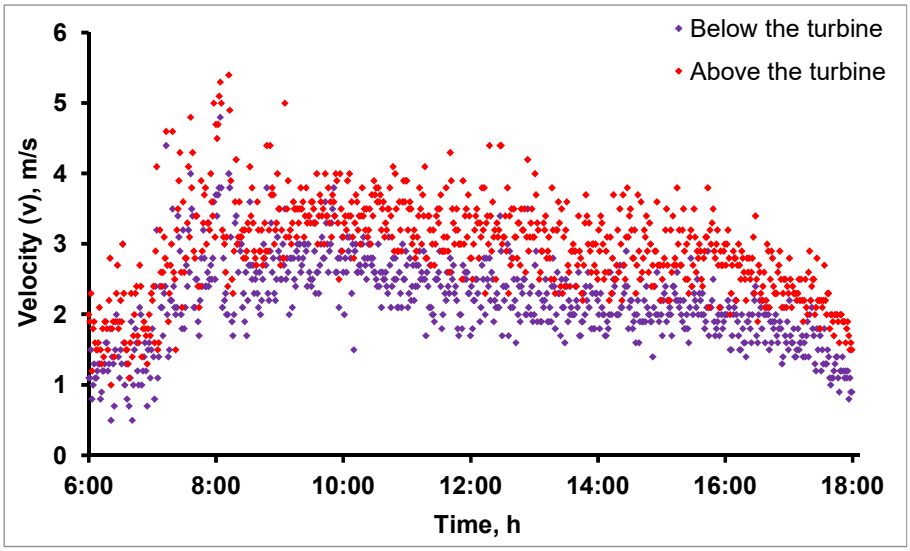

Fig. 5.12. Transient air velocity variation just below and above the turbine

5.5. Air pressure variation inside the setup

The absolute pressure variation of air inside the SUT plant was measured from 6.00 AM to 6.00 PM and plotted in **Fig. 5.13**. Measurements were taken at each minute. The air pressure inside the chimney increases and reaches a maximum value at 11.00 AM and again decreases when time goes on increasing because the air is heated up to 11.00 am. After this time region, the air is fully heated and loses its pressure. It was noticed that the air pressure at the chimney base (or a region below the turbine) is higher than at the turbine outlet. It means that the pressure drop occurs across the turbine. The average air pressure at below and above turbine are 97973 and 97970.8 N/m^2, respectively. The average pressure drop across the turbine in day time (6.00 AM to 6.00 PM) is 2.22 N/m^2 with a maximum of 4 N/m^2. It is also observed that the average ambient air pressure on day time is 97980 N/m^2 (this is measured with the help of Electronic Arduino Board with the help of computer code, Arduino 1.8.9).

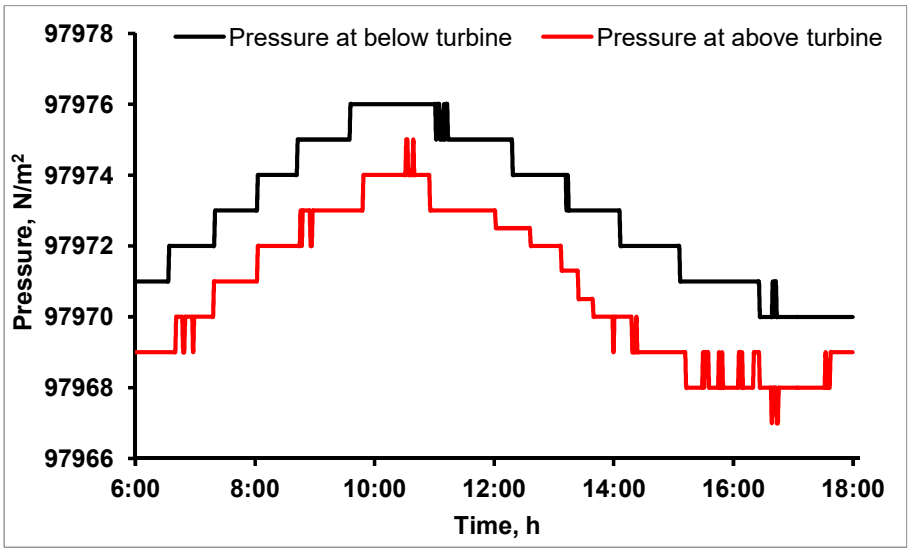

Fig. 5.13. Air pressure variation with respect to time

5.6. Speed measurement of turbine

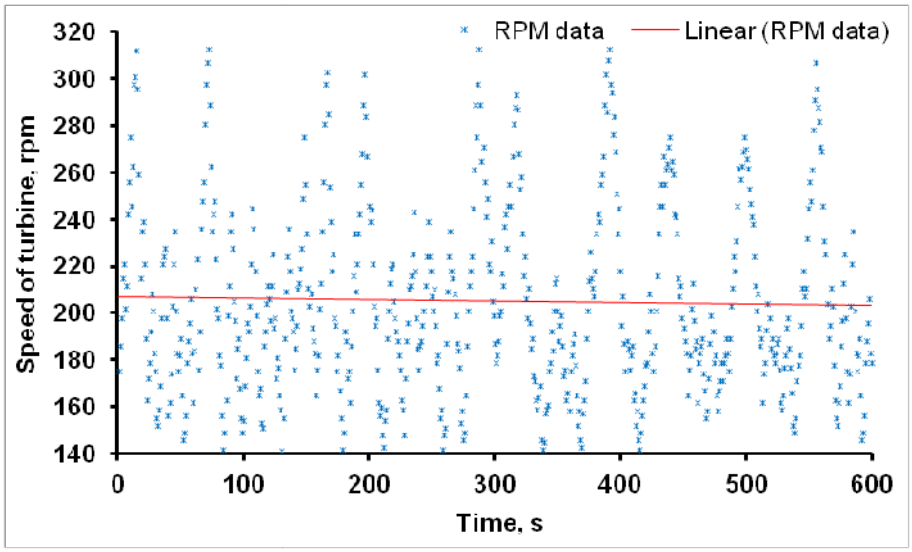

Fig. 5.14. Speed measurement of turbine

Turbine shaft revolutions were recorded for a particular period of time (between 1:00 PM to 1:10 PM) on 23rd March, 2019 and presented in **Fig. 5.14**. The maximum and minimum speeds are 317 and 142 rpm, respectively. The average speed of the shaft is 204.3 rpm and is mentioned in **Fig. 5.14**.

5.7. Estimation of power output and efficiencies of SUT plant

Pressure drop (Δp) occurs across the wind turbine (below and above the turbine) and reached its average value of 2.22 N/m^2.

Average air velocity at chimney base was experimentally evaluated and is 2.18 m/s.

Volumetric flow rate of air through the chimney was estimated using Eqs. (2.49 and 2.55) and is 0.6164 m^3/s.

Theoretical electric power (P) generated by SUT plant can be estimated by E. (2.56), and is 1.37 W.

The chimney efficiency is estimated by Eq. (2.57), and it's value is 0.0187 %.

The overall efficiency (η_o) of the plant can be calculated by Eq. (2.58), and is 0.0128 %.

Table 5.1 provides the complete details of estimated parameters of SUT.

Table 5.1: Estimated output parameters of SUT

Parameter	Value
Pressure drop (Δp)	2.22 N/m^2
Volumetric flow rate of air (Q)	0.6164 m^3/s
Theoretical power output (P)	1.37 W
Chimney efficiency (η_{ch})	0.0187 %
Overall plant efficiency (η_o)	0.0128 %

5.8. Actual power generated by turbine

Theoretical electric power (P) generated by SUT plant is 1.37 W (**Table 5.1**).

If the turbine efficiency is 66.67% [49] and the transmission losses are 10% [73], then the actual average power produced by the turbine is, P_{avg} = 0.82 W.

Then the total electric power produced in W-h for 15 h, 06:00 AM to 09:00 PM in a whole day is, $= 15 \times P_{avg} = 12.3$ *W-hr*

By using the above calculated power in W-h, the following electrical appliances can be worked freely for a particular period of time and the details are given in **Table 5.2.**

Table 5.2: Working time of household electrical appliances

House hold electrical appliance	Power consumption	Run Time
32" LED TV	60 W	12 min 18 s
Refrigerator	180 W	4 min 6 s
Ceiling Fan	75 W	9 min 50 s
LED Bulb	9/12/15 W	1 h 22 m /1 h 2 min /49 min 12 s
Laptop	50 W	14 min 46 s
All the above can run simultaneously in a home	401 W	1 min 50 s

The average energy consumption by an ordinary family for a period of one complete day is about: 20 kWh (maximum)**.** Therefore for a month, it is around 600 kWh. The following geometrical dimensions of SUT are necessary for producing 20 kWh power, 1). D_c = 70 m, 2). H_{ch} = 40 m and 3). D_{ch} = 2 m.

5.9. Results of uncertainty analysis

Uncertainty analysis was conducted using Eqs. (2.93) to (2.95) and the results are presented in this section. The number of readings (n) chosen for error analysis is 720. The performance parameters such as air velocity, pressure, temperature and solar radiation were selected for uncertainty analysis. Statistical analysis of experimental data includes x_m, σ and σ_m. Readings are taken for day time on 23rd March 2019 from 6:00 AM to 6:00 PM. The total uncertainty was measured using the accuracy and readability of instruments and uncertainty of measured data. **Table 5.3** provides the total uncertainty values of various parameters.

Table 5.3: Total uncertainties of experimental parameters

Parameters	Total uncertainty
Velocity, m/s	±0.223
Temperature, °C	±0.751
Pressure, N/m^2.	±1.077
Solar radiation, W/m^2	± 31.93
Speed, rpm	± 0.757

Volumetric flow rate of air (Q), m^3/s	± 0.007
Power output (P), W	± 0.019
Chimney efficiency (η_{ch}), %	± 0.000016
Overall SCPP efficiency (η_o), %	± 0.011

5.10. Results validation

The theoretical and numerical results were compared with experimental results and mentioned in **Table 5.4.**

Table 5.4: Comparison of theoretical and numerical results with experimental results

	D_{ch} (m)	H_{ch} (m)	D_c (m)	Maximum temperature (K)	Maximum velocity (m/s)	Chimney efficiency (%)	Maximum Power (W)
Theoretical results	0.6	6	3.5	324.2	2.1	0.0195	0.63
Numerical results	0.6	6	3.5	322	2.4	0.0182	0.51
Experimental results	0.6	6	3.5	318.9	5.3	0.0187	0.82

5.11. Summary

An SUT plant was designed and developed with the base parameter, ratio of chimney height (H_{ch}) and collector diameter (D_{cp}) as 1.7. The remaining dimensions were estimated based on H_{ch}/D_{cp} ratio and these were: D_{cp} of 3.5 m, H_{ch} of 6 m and chimney diameter (D_{ch}) of 0.6 m. A roof top with an approximate floor area of 400 m^2 was selected for erecting the plant. The selected roof area for installation of plant was free from shades of tree and other buildings. Solar collector cover angle (θ_{cp}) was chosen according to the latitude of Warangal, India. Different locally available materials were considered and analyzed for selecting the components of the plant.

The following materials were selected for the components of solar collector - Anti-refluxing glass, absorber plate - copper, chimney - polycarbonate, thermal energy storage (TES) material – sand and gravel, guide vanes - Carbon steel, base cone - wood, etc. Detailed procedures for the fabrication of setup and installation of components were explained such as

concrete foundation, supporting rods, TES system, absorber plates, structural steel frame, glass plates, canopy cover, guide vanes, wooden cone, solar chimney, strings etc.

The experiments were carried out for a period of 10 days and the results of one such day were presented. A brief analysis of the experimental data collected was presented. The solar intensity, temperature distribution of air and absorber plate, air velocities and pressures at different locations inside SUT were measured and recorded in a data logger.

- The average solar radiation from 7:00 AM to 6:00 PM was 534.5 W/m^2.
- The temperatures of south side absorber plate were slightly higher (almost reached to 67.5°C) than all the three sides (north, east and west) plate because the plant was located in northern hemisphere.
- The absolute air pressure before the turbine blade was in between 97970 to 97976 N/m^2. Similarly the air pressure above the turbine blade was in the range of 97967 to 97975 N/m^2. The maximum pressure drop that occurred across the wind turbine was 4 N/m^2.
- The maximum air velocity below and above turbine fan was 4.7 m/s (with an average of 2.18 m/s) and 5.5 m/s (average of 2.98 m/s), respectively.
- The temperature of TES system (sand and gravel mixture) on the east side was higher than that in the west side due to greater radiation in the east side in the morning. TES temperature was high (39.95°C, in west side and 32.54°C, in east side) compared to ambient air (24°C) during absence of sunlight time between 6.00 PM to 7.00 AM of the next day. The TES system worked well for the setup, and thus proved that the system can work round-the-clock.
- Average speed of turbine was 204.3 rpm.
- The theoretical power output, actual power output, chimney efficiency and overall plant efficiency were estimated as 1.37 W, 0.82 W, 0.0187 % and 0.0128 % respectively.
- The total electric power produced in kW-hr for 15 h, (06:00 AM to 09:00 PM) for a whole day was 12.3 kW-hr. Using the electrical power, a 32" LED TV can work more than 12 min 18 s, a refrigerator can sustain itself for up to 4 min 6 s, a ceiling fan can be used continuously for a period of 9 min 50 s and a laptop can function up to 14 min 46 s.
- Uncertainty analysis was performed for all the observed and estimated parameters.

The setup designed is enough to produce electrical power and therefore, the trial was successful.

Chapter 6

Conclusions

Chapter 6

6. Conclusions

A theoretical study was carried out to investigate the flow parameters and heat transfer characteristics of a prototype of solar updraft tower (SUT) power plant. The diameters of the solar collector and chimney are of the 3.5 and 0.6 m respectively. The objective of this work is to investigate the performance of SUT and to tabulate all the inputs and estimated parameters with the materials of a SUT power plant. All the three main components' (turbine, solar collector and a chimney) process parameters were estimated and discussed. Appropriate materials were discussed and selected for solar collector, chimney, turbine and heat storage materials. Solar beam, diffuse and global radiation were estimated to analyze the performance of collector cover. Energy losses in solar collector cover and transmissivity estimations were performed to calculate theoretical energy collected in solar collector. Pressure drop inside the chimney was estimated and from that the actual power output of the turbine was calculated. The quantity of heat storage materials needed was evaluated in terms of both mass and volume.

In numerical study, different cases (case-I, both collector and absorber plates are inclined; case-II, inclined collector and horizontal absorber plates; case-III, both horizontal collector and absorber plates), have been developed to evaluate and examine the flow and performance parameters of SUT power plant. A trial was made to suggest a model for better performance. A step was taken to find the location of turbine to absorb maximum kinetic energy for all the three cases. The output parameters such as power output and efficiencies were estimated for all models. The optimum collector roof angle and absorber plate angle were investigated, so that one can obtain maximum power output of the SUT case. The best case was recommended based on superior performance of system.

In the experimental work, a small scale solar chimney power plant (SCPP) was developed. Appropriate location, dimensions of each component, selection of materials for different components and a detailed procedure followed during the fabrication of SCPP plant were explained in this work. The setup was constructed based on locally available materials. Velocity, pressure and temperature were measured at various locations inside the setup.

Performance parameters of SCPP plant were estimated. The experiments were carried out for a period of 10 days and the data of a day was presented in this work.

6.1. Overall conclusions

The following overall conclusions were derived from theoretical, numerical and experimental analyses of SUT plant.

6.1.1. Theoretical analysis

2 Geometrical dimensions of the SUT plant model were optimised as H_{ch} = 6m, D_{ch} = 0.6 m and D_c = 3.5 m for getting maximum power output.

3 The average global radiation was 985 W/m^2. The minimum and maximum solar radiation fell on solar collector were estimated as 851.2 W/m^2 and 1059.4 W/m^2.

4 The maximum air velocity at chimney base was varied in between 1.82 to 2 m/s.

5 The pressure drop between inside and outside of the system was changed from 0.602 to 1.065 N/m^2.

6 The maximum power output of the SUT system was obtained in the month of April and is 0.633 W and similarly the minimum electricity generation was achieved in the month of December (0.309 W).

7 The chimney efficiency varied in between 0.0188 % to 0.0195 % in throughout the year. If we need to achieve optimum efficiency of the plant, then the chimney height should be 27 km, which is impossible for all practical purposes.

8 The maximum and minimum solar collector efficiencies were obtained as 53.9 % and 41.4 % in the months of April and December, respectively.

9 Similarly, the maximum and minimum overall efficiencies of the SUT system were achieved as 0.0028 % and 0.0017 % in the months of April and December, respectively.

10 The maximum power produced by various wind turbines (NACA 0012, NACA 4412 and NACA 23012) was estimated as 0.59 W, 0.624 W and 0.61 W respectively.

6.1.2. Numerical analysis

11 The maximum and average air velocities were obtained at chimney base (CB) of SUT system and these were 3.06 and 1.63 m/s for case-I, 2.4 and 1.34 m/s for case-II and 2.9 m/s and 1.57 m/s for case-III, respectively under the constant solar radiation of 850 W/m^2.

12 The maximum air velocity is found at 0.5 m above CB for case-I. For case-II, it is found in the range of 0.1 to 0.5 m from CB and for case-III, it is from 0.3 to 0.4 m. Therefore, these are the preferred locations for fixing the turbine.

13 The maximum and average air temperatures were estimated and these were 312 K & 305.8 K for case-I, 322 K & 306 K for case-II and 318 K & 306.3 K for case-III.

14 The maximum power output of case-II is higher (0.51 W) than case-I (0.4 W) and case-III (0.22 W).

15 The average chimney efficiency of case-I was higher (0.0187 %) than other two models (0.0182 % for case-II and 0.0184 % for case-III). Similarly, the maximum overall efficiency of case-II is higher (0.006 %) than other two models (0.005% for case-I and 0.003% for case-III).

Comparing in all aspects, the case-II could produce maximum power output and also gave highest overall system efficiency. Therefore, it is suggested that case-II can be preferred while erecting SUT setup.

6.1.3. Experimental analysis

16 The maximum air velocity below and above turbine fan was measured experimentally and it was 4.7 m/s (with an average of 2.18 m/s) and 5.5 m/s (average of 2.98 m/s), respectively.

17 The maximum pressure drop that occurred across the wind turbine was 4 N/m^2.

18 The theoretical power output (P), actual average power output (P_{avg}), chimney efficiency (η_{ch}) and overall plant efficiency (η_o) were estimated experimentally and these were 1.37 W, 0.82 W, 0.0187 % and 0.0128 %, respectively.

19 TES temperature was high (39.95°C, in west side and 32.54°C, in east side) compared to ambient air (24°C) during absence of sunlight time between 6.00 PM to 7.00 AM of the next day. The TES system worked well for the setup, and thus proved that the system can work round-the-clock.

20 The total electric power produced in kW-hr for 15 h, (06:00 AM to 09:00 PM) for a whole day was 12.3 kW-hr. Using the electrical power, a 32" LED TV can work more than 12 min 18 s, a refrigerator can sustain itself for up to 4 min 6 s, a ceiling fan can be used continuously for a period of 9 min 50 s and a laptop can function up to 14 min 46 s.

21 The average energy consumption by an ordinary family for a period of one complete day is about: 20 kWh (maximum)**.** Therefore for a month, it is around 600 kWh. The following geometrical dimensions of SUT are necessary for producing 20 kWh power,

a). Diameter of the collector (or) absorber plate = 70 m,

b). Height of the chimney = 40 m,

c). Diameter of the chimney = 2 m.

22 The setup designed was enough to produce electrical power and therefore, the trial was successful.

6.2. Future scope

- Numerical investigation of the performance parameters estimation of a solar updraft tower (SUT) plant coupled with various wind turbines using ANSYS FLUENT package (with dynamic mesh model (DMM) approach).
  - NACA 4412 wind turbine
  - NACA 23012 wind turbine
  - NACA 0012 wind turbine

- Experimental analysis of a small scale solar updraft tower (SUT) plant coupled with a real turbine (turbine will be manufactured by 3-D Printer with optimised dimensions).
- Numerical analysis on estimation of flow and heat transfer characteristics of a solar updraft tower (SUT) plant coupled with guide vanes and wooden base cone at chimney base using ANSYS FLUENT package.
- Numerical investigation of the performance parameters estimation of a SUT plant coupled with thermal energy storage system (rocks and lime stones) using ANSYS FLUENT package.

References

[1]. Asnaghi A, and Ladjevardi S.M. Solar chimney power plant performance in Iran. *Renewable and Sustainable Energy Reviews* 2012;16(5):3383-3390.

[2]. Ming T. A text book of solar chimney power plant generating technology. Zhejiang University Press Co., Ltd, China: 2016.

[3]. Haaf W, Freidrich K, Mayr G and Schlaich J. Solar Chimneys Part 1: Principle and Construction of the Pilot Plant in Manzanares. *Int. J. Solar Energy* 1983;2:3-20.

[4]. Kasaeian A, Mahmoudi A.R, Astaraei F.R and Hejab A. 3D simulation of solar chimney power plant considering turbine blades. *Energy conversion and management* 2017;147:55-65. DOI:10.1016/j.enconman.2017.05.029.

[5]. Ayadi A, Driss Z, Bouabidi A, Nasraoui H, Bsisa M, and Abid M.S. A computational and experimental study on the effect of the chimney height on the thermal characteristics of a solar chimney power plant. *J Process Mechanical Engineering* 2017; 0(0):1-14. DOI:10.1177/0954408917719776.

[6]. Ayadi A, Driss Z, Bouabidi A, and Abid M.S. Experimental and numerical study of the impact of the collector roof inclination on the performance of a solar chimney power plant. *Energy and Buildings* 2017;139:263-276. DOI:10.1016/j.enbuild.2017.01.047.

[7]. Tingzhen M, Wei L, and Guoliang X. Analytical and numerical investigation of the solar chimney power plant systems. *Int. J. Energy Research* 2006;30:861-873. DOI:10.1002/er.1191.

[8]. Cottam P.J, Duffor P, Lindstrand P, and Fromme P. Effect of canopy profile on solar thermal chimney performance. *Solar Energy* 2016;129:286-296. DOI:10.1016/j.solener.2016.01.052.

[9]. Bernardes M.A.S, and Zhou X. On the heat storage in solar updraft tower collectors – water bags. *Solar Energy* 2013;91:22-31. DOI:10.1016/j.solener.2012.11.025.

[10]. Tingzhen M, Wei L, Derichter R.K, Meng F, and Pan Y. Chimney shape numerical study for solar chimney power generating systems. *Int. J. Energy Research* 2006;30:861-873. DOI:10.1002/er.1910.

[11]. Zhou X, Bernardes M.A.S, and Ochieng R.M. Influence of atmospheric cross flow on solar updraft tower inflow. *Energy* 2012;42(1):393-400. DOI:10.1016/j.energy.2012.03.037.

[12]. Petela R. Thermodynamic study of a simplified model of the solar chimney power plant. *Solar Energy* 2008;83(1):94-107. DOI:10.1016/j.solener.2008.07.001.

[13]. Nasirivatan S, Kasaeian A, Ghalamchi M, and Ghalamchi M. Performance optimization of solar chimney power plant using electric/corona wind. *Journal of Electrostatics* 2015;78:22-30. DOI:10.1016/j.elstat.2015.09.007.

[14]. Koonsrisuk A, and Chitsomboon T. Effects of flow area changes on the potential of solar chimney power plants. *Energy* 2013;51:400-406. DOI:10.1016/j.energy.2012.12.051.

[15]. Koonsrisuk A, Lorente S, and Bejan A. Constructal solar chimney configuration. *Int. J. Heat mass transfer* 2010;53(1-3):327-333. DOI:10.1016/ijheatmasstransfer.2009.09.026.

[16]. Chen K, Wang J, Dai Y, and Liu Y. Thermodynamic analysis of a low temperature waste heat recovery system based on the concept of solar chimney. *Energy conversion and management* 2014;80:78-86. DOI:10.1016/j.enconman.2014.01.007.

[17]. Ming T, Liu W, Pan Y, and Xu G. Numerical analysis of flow and heat transfer characteristics in solar chimney power plants with energy storage layer. *Energy conversion and management* 2008;49(10):2872-2879. DOI:10.1016/j.enconman.2008.03.004.

[18]. Li J, Guo H, and Huang S. Power generation quality analysis and geometric optimization for solar chimney power plants. *Solar Energy* 2016;139:228-237. DOI:10.1016/j.solener.2016.09.033.

[19]. Shirvan K.M, Mirzakhanlari S, Mamourian, and Hamdeh N.A. Numerical investigation and sensitivity analysis of effective parameters to obtain potential maximum power output: A case study on Zanjan prototype solar chimney power plant. *Energy conversion and management* 2017;136:350-360. DOI:10.1016/j.enconman.2016.12.081.

[20]. Okoye C.O, and Taylan O. Performance analysis of a solar chimney power plant for rural areas in Nigeria. *Renewable Energy* 2017;104:96-108. DOI:10.1016/j.renene.2016.12.004.

[21]. Chan C-Y, Hu S-Y, Raynal M, Leung D.Y.C, Chang A.P.S, and Yao J.B. A telescopic divergent chimney for power generation based on forced air movement: principle and theoretical formulation. *Applied Energy* 2014;136:873-880. DOI: 10.1016/j.apenergy.2014.04.086.

[22]. Gholamalizadeh E, and Mansouri S.H. A comprehensive approach to design and improve a solar chimney power plant: A special case – Kerman project. *Applied Energy* 2013;102:975-982. DOI: 10.1016/j.apenergy.2012.06.012.

[23]. Zuo L, Liu Z, Zhou X, Ding L, Chen J, Ning Q, and Yuan Y. Preliminary study of wind supercharging solar chimney power plant combined with sea water desalination by indirect condensation freshwater production. *Desalination* 2019;455:79-88.

[24]. Cao F, Liu Q, Yang T, Zhu T, Bai J, and Zhao L. Full year simulation of solar chimney power plants in Northwest China. *Renewable Energy* 2018;119:421-428.

[25]. Jafarifar N, Behzadi N.M, and Yaghini M. The effect of strong ambient winds on the efficiency of solar updraft tower power plants: A numerical case study for Orkney. *Renewable Energy* 2019;136:937-944.

[26]. Hassan A, and Waqas M.M.A. Numerical investigation on performance of solar chimney power plant by varying collector slope and chimney diverging angle. *Energy* 2018;142:411-425.

[27]. Rabehi R, Chaker A, Ming T, and Gong T. Numerical simulation of solar chimney power plant adopting the fan model. *Renewable Energy* 2018;126:1093-1101.

[28]. Huang M-H, Chen L, He Y-L, J.J. Cao J.J, and Tao W.Q. A two dimensional simulation method of the solar chimney power plant with a new radiation model for the collector, *International Communications in Heat and Mass Transfer* 2017;85:100-106.

[29]. Elwekeel F.N.M, Abdala A.M.M, and Rahman M.M. Effects of novel collector roof on solar chimney power plant performance. *Journal of Solar Energy Engineering* 2019;141:031004-1-16.

[30]. Cottam P.J, Duffour P, Lindstrand P, and Fromme P. Solar chimney power plants – Dimension matching for optimum performance. *Energy Conversion and Management* 2019;194:112–123. DOI:10.1016/j.enconman.2019.04.074.

[31]. Bouabidi A, Ayadi A, Nasraoui H, Driss Z, and Abid M.S. Study of solar chimney in Tunisia: Effect of the chimney configurations on the local flow characteristics. *Energy & Buildings* 2018;169:27-38.

[32]. AL-kayeim H.H, Aurybi M.A, Gilani S.I.U. Influence of canopy condensate film on the performance of solar chimney power plant. *Renewable Energy* 2019;136:1012-1021.

[33]. Asnaghi A, Ladjevardi S.M, Kashani A.H, and Izadkhast P.S. Solar chimney power plant performance analysis in the central regions of Iran. *Journal of Solar Energy Engineering, Transactions of ASME* 2013;135:111-117.

[34]. Kalash S, Naimeh W, and Ajib S. Experimental investigation of the solar collector temperature field of a sloped solar updraft power plant prototype. *Solar Energy* 2013;98:70-77.

[35]. Ghalamchi M, Kasaeian A, and Mehrad G. Experimental study of geometrical and climate effects on the performance of a small solar chimney. *Renewable and Sustainable Energy Reviews* 2015;43:425- 431.

[36]. Ghalamchi M, Kasaeian A, Mehrad G, and Alireza H.M. An experimental study on the thermal performance of a solar chimney with different dimensional parameters. *Renewable Energy* 2016;91:477-483.

[37]. Sangi R, Amidpour M, and Hosseinizadeh B. Modeling and numerical simulation of solar chimney power plants. *Solar Energy* 2011;85:829–838.

[38]. Mohiuddin A, and Uzgoren E. Computational analysis of a solar energy induced vortex generator. *Applied Thermal Engineering* 2016;98:1036-1043.

[39]. Zhou X, Yang J, Xiao B, and Hou G. Experimental study of temperature field in a solar chimney power setup. *Applied Thermal Engineering* 2007;27:2044-2050.

[40]. Kasaeian A.B, Heidari E, and Nasirivatan Sh. Experimental investigation of climatic effects on the efficiency of a solar chimney pilot power plant. *Renewable and Sustainable Energy Reviews* 2011;15:5202- 5206.

[41]. Kasaeian A, Ghalamchi M, and Ghalamchi M. Simulation and optimization of geometric parameters of a solar chimney in Tehran. *Energy Conversion and Management* 2014;83:28- 34.

[42]. Gholamalizade E, and Chung J.D. Analysis of fluid flow and heat transfer on a solar updraft tower power plant coupled with a wind turbine using computational fluid dynamics. *Applied Thermal Engineering* 2017;126:548-558.

[43]. Koonsrisuk A, and Chitsomboon T. Partial geometric similarity for solar chimney power plant modelling. *Solar Energy* 2009;83:1611-1618.

[44]. Lal S, Kaushik S.C, and Hans R. Experimental investigation and CFD simulation studies of a laboratory scale solar chimney for power generation. *Sustainable Energy Technologies and Assessments* 2016;13:13-22.

[45]. Schlaich J, Bergermann R, Schiel W, and Weinrebe G. Design of commercial solar updraft tower systems – utilization of solar induced convective flows for power generation. *Journal of Solar Energy Engineering, Transactions of ASME* 2005:127:117-124.

[46]. Prabhukhot P.R and Prabhukhot A.R. Computer analysis of S822 Aerofoil section for blades of small wind turbines at low wind speed. *Journal of Solar Energy Engineering, Transactions of ASME* 2017;139:051008-1-4.

[47]. Pretorius J.P and Kröger D.G. Critical evaluation of solar chimney power plant performance. *Solar Energy* 2006;80:535-544.

[48]. Tian Y and Zhao C.Y. A review of solar collectors and thermal energy storage in solar thermal applications. *Applied Energy* 2013;104:538–553.

[49]. Gannon A.J and Von Backström T.W. Solar chimney turbine performance. *Journal of Solar Energy Engineering, Transactions of ASME* 2003;125:101-106.

[50]. Gitan A.A, Abdulmalek S.H and Dihrab S.S. Tracking collector consideration of tilted collector solar updraft tower power plant under Malaysia climate conditions. *Energy* 2015;93(2):1467-77.

[51]. Guo P, Li J, Wang Y and Wang Y. Numerical study on the performance of a solar chimney power plant, *Energy Conversion and Management* 2015;105:197-205.

[52]. Hu S, Leung D.Y.C and Chan J.C.Y. Impact of the geometry of divergent chimneys on the power output of a solar chimney power plant. *Energy* 2017;120:1–11.

[53]. Maghrebi M.J, Nejad R.M and Masoudi S. Performance analysis of sloped solar chimney power plants in the southwestern region of Iran. *International Journal of Ambient Energy* 2017;38(6):542-549.

[54]. Zhou X and Yang J. A novel solar thermal power plant with floating chimney stiffened onto a mountain side and potential of the power generation in china's deserts, *Heat Transfer Engineering* 2009;30(5):400-407.

[55]. Maia C.B, Ferreira A.G, Valle R.M and Cortez M.F.B. Analysis of the air flow in a prototype of a solar chimney drier. *Heat Transfer Engineering* 2009;30(5):393-399.

[56]. Zhou X, Yang J, Xiao B, Hou G and Xing F. Analysis of chimney height for solar chimney power plant, *Applied Thermal Engineering* 2009;29:178-185.

[57]. Zxou X, Yang J, Xiao B, Hou G and Yingying W.U. Numerical investigation of a compressible flow through a solar chimney. *Heat Transfer Engineering* 2009;30(8):670-676.

[58]. Ozgen F, Esen M and Esen H. Experimental investigation of thermal performance of a double flow solar air heater having aluminium cans. *Renewable Energy* 2009;34:2391-2398.

[59]. Esen H, Ozgen F, Esen M, Sengur A. Artificial neural network and wavelet neural network approaches for modeling of a solar air heater. *Expert systems with applications* 2009;36:11240-11248.

[60]. Esen H, Ozgen F, Esen M, Sengur A. Modelling of a new solar air heater through least squares support vector machines. *Expert systems with applications* 2009;36:10673-10682.

[61]. Esen M and Yuksel T. Experimental evaluation of using various renewable energy sources for heating a green house. *Energy and Buildings* 2013;65:340-351.

[62]. Kalogirou S.A. Solar thermal collectors and applications. *Progress in Energy and Combustion Science* 2004;30:231-295.

[63]. Khurmi R.S, Gupta J.K. A text book of machine design. First multicolor ed. Eurasia publishing house (pvt) Ltd; 2005.

[64]. Sukhatme S.P and Nayak J.K. Solar energy-principles of thermal collection and storage, 3rd ed. Tata McGraw Hill Education Private Limited, New Delhi, India: 2008.

[65]. Threlkeld J.L, Jordan R.C. Direct solar radiation available on clear days. ASHRAE Transactions, 1958: 64:45.

[66]. Iqbal M. An introduction to solar radiation, 1sted.Academic press, Canada: 1983.

[67]. Coetzee H. Design of solar chimney to generate electricity employing a convergent nozzle, Ph.D thesis, Botswana Technology Center, Private Bag 0082, Gaborone, Botswana, South Africa, 1999.

[68]. Ghalamchi M, Kasaeian A and Ghalamchi M. Experimental study of geometrical and climate effects on the performance of a small solar chimney. *Renewable and sustainable energy reviews* 2015;43:425-431.

[69]. Zhou X.P, Wang F and Ochieng R.M. A review on solar chimney power technology. *Renewable and Sustainable Energy Reviews* 2010;14:2315–38.

[70]. Harte R, Höffer R, Krätzig W.B, Mark P and Niemann H.J. Solar updraft power plants: Engineering structures for sustainable energy generation. *Engineering Structures* 2013;56:1698-1706.

[71]. Larbi S, Bouhdjar A, Meliani K, Taghourt A, and Semai H. Solar chimney power plant with heat storage system performance analysis in south region of Algeria, *2015 3rd International Renewable and Sustainable Energy Conference (IRSEC)*, *IEEE Conference Publications*, 1 - 6, DOI: 10.1109/IRSEC.2015.7454948.

[72]. Kaygusuz K. The viability of thermal energy storage, *Energy Sources* 2010;21(8):745-755.

[73]. Soren G. A text book of Wind Turbines. 2nd ed. University college of Arhaus, Arhaus; 2009.

[74]. Gasch R, Twele J. Wind power plants. 2nd ed. Springer Heidelberg Dordrecht, London; 2012.

[75]. Tyagi A.P. Solar radiant energy over India, India Meteorological department, Ministry of earth sciences, Government of India: 2016.

[76]. Abhay L, Chandramohan V.P and Raju V.R.K. Design, development and performance of indirect type solar dryer for banana drying. *Energy Procedia* 2017; 109: 409 – 416.

[77]. Pasumarthi N, Sherif S.A. Experimental and theoretical performance of a demonstration solar chimney model—Part II: Experimental and theoretical results and economic analysis, *International Journal of Energy Research* 1998;22:443-461.

[78]. W. Haaf, Solar Chimneys Part 2: Preliminary test results from the Manzanares pilot plant, International Journal of Solar Energy 1984; 2: 141-161.

[79]. Durrani N, Hameed H, Rahman H, Chaudhry S.R. A detailed aerodynamic design and analysis of a 2D vertical axis wind turbine using sliding mesh in CFD. *49th AIAA Aerospace Sciences Meeting including the New Horizons Forum and Aerospace Exposition* 4 - 7 Orlando, Florida (2011).

[80]. Al-Kayeim H.H, Aurybi M.A, Gilani S.I.U, Ismaeel A.A, and Mohammad S.T. Performance evaluation of hybrid solar chimney for uninterrupted power generation. *Energy* 2019; 166:490-505.

[81]. Ahmed M.R, and Patel S.K. Computational and experimental studies on solar chimney power plants for power generation in pacific island countries. *Energy Conversion and Management*2017; 149:61-78. DOI:10.1016/j.enconman.2017.07.009.

[82]. Nasraoui H, Driss Z, Ayadi A, Bouabidi A, and Kchaou H. Numerical and experimental study of the impact of conical chimney angle on the thermodynamic characteristics of a solar chimney power plant. *J. Process Mechanical Engineering* 2019; 0(0):1-15. DOI:10.1117/0954408919859160.

[83]. Fadaei N, Kasaeian A, Akbarzadeh A, and Hashemabadi S.H. Experimental investigation of solar chimney with phase change material (PCM). *Renewable Energy* 2018;123:26-35. DOI: 10.1016/j.renene.2018.01.122.

Publications

Published Journal papers

1. Balijepalli, R., Chandramohan, V.P. and Kirankumar, K. (2017) Performance Parameter Evaluation, Materials Selection, Solar Radiation with Energy Losses, Energy Storage and Turbine Design Procedure for a Pilot Scale Solar Updraft Tower, *Energy Conversion and Management,* **Elsevier***,* 150: pp.451-462. DOI: 10.1016/j.enconman.2017.08.043. (SCI)

2. Balijepalli, R., Chandramohan, V.P. and Kirankumar, K. (2018) A Complete Design Data and Performance Parameter Evaluation of a Pilot Scale Solar Updraft Tower, *Heat Transfer Engineering,* **Taylor & Francis**, 41: pp.5-6. DOI: 10.1080/01457632.2018.1546811. (SCI)

3. Balijepalli, R., Chandramohan, V.P. and Kirankumar, K. (2018) Optimized Design and Performance Parameters for Wind Turbine Blades of a Solar Updraft Tower (SUT) Plant Using Theories of Schmitz and Aerodynamics Forces, *Sustainable Energy Technologies and Assessments*, **Elsevier,** 30: pp.192-200. DOI: 10.1016/j.seta.2018.10.001. (SCI)

4. Balijepalli, R., Chandramohan, V.P. and Kirankumar, K. (2019) Development of a Small Scale Plant for a Solar Chimney Power Plant (SCPP): A Detailed Fabrication Procedure, Experiments and Performance Parameters Evaluation, *Renewable Energy,* **Elsevier,** 148: pp.247-260. DOI: 10.1016/j.renene.2019.12.001. (SCI)

Journal communicated:

1. Balijepalli, R., Chandramohan, V.P. and Kirankumar, K. (2019) Numerical investigation of flow parameters and thermodynamic characteristics of different solar updraft tower models with a suggested model for better performance. Manuscript submitted on December 2019, *Energy, **Elsevier***.

2. Balijepalli, R., Chandramohan, V.P. and Kirankumar, K. (2019) Numerical analysis on flow and performance characteristics of a small scale solar updraft tower (SUT) with horizontal absorber plate and collector glass. Manuscript submitted on November 2019, *Journal of Thermal Analysis and Calorimetry, **Springer.***

International Conferences

1. Ramakrishna Balijepalli, Chandramohan, V.P. and Kirankumar, K. (2017) Design and performance parameter evaluation of a pilot scale solar updraft tower, Proceedings of the 1st International and 18th ISME Conference, February 23rd – 25th, 2017, **NIT Warangal**, Warangal.
2. Ramakrishna Balijepalli, Chandramohan V.P and Kirankumar, K. (2017) Design and Performance Investigation of Wind Turbine Blade for Solar Updraft Tower under Low Wind Speeds, 6th international conference on advances in energy research (ICAER), 12th – 14th December, **Indian Institute of Technology Bombay**, Bombay, India.
3. Ramakrishna Balijepalli, Chandramohan V.P and Kirankumar, K. (2018) Design parameters estimation of a wind turbine using theory of conservation of angular momentum and aerodynamic forces: An optimised solution for the application of SUT, International conference on thermal analysis and energy systems (ICTAES), 12th – 13th April, Hindusthan college of engineering and Technology, Coimbatore, Tamilanadu, India.
4. Ramakrishna Balijepalli, Chandramohan V.P and Kirankumar, K. (2019) Numerical analysis on flow and performance characteristics of a small scale solar updraft tower (SUT) with horizontal absorber plate and collector glass, International Mechanical Engineering Congress – 2019 (IMEC-2019), 29th November - 1st December -2019, **National Institute of Technology, Tiruchirappalli**, Tamil Nadu, India.